WL-TR-94-2043

HIGH FLUX HEAT EXCHANGER

EDWARD M. FLYNN
R. SCOTT DOWNING
DAM C. NGUYEN

MCDONNELL DOUGLAS AEROSPACE
PO BOX 516
ST LOUIS MO   63166-0516

FEBRUARY 1994

FINAL REPORT FOR 10/30/91-12/31/93

DTIC
ELECTE
S MAR 03 1995
G
D

APPROVED FOR PUBLIC RELEASE; DISTRIBUTION IS UNLIMITED.

DTIC QUALITY INSPECTED 4

AEROPROPULSION AND POWER DIRECTORATE
WRIGHT LABORATORY
AIR FORCE MATERIEL COMMAND
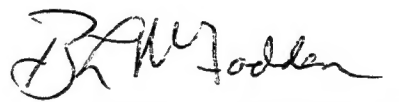WRIGHT PATTERSON AFB OH 45433-7251

19950227 092

NOTICE

WHEN GOVERNMENT DRAWINGS, SPECIFICATIONS, OR OTHER DATA ARE USED FOR ANY PURPOSE OTHER THAN IN CONNECTION WITH A DEFINITELY GOVERNMENT-RELATED PROCUREMENT, THE UNITED STATES GOVERNMENT INCURS NO RESPONSIBILITY OR ANY OBLIGATION WHATSOEVER. THE FACT THAT THE GOVERNMENT MAY HAVE FORMULATED OR IN ANY WAY SUPPLIED THE SAID DRAWINGS, SPECIFICATIONS, OR OTHER DATA, IS NOT TO BE REGARDED BY IMPLICATION, OR OTHERWISE IN ANY MANNER CONSTRUED, AS LICENSING THE HOLDER, OR ANY OTHER PERSON OR CORPORATION; OR AS CONVEYING ANY RIGHTS OR PERMISSION TO MANUFACTURE, USE, OR SELL ANY PATENTED INVENTION THAT MAY IN ANY WAY BE RELATED THERETO.

THIS REPORT HAS BEEN REVIEWED BY THE OFFICE OF PUBLIC AFFAIRS (ASD/PA) AND IS RELEASABLE TO THE NATIONAL TECHNICAL INFORMATION SERVICE (NTIS). AT NTIS IT WILL BE AVAILABLE TO THE GENERAL PUBLIC INCLUDING FOREIGN NATIONS.

THIS TECHNICAL REPORT HAS BEEN REVIEWED AND IS APPROVED FOR PUBLICATION.

JERRY E. BEAM, Section Chief
Thermal Technology Section
Power Technology Branch

BURYL L. MCFADDEN, Chief
Power Technology Branch
Aerospace Power Divicion

FOR THE COMMANDER

MICHAEL D. BRAYDICH, Lt Col, USAF
Deputy Director
Aerospace Power Division

IF YOUR ADDRESS HAS CHANGED, IF YOU WISH TO BE REMOVED FROM OUR MAILING LIST, OR IF THE ADDRESSEE IS NO LONGER EMPLOYED BY YOUR ORGANIZATION PLEASE NOTIFY WL/POOS , WRIGHT-PATTERSON AFB, OH 45433-7251 TO HELP MAINTAIN A CURRENT MAILING LIST.

COPIES OF THIS REPORT SHOULD NOT BE RETURNED UNLESS RETURN IS REQUIRED BY SECURITY CONSIDERATIONS, CONTRACTUAL OBLIGATIONS, OR NOTICE ON A SPECIFIC DOCUMENT.

# REPORT DOCUMENTATION PAGE	*Form Approved* *OMB No. 0704-0188*

Public reporting burden for this collection of information is estimated to average 1 hour per response, including the time for reviewing instructions, searching existing data sources, gathering and maintaining the data needed, and completing and reviewing the collection of information. Send comments regarding this burden estimate or any other aspect of this collection of information, including suggestions for reducing this burden, to Washington Headquarters Services, Directorate for Information Operations and Reports, 1215 Jefferson Davis Highway, Suite 1204, Arlington, VA 22202-4302, and to the Office of Management and Budget, Paperwork Reduction Project (0704-0188), Washington, DC 20503.

1. AGENCY USE ONLY *(Leave blank)*	2. REPORT DATE FEB 1994	3. REPORT TYPE AND DATES COVERED FINAL AND DATES 10/30/91--12/31/93	
4. TITLE AND SUBTITLE HIGH FLUX HEAT EXHANGER			5. FUNDING NUMBERS C F33615-90-C-2054 PE 62203 PR 3145 TA 20 WU C1
6. AUTHOR(S) EDWARD M. FLYNN R. SCOTT DOWNING DAM C. NGUYEN			
7. PERFORMING ORGANIZATION NAME(S) AND ADDRESS(ES) MCDONNELL DOUGLAS AEROSPACE PO BOX 516 ST LOUIS MO 63166-0516			8. PERFORMING ORGANIZATION REPORT NUMBER
9. SPONSORING/MONITORING AGENCY NAME(S) AND ADDRESS(ES) AEROPROPULSION AND POWER DIRECTORATE WRIGHT LABORATORY AIR FORCE MATERIEL COMMAND WRIGHT PATTERSON AFB OH 45433-7251			10. SPONSORING/MONITORING AGENCY REPORT NUMBER WL-TR-94-2043
11. SUPPLEMENTARY NOTES			
12a. DISTRIBUTION/AVAILABILITY STATEMENT APPROVED FOR PUBLIC RELEASE; DISTRIBUTION IS UNLIMITED.			12b. DISTRIBUTION CODE

13. ABSTRACT *(Maximum 200 words)*

This final report documents the results of the final two phases of a four-phase program to develop a high flux heat exchanger for cooling future high-performance aircraft electronics. Phases I and II, documented in interim report WL-TR-93-2027, defined future avionics cooling requirements and summarized a trade study of applicable cooling technologies. The Phase II trade study selected the Compact High Intensity Cooler (CHIC) for further development in Phases III and IV. This report describes the design, fabrication, and testing of the CHIC. The CHIC was designed to minimize system penalties (weight, cost, etc.) to a typical advanced fighter aircraft. Design objectives included a heat exchanger shape factor meeting Standard Electronics Module Format "E" (SEM-E) specification, local heat flux capability of 100 W/cm^2, total module heat flux capability of 2000 W, maximum junction temperature of 90 °C, and the use of poly alpha olefin (PAO) as the coolant. The CHIC was fabricated by diffusion bonding a stack of 24 copper alloy laminations (of eight different patterns) produced by photo-chemical etching. It was leak checked, proof-pressure tested, and then subjected to a series of thermal tests to verify performance. This was the first demonstration of 100 W/cm^2 local heat flux capability and 2000 W module capability using PAO.

14. SUBJECT TERMS ELECTRONIC COOLING, HIGH POWER ELECTRONICS, AVIONICS COOLING			15. NUMBER OF PAGES 131
			16. PRICE CODE
17. SECURITY CLASSIFICATION OF REPORT UNCLASSIFIED	18. SECURITY CLASSIFICATION OF THIS PAGE UNCLASSIFIED	19. SECURITY CLASSIFICATION OF ABSTRACT UNCLASSIFIED	20. LIMITATION OF ABSTRACT UL

NSN 7540-01-280-5500

Standard Form 298 (Rev. 2-89)
Prescribed by ANSI Std. Z39-18
298-102

TABLE OF CONTENTS

LIST OF FIGURES

LIST OF FIGURES (CONTINUED)

LIST OF TABLES

FOREWORD

This report presents results developed by McDonnell Douglas Aerospace (MDA) under Air Force Contract F33615-90-C-2054 "High Flux Heat Exchanger." This development program was conducted under sponsorship of the Air Force Wright Laboratory, with Dr. Jerry E. Beam, POOS, as Project Manager. The program was divided into four phases:

1. Cooling Requirements for Future Avionics

2. Cooling Concept Trade Study

3. Cooling Concept Design

4. Fabrication, Test, and Data Analysis

This final report documents the results of the final two phases. Results of Phases 1 and 2 are documented in Report WL-TR-93-2027.

The final two phases of this program reported herein were managed at MDA by Mr. Brian K. Bennett. The principal investigator was Mr. Edward M. Flynn. The principal subcontractor was Sundstrand Aerospace. The subcontractor program manager was Mr. Timothy J. Bland, and the subcontractor principal investigators were Mr. R. Scott Downing and Mr. Dam Nguyen.

Aeroquip, Lockhart Industries, Mechtronics, MicroStar Inc., Mini Systems Inc., and REFRAC Systems also contributed to this program.

SECTION 1

INTRODUCTION

1.1 Background

Future aerospace systems designs must employ a new generation of electronics components while meeting requirements for lower cost, improved performance, and higher reliability. These components have functional densities several orders of magnitude greater than their predecessors, yet with only marginally improved reliability. The net result is that, although the reliability of the individual components has improved, the far greater number of components decreases system reliability. New cooling technology is needed to improve the reliability of electronics systems. With the advent of VHSIC technology and the increased power in switching devices, thermal densities have dramatically risen, but methods capable of dissipating this thermal load need to be developed. Conventional solutions, such as air or liquid convection cooling, are heavy and bulky. Future platforms offering combinations of high speed and/or low observability will require avionics cooling systems that minimize the use of external ram or bleed air. Current conduction cold plate technology limits power dissipation to roughly 30 to 40 W on each SEM-E printed circuit board (PCB), while recently developed flow-through modules can handle about 200 to 400 W. These flow-through modules limit the local heat dissipation at individual devices to about 10 to 15 W/cm^2. Within the next five to ten years, local heat load at the device level is projected to increase to about 30 to 50 W/cm^2 for digital processors and to several hundred W/cm^2 for power processors (refernece [1]). Therefore, development of novel cooling techniques is needed to provide waste heat removal, temperature control, and reliability improvement.

1.2 Objective

The objective of this program is to analyze, design, develop, and demonstrate a novel high flux heat exchanger for cooling future high-performance electronics. The results of the first two phases of this four-phase program are reported in reference [1], which describes cooling requirements and a cooling concept trade study. The results of the final two phases are included in this report. The objective of Phase III is to perform a detailed design of the heat exchanger selected from the Phase II trade study. The objective of Phase IV is to fabricate and test the heat exchanger, and to measure performance against the cooling requirements established in Phase I.

Specific objectives included the following advancements in avionics cooling technology:

1. Using a cooling concept with proven feasibility but limited development, to redesign the concept for suitability in an aircraft operating environment. This, for instance, could require changing coolants from a thermally desirable coolant such as water to a thermally poorer but better-suited aircraft coolant such as poly alpha olefin (PAO).

1

2. To demonstrate heat removal capabilities for aircraft avionics significantly greater than those obtainable with currently used heat exchangers.

3. To demonstrate high heat flux capability *and* high packaging density (i.e., to not rely on extensive heat spreading).

1.3 Summary

A heat exchanger was designed, fabricated, and tested which meets the high heat flux requirements established in Phase I. High local heat flux capability (100 W/cm^2) was achieved by combining the high heat transfer characteristics of multiple jet impingement with the compact extended surface area enhancement of laminated construction. Total module heat load capability of 2000 W was projected based on successful sample testing of several of the twenty 100-W cooling locations. The HFHE was integrated into the Lockhart LOC-E-JECT ™ liquid cooled SEM-E format module used for F-22 avionics cooling. The heat exchanger shape factor conforms to SEM-E packaging specifications (MIL-STD-1389D) in lateral dimensions, with thickness slightly exceeding SEM-E standards due to cost-savings interests in developing a prototype. No technical obstacles are forseen for eventually reducing thickness to SEM-E standards. The aircraft coolant PAO was used under conditions of coolant supply temperature, flow rate, and pressure drop available in a fighter aircraft environment. Repeatable thermal and hydraulic performance were obtained over a one-month period of testing, including 22 hours of flowing coolant.

SECTION 2

PRELIMINARY DESIGN

A parametric design study was performed in order to understand and minimize heat exchanger impact on a typical, notional advanced fighter aircraft. Heat exchanger design parameters included coolant pressure drop, flow rate, coolant supply temperature, heat exchanger material, manifolding, and flow distribution. Aircraft system impact was assessed in terms of aircraft weight increase, cold-start performance, cost, and risk.

2.1 Requirements and Assumptions

Heat exchanger performance requirements and design constraints, specified in the Air Force Statement of Work and developed in the first two phases of this program, are shown in Table 1.

Table 1

Heat Exchanger Design and Performance Requirements and Objectives

Form Factor	SEM-E Size (Approx. 15 cm x 17 cm, on 1.5 cm pitch, approx. 200 cm^2 device mounting area per side, defined by MIL-STD-1389D). (Objective)
Steady-State Heat Flux	Steady-state module heat load of 2180 W, distributed as 100 W/cm^2 to 20 cm^2 of board surface area, and 1.0 W/cm^2 heat flux over the remaining 180 cm^2 (assuming single-sided heat addition). (Requirement)
Transient Heat Flux	100 W/cm^2. (Requirement)
Junction Temp.	$\leq 90\,°C$. (Requirement)
Coolant Temp.	$\geq 0\,°C$. (Requirement)
Module Pressure Drop	< 311 kPa (45 psi) at Design Point (Requirement) < 690 kPa (100 psi) for Cold Start (Requirement)

From the Phase 1 requirements study, no SEM-E application was found which would require 100 W/cm^2 local cooling capability or 2000 W total module capability. However, devices such as More-Electric-Aircraft power conditioners, which might not

3

be mounted on SEM-E modules, are predicted to dissipate heat in excess of 100 W/cm^2, while SEM-E module cooling requirements are expected to continue to grow. Therefore, while SEM-E modules may not require 100 W/cm^2 capability in the forseeable future, such demonstration achieves the objectives of exceeding any expected SEM-E cooling needs while meeting requirements of certain non-SEM-E cooling applications. Two pressure drop requirements are given in Table 1. The pressure drop of 311 kPa is the maximum assumed to be available to the module during normal operation, and is used as an upper bound for calculating design-point flow rate and thermal performance. The value of 690 kPa is the maximum pressure drop assumed during low-flow start-up conditions, and is used for structural design purposes.

Table 2 lists several assumptions made in order to conduct the preliminary design. Assumption #3 concerns electronics device thermal resistance from junction to heat exchanger wall. Maximum junction temperature of 90 °C is a requirement, but actual electronics devices were not tested, so a measurement of junction temperature could not be made. Therefore, heat exchanger wall temperature was used as a test requirement, and a relationship was assumed between wall temperature and junction temperature for a typical high power device. Figure 1 depicts thermal resistance paths between an electronics device junction and heat exchanger coolant. Thermal resistances between junction and device case, and between device case and heat exchanger wall of 0.20 °C/(W/cm^2) each were assumed. Thus, at a heat flux of 100 W/cm^2, the wall temperature requirement is:

$$T_{wall} (max) = T_j (max) - (R_{jc} + R_{cw})*Q$$
$$= 90 \text{ °C} - (0.2 + 0.2) \text{ °C/(W/cm}^2) * 100 \text{ W/cm}^2$$
$$= 50 \text{ °C}$$

Table 2

Assumptions Made for Preliminary Design

1.	Single-sided heat addition to module.
2.	20 cm^2 of high heat area is comprised of twenty discrete 1.0 cm x 1.0 cm locations.
3.	Junction-to-case thermal resistance = 0.20 °C/(W/cm^2). Device case to heat exchanger wall thermal resistance = 0.20 °C/(W/cm^2).
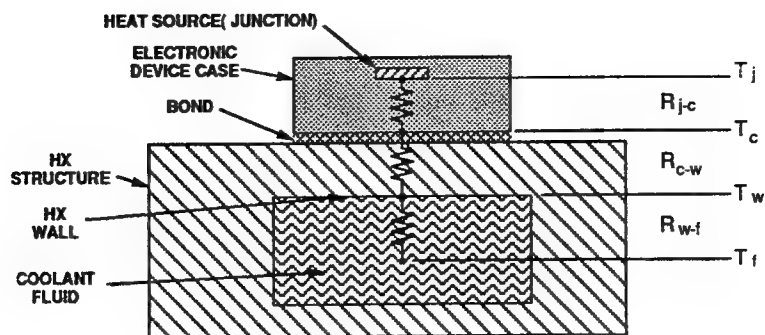
Figure 1. Definition of Thermal Resistances

A maximum heat exchanger wall temperature of 50 °C was therefore used in place of the 90 °C junction temperature requirement.

Junction temperature requirements for digital applications sometimes are lower than 90 °C. The Air Force Advanced Aircraft Avionics Packaging Technology (AAAPT) program (reference [2]), for example, specifies 65 °C. As mentioned above, digital applications, AAAPT included, will not experience 100 W/cm^2 heat dissipation. The lower heat dissipations experienced by digital applications will result in junction temperatures lower than 90 °C. The 90 °C junction temperature requirement of this program pertains to devices which dissipate heat on the order of 100 W/cm^2, representative of very high-power transistors designed to operate at higher junction temperatures.

2.2 CHIC Concept Review

An overview of CHIC construction and operating characteristics is given in this section. Greater detail on CHIC operating principles may be found in Appendix A.

The CHIC device was first introduced by Sundstrand in 1983 (Bland, et al., reference [3]). This liquid single-phase cooler combines the thermal efficiency of multiple jet impingement with extended surface area enhancement to produce a high effective heat transfer coefficient. Figure 2 shows the basic elements of a CHIC device. Various laminates are fabricated separately, then stacked and bonded to form a single cooler element.

The arrows in Figure 2 show the direction of coolant flow. Entering the inlet port in the end cover, the liquid is pumped through the feed manifold and to the jet orifice plate. This plate usually contains about 50 to 200 small circular holes. In the simplest form, the liquid impinges on the target plate, and then is directed back to the drain manifold and ultimately to the exit port. The electronics device is attached to the base side of the target plate. Figure 2 shows a single orifice plate and spacer. Usually the orifice plate and spacer are repeated several times, with each successive

5

orifice plate acting as a target for the jets from the orifice plate immediately upstream. The orifices are offset by one-half their pitch from plate to plate, so that the liquid impinges midway between the next set of orifices, then cascades downward as it passes through subsequent orifice plates. The greater the number of plates, the greater the fin effect and thus the higher the effective heat transfer coefficient. The penalties for a large number of orifice plates are higher pressure drop in the CHIC and a thicker heat exchanger.

Typically, the laminates are photoetched, then stacked and bonded. Diffusion bonding has been demonstrated for copper modules and vacuum brazing for aluminum modules, although the copper technology is more mature. The photoetching process allows virtually anything that can be drawn to be fabricated, so that the designer has liberty in laying out locations and sizes of the various CHICs on the module.

END COVER

DRAIN MANIFOLD

BACK PLATE DRAIN

FEED DRAIN DIVIDER

FEED MANIFOLD

JET ORIFICE PLATE

SPACER PLATE

TARGET DRAIN

TARGET PLATE
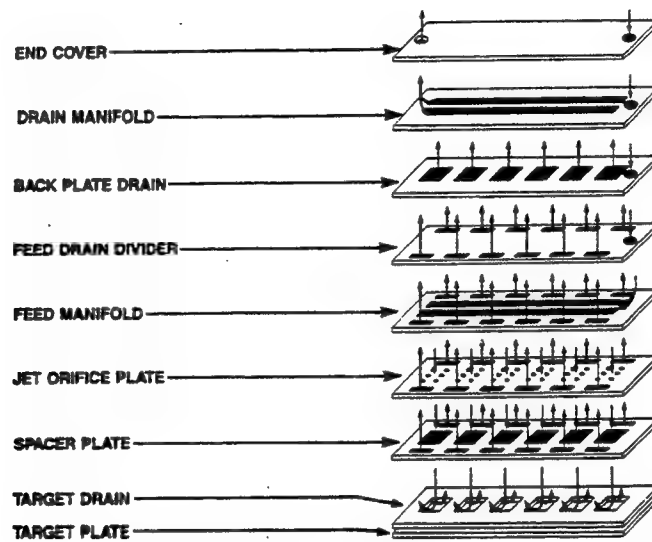
Figure 2. CHIC Elements and Fluid Flowpaths

Since the 1983 prototype, several versions of the CHIC have been built from copper and aluminum. Recently, a single module containing multiple CHICs was built by Sundstrand. References [3] through [5] provide heat flux and thermal resistance measurements on a variety of CHIC devices tested with water, Freon-11, and Freon-113. Using much of this data, Sundstrand has developed a validated analytical model to predict the thermal and hydraulic performance of arbitrary CHIC configurations. Since CHIC devices had not yet been tested with PAO, which is highly viscous, the Sundstrand model predictions for this program were based on extrapolations to low Reynolds numbers.

2.3 Heat Exchanger Design Variables

Design variables included coolant selection, flow rate, flow distribution, heat exchanger construction materials, and geometric details.

2.3.1 Coolant Selection

CHIC coolers have been tested with water, Freon-11, and Freon-113 (references [3], [4], and [5]). Water cannot be used by a CHIC in a fighter aircraft application because freezing could cause damage. Freon presents supportability difficulties because it is not always stocked. An aircraft coolant currently in use was preferred.

Coolanol has been a standard coolant on fighter aircraft, but is prone to decomposition and associated increase in flammability. It is being replaced by poly alpha olefin (PAO) (references [6], [7], [8], and [9]) which is more stable. Based on these considerations, PAO was selected as the coolant for HFHE tests. The thermal properties of PAO are similar to those of Coolanol (although the viscosity of PAO is higher), and inferior to those of water.

2.3.2 Other Design Variables

Other variables traded off in the preliminary design are listed in Table 3:

Table 3

Design Variables Traded Off

PARAMETER	RANGE STUDIED	COMMENTS
Coolant Flow Rate	150 to 1100 kg/hr	Key parameter. Must avoid excessive sensible heat rise (low flows) and excessive pressure drops (high flows).
Module Material	Copper or aluminum	Affects thermal performance, weight, stiffness, and fabrication.
Series/Parallel Flow Arrangement (for cooling 20 heat sources)	1, 2, 4 in series (20, 10, 5 in parallel)	Strongly affects pressure drop and requirements on coolant supply temperature and flow rate.
CHIC Plate Thickness	0.010, 0.015, 0.020 cm (0.004, 0.006, 0.008 in)	Minor impact to optimization
Number of Orifice Plates	N = 3 to 9	Large number of plates gives improved thermal performance but is more costly.
Orifice Hole Diameter	D_j = 0.028, 0.023, .018 cm (0.011, 0.009, 0.007 in)	Smaller orifice diameters generally show best performance, but lead to increased filtration need. Orifice diameter kept larger than plate thickness.

Coolant routing for the three configurations studied (one, two, and four CHICs cooled in series) is shown in Figure 3.

The number of orifices per spacer plate was taken as a constant value of 135 for these preliminary design studies. This number of holes gives adequate uniformity of coverage of the targeted area without forcing the orifice diameter to be too small. Very small jet diameters increase the need for filtration.

2.4 Evaluation Criteria

The design variables listed above were assessed against their impact on a typical advanced fighter aircraft. Evaluation criteria are listed below:

- Take-Off Gross Weight (TOGW) penalty
- Life Cycle Cost
- Risk
- Cold start considerations
- Heat exchanger thickness

2.4.1 TOGW Impact

The effect of HFHE design parameters on fighter aircraft Take-Off Gross Weight (TOGW) was estimated for a notional advanced fighter in its baseline mission role. The process consisted of two steps. First, an aircraft environmental control system (ECS) typical of advanced fighters was modeled, and sensitivity of TOGW to heat exchanger weight, flow rate, pressure drop, and the coolant supply temperature was calculated. Second, parametric variations in heat exchanger design features (number of orifice plates, parallel versus series cooling of the twenty heat source locations, material selection, etc.) were studied for their impact on the four parameters listed above (weight, flow rate, pressure drop, and coolant supply temperature). The results obtained from Step 1 could then be used to determine the impact of heat exchanger design parameters on TOGW. These two steps are discussed in the following two subsections.

Step 1 - TOGW Sensitivity to Fixed Weight and Operating Conditions

The calculated sensitivites of aircraft TOGW to heat exchanger weight, flow rate, pressure drop, and coolant supply temperature are shown in Appendix C, Figures C.1 through C.4. These sensitivities assume a single electronics module removing 2000 W of waste heat. For other total heat fluxes, the TOGW penalties shown would be approximately proportional to total heat flux. The results indicate that, over the range of candidate design conditions, TOGW is more sensitive to flow rate and coolant supply temperature than to pressure drop and heat exchanger weight. These results provide guidance for heat exchanger design. For example, by increasing the number of orifice plates, a higher pressure drop may be incurred, but TOGW increases only modestly. The use of a greater number of plates results in increased fin area and improved thermal performance; thus, flow rate can be reduced or coolant supply temperature increased. Since TOGW is more sensitive to flow rate and coolant supply temperature than to pressure drop, increasing the number of orifice plates will, up to a point, reduce TOGW.

2 CHICS IN SERIES (10 PARALLEL FLOW PATHS)

1 CHIC IN SERIES (20 PARALLEL FLOW PATHS)

4 CHICS IN SERIES (5 PARALLEL FLOW PATHS)
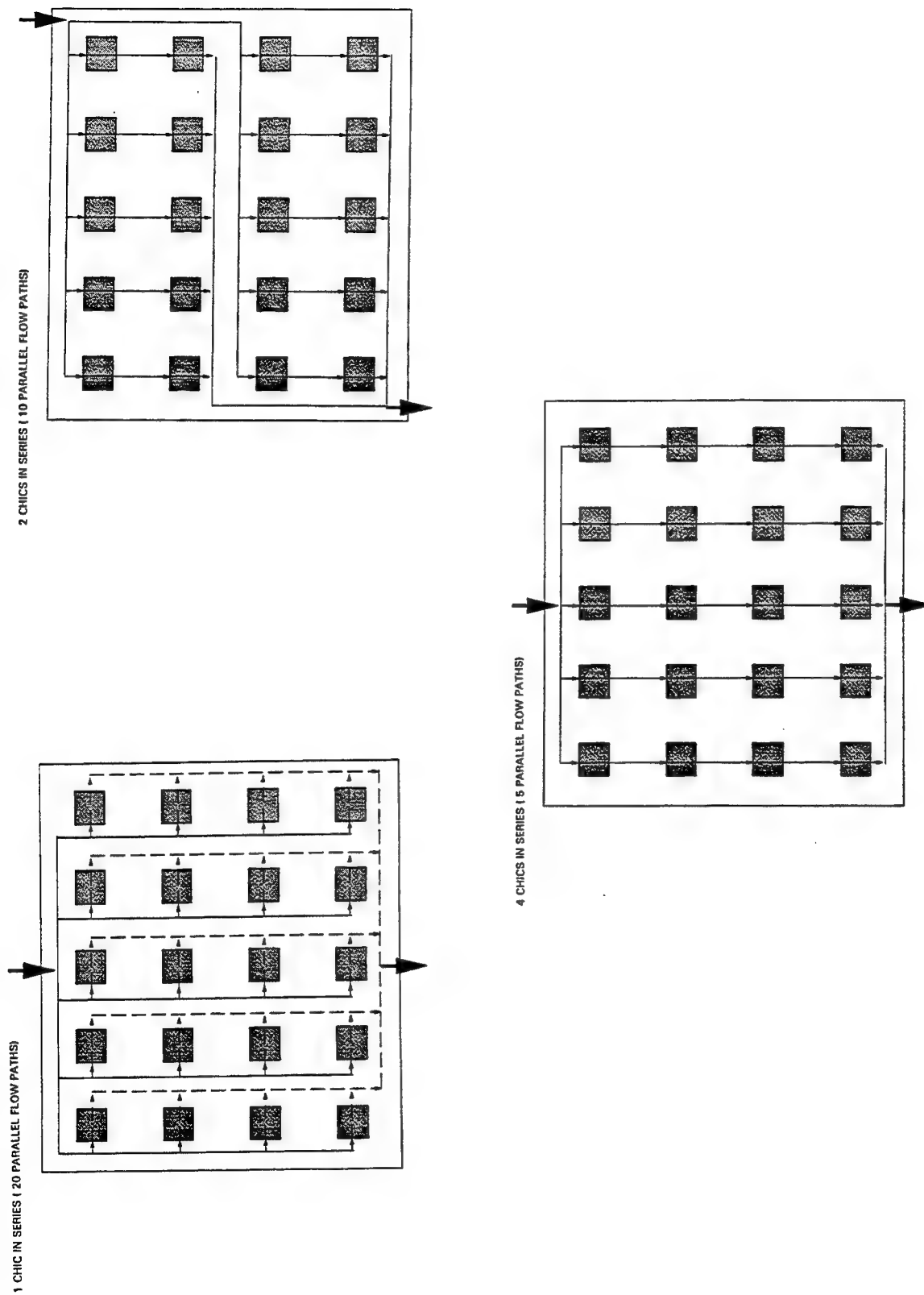
Figure 3. Coolant Routing Methods Studied

9

Step 2 - Impact of HFHE Design Parameters on TOGW

The Sundstrand analytical model was used for this step. Appendix B describes thermal performance correlations available in the model and shows comparisons between model predictions and test data from previous studies. Pressure drop was calculated using a detailed model of the CHIC, and pipe equations with equivalent lengths for other regions. Heat exchanger design parameters were:

- Flow rate
- Number of orifice plates
- Orifice configuration
- Plate thickness
- Series/parallel flow configuration
- Material selection and construction

Of the three heat exchanger operating conditions used to determine TOGW impact in Step 1 (flow rate, pressure drop, and coolant supply temperature), flow rate was chosen as the independent variable. Pressure drop and coolant supply temperature requirements were then calculated based on the flow rate, specific set of design parameters, and the requirement to maintain 50 °C wall temperature at a heat flux of 100 W/cm^2.

Results

A detailed discussion of the impact of HFHE design parameters on TOGW is given in Appendix D; results are summarized in Table 4:

Table 4

TOGW Sensitivity to Design Parameter Changes

PARAMETER	TOGW SENSITIVITY *
Flow Rate	Very sensitive. High flow rate incurs excessive Δp and flow rate penalties. Low flow rate requires very low coolant supply temperature. Optimum flow rate is about 270 kg/hr.
Material Selection	Copper incurs lower TOGW penalty than aluminum. Superior thermal performance of copper more than offsets its greater fixed weight penalty.
Series/Parallel Flow Configuration	More in parallel (fewer in series) incurs lower TOGW penalty than when arranged two or more in series, due primarily to reduced pressure drop.
Number of Orifice Plates	Moderate. Strongly flow rate dependent.
Orifice Configuration / Size	With more CHICs in parallel (20 vs. 10 or 5), smaller orifice diameters incur slightly lower TOGW penalty.
Plate Thickness	Insensitive

* See Appendices C and D for detailed results.

2.4.2 Cost, Risk, and Thickness Trade-off

The TOGW penalty study discussed above and in Appendices C and D showed that an HFHE constructed from copper incurs a lower TOGW penalty than one constructed from aluminum. Factors other than TOGW must also be considered in the final selection of material and fabrication methods. These factors include:

- Design Costs
- Material Costs
- Fabrication Costs
- Installation and Maintenance Costs
- Safety Considerations
- Packaging Volume
- Ruggedness of Construction (Handling Requirements)

A top level trade study examined these factors along with TOGW results. Seven combinations of heat exchanger material and construction technique were considered and are summarized in Table 5. Materials include pure copper, pure aluminum, and copper- and aluminum-alloys. Manufacturing methods include photochemical machining (PCM) and investment casting. PCM is the typical technique used to produce CHIC laminates from sheet stock of materials. Laminate consolidation included either diffusion bonding or vacuum brazing.

Table 5

Constructions Selected for Trade Study

CONFIG-URATION*	CONSTRUCTION MATERIALS AND SEQUENCE
A	Pure Copper - laminations photoetched, diffusion bonded, and machined as needed for fittings, clamp features, and surface flushing.
B	Pure Aluminum - laminations photoetched, diffusion bonded, and machined as needed for fittings, clamp features, and surface flushing.
C	Copper Alloy - laminations photoetched, diffusion bonded and machined for fittings, clamp features, surface flushing on lamination edges required.
D	Aluminum Alloy - laminations photoetched, diffusion bonded, and machined for fittings, clamp features, and surface flushing.
E	Pure Copper Insert, Copper Alloy Frame - a single hot zone pure copper insert, one or two piece copper alloy frame, laminations photoetched, brazed, and machined for fittings.
F	Copper Alloy Insert, S.S. Frame - a single hot zone alloy copper insert, one or two piece copper alloy frame, laminations photoetched, brazed, and machined for fittings.
G	Individual Copper CHIC Inserts, Aluminum Module, - twenty individual copper CHICs each comprised of photoetched and diffusion bonded laminations, inserted into aluminum module, which is comprised of photoetched and brazed laminations. CHICs adhesively bonded into module, flush with module surface.

* See Figures 4, 5, and 6.
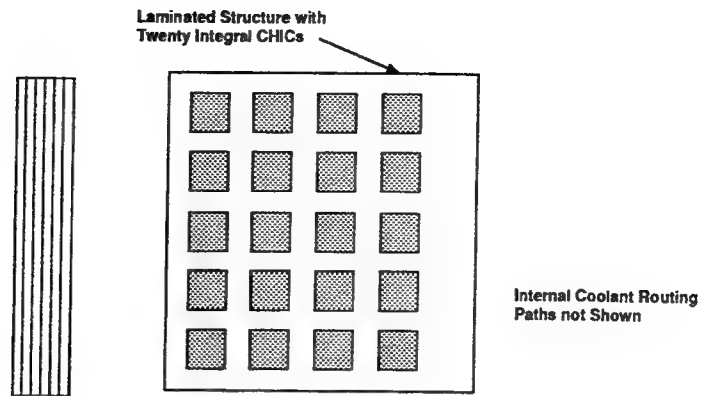
Figure 4. Monolithic HFHE Construction (Designs A, B, C, and D)
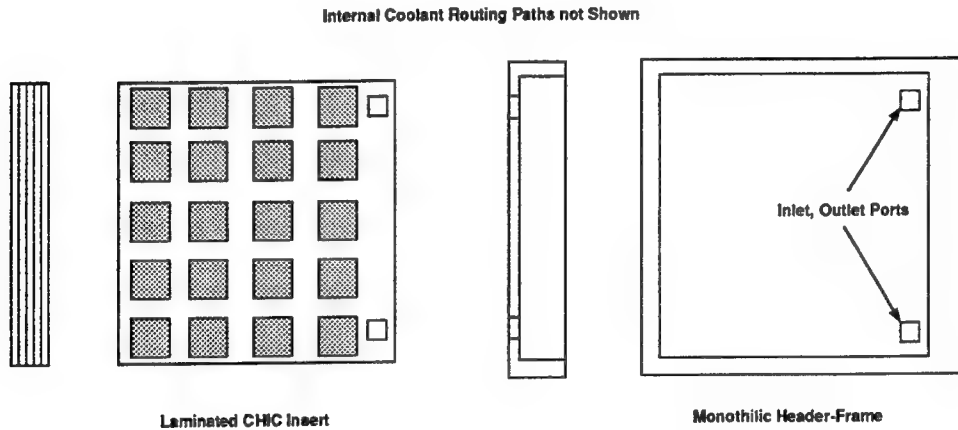
Figure 5. HFHE Design Consisting of CHIC Array Inserted into Header-Frame. (Designs E, F)
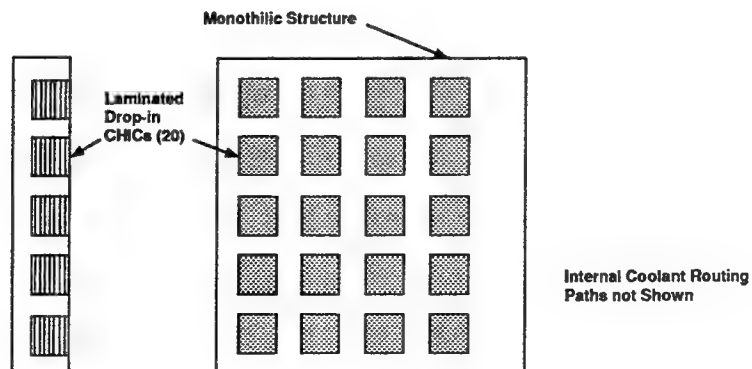
Figure 6. HFHE Design Consisting of Twenty Individual CHICs Inserted into Module. (Design G)

12

Table 6 presents many of the parameters such as risk, TOGW penalty, mechanical properties, thermal properties, and other factors which were considered in the selection process. A top level design-to-cost analysis is discussed in Section 3.8.

Design G offers the highest performance and lowest TOGW penalty, but brings with it the greatest fabrication and leak risks and highest cost. Design G therefore was not selected as the optimum configuration.

Table 6

Trade-off of Seven Candidate Designs

FACTOR	CONFIGURATION						
	A	**B**	**C**	**D**	**E**	**F**	**G**
Description	Pure Cu, one piece.	Pure Al, one piece.	Cu Alloy, one piece.	Al Alloy	Pure Cu Laminates, Cu Alloy Frame	Cu Alloy Laminates, S.S. frame.	20 Cu CHIC Inserts in Al Module.
Thermal Conductivity (W/m·°C)	400	225	330-360	170-190	400	330-360	400
Mechanical Properties	Softest, weakest. Must be thick.	High strength. Oxidizes.	Harder and stronger than pure Cu.	Good strength and machinability.	Better than pure Cu.	S.S. provides high strength.	Good strength and machinability.
Module Wt.	Heaviest	Low	Heavy	Lowest	Heavy	Moderate	Low
TOGW Impact	Low	High	Low	High	Low	Very Low	Lowest
Other Factors	Difficult to machine. Care in handling.	Must be plated to prevent oxidation. Requires glovebox cleanliness / Cu flash used.		Must control excess braze material.			Highest leak potential. Costliest.
Experience	Extensive. Many CHICs up to 2.54 x 10 cm		Limited. Diffusion parameters need to be found.	Previous 10 x 20 cm HFHX and jet fin HXs.	CHIC/ Tubing bond experience	Cu CHIC experience	None
Risk	Lowest	Moderate/ High	Low/ Moderate	Low	Moderate	2nd Lowest	Highest

13

Designs A, C, and E are constructed from copper or high conductivity copper alloys, and therefore are heaviest. However, because of their excellent thermal performance, flowrate requirement is minimized and thus the TOGW penalties they incur are lowest. Conversely, the aluminum (B and D) designs have the lowest module weights but incur higher TOGW penalties.

In the down-selection process, the designs which consisted entirely of copper or copper alloys (A, C, and E) were eliminated because of their poor mechanical properties, machining difficulties, and high fabrication costs.

The diffusion-bonded aluminum design (B) would require considerable developmental work in the diffusion bond process of a material with very high oxidation potential. This design was considered to have too high of a developmental risk.

It was determined that the two best candidates were Configurations D and F. A preliminary design-to-cost study showed that the aluminum design (D) would have lowest fabrication cost in a production environment. Depending on quantity, the laminations would be either photoetched, punched, or stamped, and the header-frame would be either machined or investment cast. The laminations would be brazed together. Sundstrand had previously built a CHIC module under internal funds (reference [3]) using photoetched aluminum alloy laminations and vacuum brazing. Although successful, significant care had to be taken to avoid excess braze alloy fouling the heat exchanger passages. Excess braze material, if not properly controlled, could clog the CHIC orifices and narrow the flow passages in the HFHE core. It was felt that this risk was too great for this program, so Configuration D was reserved as the backup design.

Therefore, Configuration F was selected as the baseline design with configuration D as a backup. Design F represents a good compromise in low TOGW and high thermal performance. Stainless steel was chosen for the header-frame because of its excellent mechanical properties, material compatibility, match in CTE to copper, and low cost. Table 7 shows the trade-off between Configurations D and F. As will be discussed in Section 3, in detailed design the header frame material for Design F was changed from stainless steel to aluminum.

Table 7

Trade-off Between Final Two Candidate Designs

	D	F
	Aluminum Alloy	Copper Alloy Insert - S.S. Frame
Cost	Cheapest to make in production	Cheapest to make as a single prototype
Risk	Risk of braze blockage. Risk could be reduced with development	Low risk Cu diffusion bond
Weight	Lowest module weight, but high TOGW	Lowest TOGW
Selection		X

2.4.3 Cold Start Considerations

Environmental specifications for military equipment often cite a low-temperature operational requirement of -40 °C to -54 °C. The kinematic viscosity of PAO increases rapidly with declining temperature, and is approximately 24 times as great at -40 °C as at room temperature, and 110 times as great at -54 °C as at room temperature. The increased viscosity at low temperature raises the concern about system start-up time under cold conditions. A first-order estimate of HFHE coolant flow characteristics at -40 °C was made.

In order to predict actual flow rate under low-temperature conditions, a real flow loop and pump pressure head-flow curve are needed. A simpler approach was taken, where the pressure drop through the HFHE alone was analyzed, and pressure drop available from the pump under low-flow conditions available to the HFHE was assumed fixed. This approach, though not rigorous, leads to general conclusions about cold-start capabilities of the various configurations. For the analysis, a pump capable of delivering 690 kPa (100 psi) pressure differential to the HFHE at a low flow rate was assumed, based on F-15 coolant pump measured pressure rise capability for PAO at low temperature (reference [9]).

In the CHIC stacks, pressure drop (Δp) arises from two sources: 1) frictional resistance through the flow distribution passages; and 2) resistance through the orifices. Frictional Δp, for laminar flow, is proportional to the product of dynamic viscosity and velocity, while orifice Δp is proportional to velocity squared and is independent of viscosity. Therefore, low temperature does not affect the orifice portion of the CHIC Δp. At room temperature, for a stack of four orifice plates, the analytical model predicted 71% of the CHIC Δp was incurred through the orifices, and only 29% through friction.

Pressure drop and flow rate at -40 °C can be predicted using the analytical model, but extrapolating predictions from 20 °C to -40 °C provides more insight. The analytical model, as described in Section 2.4.1, predicts, for the condition of all CHICs in parallel and a module flow rate of 270 kg/hr, a CHIC Δp of 13.3 kPa (1.93 psi) at 20 °C. This is the first condition shown in Table 8. Frictional pressure drop in the CHIC stacks (Δp_f) is 3.9 kPa (0.56 psi), and orifice pressure drop (Δp_o) is 9.5 kPa (1.37 psi). Pressure drop through the headers and flow distribution (Δp_h) was estimated as 103 kPa (15 psi), and was later verified in detailed design to be a reasonable estimate. Total module pressure drop (Δp_{total}) is the sum of CHIC and header/distribution values and is 117 kPa (16.9 psi). These Δp's can be extrapolated to the condition of -40 °C coolant temperature using the following groundrules:

Total Δp available at -40 °C = 690 kPa (100 psi)
Δp_h is proportional to viscosity and module flow rate
Δp_f is proportional to viscosity and CHIC flow rate
Δp_o is proportional to CHIC flow rate squared

Applying these groundrules, Table 8 shows the resultant flow rates and pressure drop breakdown in the HFHE. These calculations assume the electronics mounted to the HFHE are unpowered and thus the coolant loop does not warm through electronics heat dissipation. Module flow rate is predicted as 72 kg/hr when all CHICs are

15

arranged in parallel, 65 kg/hr when two CHICs are in series, and 46 kg/hr when four CHICs are in series. These flow rates represent a sizeable fraction of the design point flow rate of 270 kg/hr; thus, significant flow can be initiated at -40 °C. (In fact, Figure 10 indicates that for -40 °C coolant and a flow rate of 72 kg/hr, the heat exchanger wall will be maintained below the required temperature of 50 °C, suggesting that the electronics could operate safely at -40 °C). The difference in flow rate for one versus four CHICs arranged in series (72 vs. 46 kg/hr) seems low enough so as not to be a deciding factor in the series/parallel layout trade-off.

Table 8

Predicted Flow Rates at -40 °C *

Coolant Temp. (°C)	Number of CHICs in Series (N)	CHIC Flow m_c (kg/hr)	Module Flow $m_m=N*m_c$ (kg/hr)	CHIC Δp_f kPa (psi)	CHIC Δp_o kPa (psi)	Total Δp in CHICs $\Delta p_c=N*$ $(\Delta p_f+\Delta p_o)$ kpa (psi)	Δp_h Headers, Distrib.) kPa (psi)	$\Delta p_{total} =$ $\Delta p_c+\Delta p_h$ kPa (psi)
20	1	13.5	270	3.9 (0.56)	9.5 (1.37)	13.3 (1.93)	103.5 15.0	117 16.9
-40	1	3.6	72	24.8 (3.6)	0.7 (0.1)	25.5 (3.7)	666.4 96.3	690 100
-40	2	6.5	65	44.9 (6.5)	2.1 (0.3)	93.8 (13.6)	596.2 86.4	690 100
-40	4	9.2	46	63.5 (9.2)	4.1 (0.6)	270.5 (39.2)	419.5 60.8	690 100

* For the case of four orifice plates.

2.5 Selected Preliminary Design

The preliminary design, described in Table 9, is based on TOGW, cost, and risk considerations.

The HFHE design has the stiffness of stainless steel while maintaining the high thermal performance of copper. The baseline construction is shown in Figure 5. A copper insert with internal flow passages is made by diffusion bonding a number of laminations. The final dimensions are 13.67 cm x 14.81 cm, and 0.43 cm thick. The fluid connections to the stainless steel header frame are on the back cover.

The stainless steel header frame provides stiffness and protection for the softer copper. Flat mounting surfaces on the stainless steel frame are designed to accomodate board locking devices such as Wedge-Lok ™. The frame is made to SEM-E standards (MIL-STD-1389D).

Table 9

Preliminary Design Summary

Coolant	PAO
Series/Parallel Configuration	All 20 CHICs fed coolant in parallel
Material	CHICs: Cu Alloy (Cu, 0.10% Zr) Header Frame: Stainless Steel
CHIC Fabrication	Photochemical etch / diffusion bond
No. Orifice Plates	7
Orifice Plate Thickness	0.10 cm (0.04 in)
Orifice Hole Pattern	20 x 3
Design Point* Flow Rate	270 kg/hr
Design Point Pressure Drop	110 kPa (16 psi) (Header+CHIC, w/o QDs))
Design Point Coolant Supply Temperature	30 °C

* Design point is defined as the condition to maintain 50 °C wall temperature when all twenty CHIC sites are subjected to 100 W heat flux each.

SECTION 3

DETAILED DESIGN

A detailed design of the selected concept from the preliminary design was performed.

3.1 Mechanical Configuration

As discussed in Section 2, trade studies on construction of the HFHE led to the selection of a copper alloy insert into a stainless steel header-frame. The outer dimensions of the header-frame meet SEM-E size specification (approximately 15 cm x 17 cm, per MIL-STD-1389D). Because a SEM-E size liquid flow-through module was recently developed under a separate Air Force program (to accomodate lower heat fluxes than the HFHE requirements), the maker of the module, Lockhart Industries, Inc. (LII), was contacted to discuss feasibility of using their module for the header-frame. Lockhart agreed to modify their newer SEM-E liquid cooled module, part number 101456 (Figure 7), by blocking the normal active flow zone and instead porting the flow into a flush-mounted removable CHIC plate. The porting locations and sizes are shown in Figure 8. The LII module is fabricated from aluminum alloy, so a departure was made from the preliminary design which had a stainless steel header-frame.
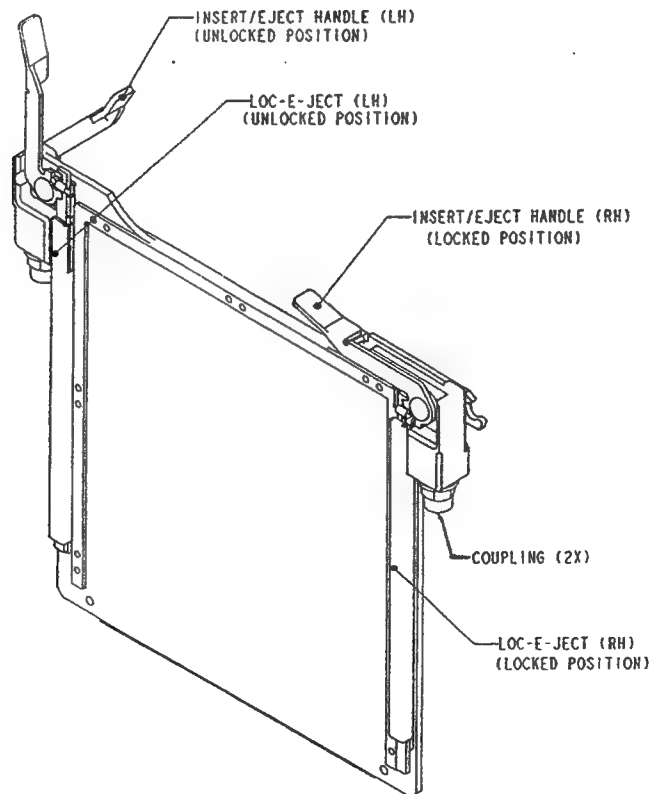
Figure 7. Lockhart SEM-E Liquid Flow-Through Module

18
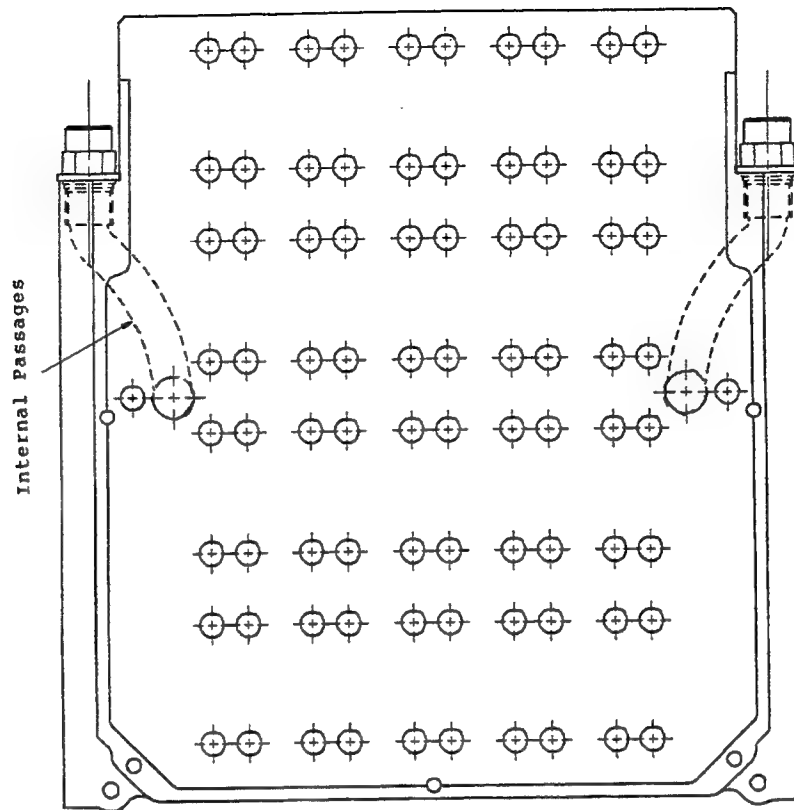
Figure 8. Porting Locations of Modified LII Module

An advantage to using the LII module as the header-frame is that it is closer to the design that would be expected to be used in production. An all-aluminum module, with vacuum brazed aluminum CHIC laminations replacing fin stock on the LII module, would probably be the preferred high-production construction over copper CHICs because of lower production costs. For this program, however, developing braze process parameters was beyond scope.

3.1.1 Overall Assembly

The HFHE consists of two principal components which are bolted together: a copper insert which contains the twenty high flux cooling locations, and an aluminum header-frame which adds stiffness to the overall assembly and extends the outer dimensions to SEM-E specifications (see Figure 5). The entire assembly measures 14.9 cm (5.88 in) by 15.6 cm (6.16 in), with a total thickness of 1.52 cm (0.60 in). The thickness of the assembly equals the SEM-E module pitch specified in MIL-STD-1389D, and thus would leave no space for mounting electronics devices if mounted in a multi-module rack. Thickness was largely the result of choosing a low-cost approach for attaching the copper CHIC insert to the aluminum header-frame, and was not necessary for thermal performance. The copper insert which contains the CHICs is 0.467 cm (0.184 in) thick, significantly less than the 1.52 cm (0.60 in) required SEM-E pitch. Thus, it is expected that a thinner HFHE could be developed meeting all SEM-E specifications without compromising thermal performance.

19

Several methods for sealing the CHIC / header-frame interface were evaluated. These included: 1) metallurgical bonding, e.g. soldering or brazing; 2) adhesives, e.g. epoxies, RTV, silicones; 3) O-ring seal; and 4) gasket seal. A gasket seal was adopted as the best choice based on cost for the prototype module. VITON-A was readily available, easy to work with, and compatible with PAO, and was selected.

Photographs of the insert, header-frame, and gasket, in both the dissambled and assembled states, are provided in Appendix I.

3.1.2 Copper Insert

The copper insert contains twenty CHIC coolers arranged in a four-by-five array, and coolant distribution/collection channels in an integral structure. It was formed by stacking 24 photo-etched copper alloy laminates, each of 0.010 or 0.038 cm (0.004 or 0.015 in) thickness, and diffusion bonding them to create a monolithic heat exchanger. Total thickness of the insert is 0.467 cm (0.184 in). The alloy is CDA 15100 (copper, 0.10% zirconium). All twenty CHICs cool the same side of module, i.e., the module is designed for single-sided heat application. Each CHIC cools a surface area of 1.0 cm^2. Each of the twenty CHICs is fed coolant in parallel.

Figure 9 shows the locations of the twenty CHIC sites (designated by dashed squares for illustration purposes). The solid outlines drawn at each site represent the footprint of an Omnirel C-6 device, which is a package style used for power MOSFETs and IGBTs.. The hole pattern shown matches that required by the device in order to add realism to the design. The device requires only two bolt holes, but four were located at each CHIC site to facilitate fastening the heat source (described in Section 5.3.3). The Omnirel C-6 device was not tested during this test program.
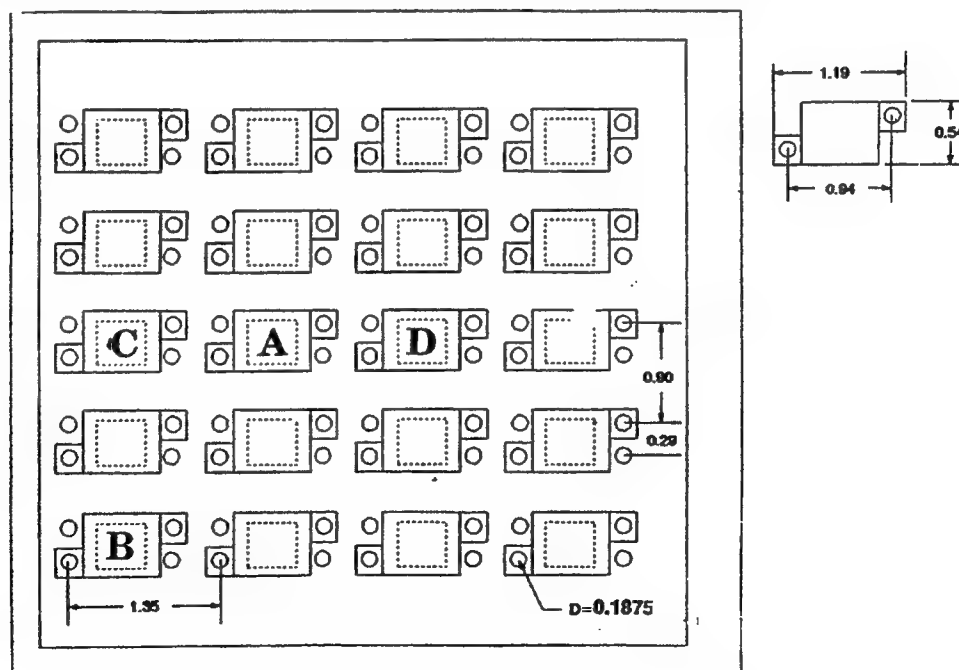
Figure 9. CHIC Locations and Bolt Hole Pattern

As described in Section 5.4.2, tests were performed at four different CHIC sites, designated "A", "B", "C", and "D".

3.1.3 Aluminum Frame

Figure 8 depicts the frame, which was adapted by Lockhart Industries from their model No. 101456 liquid flow-through module to include coolant inlet and outlet ports. The array of bolt holes shown matches the pattern on the copper insert shown in Figure 9.

3.2 Lamination Description

The CHIC insert was designed to be formed from a set of bonded laminates using eight types of plates. Two plate thicknesses were used: 0.010 cm (0.004 in) and 0.038 cm (0.015 in), based on material availability and cost. Plate drawings, not fully dimensioned, are shown in Appendix E, Figures E.2 through E.9, as Plates A, B, C, C*, D, E, F, and G. Plates C and C* are mirror images and could be produced from the same drawing. The stacking order of the plates is given in Figure E.1. A total of 24 plates was used. A photograph of the laminates is shown in Appendix I.

3.2.1 Number of Orifice Plates

In preliminary design (Section 2), the UMW jet impingement correlation (see Appendix B for impingement correlations) was used for thermal performance predictions. In detailed design, the most conservative (open literature) correlation was used. This led for the need to increase the number of orifice plates beyond the seven selected in preliminary design. In preliminary design, TOGW was determined to increase as the number of orifice plates was increased, due to higher CHIC pressure drop. After a hydraulic analysis of the headers was included in detailed design, however, it was realized that by increasing the number of plates beyond seven, pressure drop actually *decreased*. As more plates were added, flow area in the headers increased, which reduced header Δp at a faster rate than the increase in Δp at the CHIC locations. The benefits of improved thermal performance and reduced Δp easily outweigh the slight penalties of increased cost and increased heat exchanger thickness. Seven, eight, and nine plates were studied (see Appendix D), and a design consisting of nine plates was selected as a compromise on thermal performance, TOGW, cost, and heat exchanger thickness.

3.3 CHIC Detailed Design Specification

Geometric design data on the CHIC regions of the heat exchanger are given in Table 10.

Table 10

Detailed Design Summary

PARAMETER	VALUE
Number of CHICs in Module	20
Active Area of Each CHIC	1 x 1 cm
Orifice Hole Diameter	0.020 cm (0.008 in)
Orifice Plate Thickness	0.010 cm (0.004 in)
Spacer Plate Thickness	0.010 cm (0.004 in)
Target Spacer Thickness	0.038 cm (0.015 in)
Target Cover Plate Thickness	0.076 cm (0.030 in)
Number of Orifice Plates	9
Number of Spacer Plates	8
Number of Holes per Slot	20
Number of Slots per CHIC	3
Slot Width	0.170 cm (0.067 in)
Slot Length	0.848 cm (0.334 in)
Conduction Bar Width	0.163 cm (0.064 in)
Hole Pitch (lengthwise) / Hole Diameter (x/D)	4.2
Hole Pitch (widthwise) / Hole Diameter (y/D)	4.2
Jet Length / Hole Diameter, Stack (z/D)	0.50
Jet Length / Hole Diameter, Target (z/D)	1.875

3.4 Predicted Thermal Performance

3.4.1 High Heat Flux Condition

Figure 10 shows predicted thermal performance of the HFHE using the most conservative thermal correlation (see Appendix B for correlations). HFHE wall and junction temperatures are shown as functions of coolant flow rate and inlet temperature, for the condition of 100 W/cm^2 heat flux. As discussed in Section 2.1, the requirement for 90 °C maximum junction temperature results in a 50 °C maximum wall temperature requirement given certain assumptions of junction-to-wall thermal resistance. These maximum temperature limits are indicated by the dotted line in Figure 10. The temperature requirement can be met with 30 °C coolant at a flow rate of 452 kg/hr, 20 °C coolant temperature at a flow rate of 214 kg/hr, 10 °C coolant

temperature at a flow rate of 135 °C, and 0 °C coolant temperature at a flow rate of 106 kg/hr. These curves may also be used to to deduce wall-to-fluid thermal resistance. For example, at a flow rate of 214 kg/hr and 20 °C coolant temperature, wall-to-fluid thermal resistance is calculated as:

$$R_{wf} = \frac{T_w - T_f}{Q/A} = \frac{50\,°C - 20\,°C}{100\,W/cm^2} = 0.30\,°C/(W/cm^2) \qquad (1)$$

Where:

R_{wf} = Wall-to-fluid thermal resistance
T_w = Heat exchanger wall temperature
T_f = Fluid (coolant) supply temperature
Q/A = Heat flux per unit area
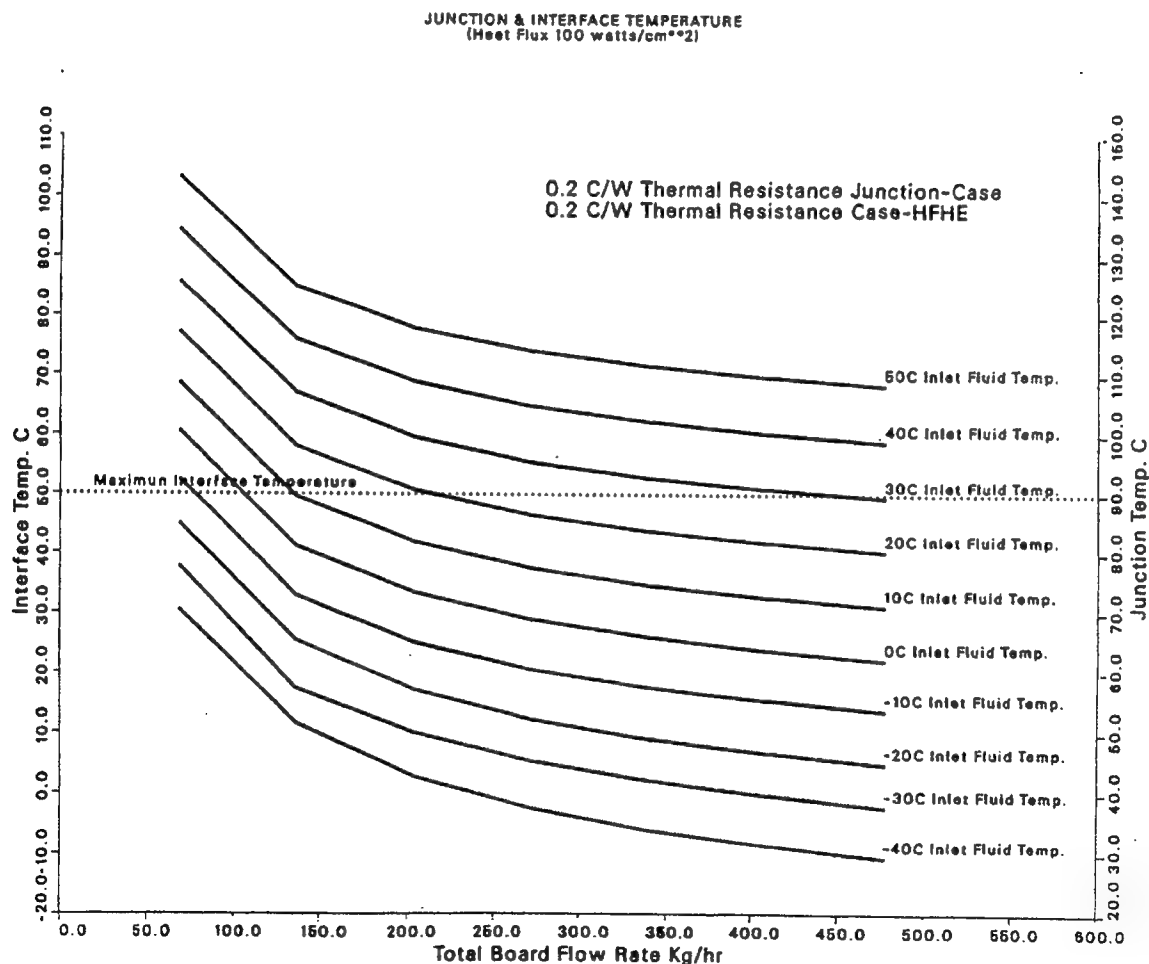
Figure 10.   Predicted Thermal Performance of HFHE

23

3.4.2 Low Heat Flux Condition

In addition to the 100 W/cm^2 heat flux requirement applied to 20 cm^2 of module surface area, the remainder of the module must be capable of removing up to 1.0 W/cm^2 heat flux while maintaining 90 °C junction temperature. In the interest of minimizing test cost, this secondary requirement was met through analysis but not test. The HFHE design employed no special provisions to meet this low level requirement; it relied on in-plane conduction through the high conductivity copper alloy from the low flux zones to the CHICs or to internal manifolds. An analysis of heat flow from the low flux region to a CHIC is shown in Figure 11. The worst-case location on the module was analyzed, at a location 1.4 cm from a CHIC site, at the module edge. A linear resistance model was used to approximate the three-dimensional nonlinear heat flow paths in the actual HFHE. Thermal resistances from junction to case, and from device case to HFHE, were assumed as 10 and 20 °C/(W/cm^2), respectively, which are in the range for lower power electronics devices. Figure 11 shows that the required coolant temperature to maintain 90 °C junction temperature under these conditions is 36.7 °C. Since the design condition specifies 20 °C coolant, the junction temperature requirement will be met and therefore this margin of safety justifies deleting the low flux test condition.

$$T_{PAO} = T_j - (\tfrac{q}{A})_{LF} (R_{jc} + R_{cb} + R_{down} + R_{fin} + R_{conv})$$

$$R_{down} = \frac{a}{2k} \quad R_{fin} = \frac{b^2}{2ak} \quad R_{conv} = \frac{b}{h_{eff}a}$$

$$\Delta T_j - PAO = 1.0 \, (10. + 20. + 0.06 + 0.62 + 22.6)$$

$$T_{PAO} = 90°C - 53.3°C = 36.7°C$$
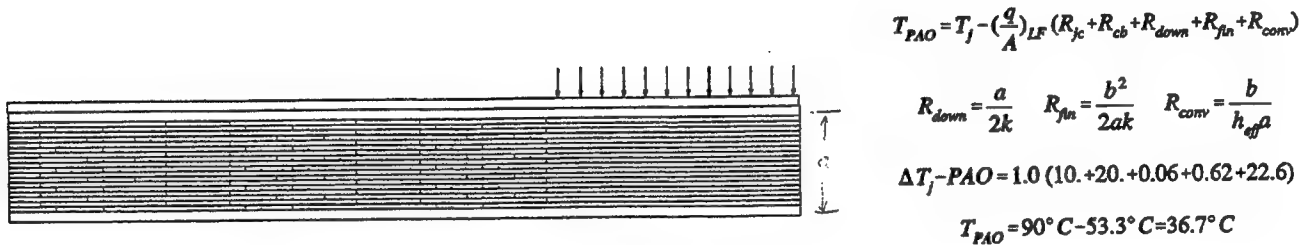
Figure 11. Thermal Analysis of Low Level Heat Flux Condition

3.5 Predicted Hydraulic Performance

Figure 12 shows the predicted hydraulic performance of the HFHE using semi-empirical models. Pressure drop through the copper insert plus aluminum header-frame is shown as a function of coolant flow rate and inlet temperature. Pressure drop was calculated using a detailed model for CHIC zones, and pipe equations with equivalent lengths for other sections.

As mentioned in Section 2.1, a maximum operational pressure drop of 311 kPa (45 psi) was imposed as a representative limit in an aircraft cooling loop (this limit will vary considerably depending on specific application). This limit is shown by a dotted

line. Also shown is a maximum allowable pressure drop assumed under cold start conditions, assuming that the pump can deliver a higher pressure at reduced flow rate. The value assumed, 690 kPa (100 psi) is close to pump test data using PAO in an F-15 coolant loop (reference [8]). At the -40 °C coolant condition, which may be the low-temperature requirement for some systems, a flow rate of 70 kg/hr can be generated at 690 kPa pressure differential. As the system warms through pump heat dissipation, flow rate will gradually increase. The CHIC devices offer a cold start advantage over channel-flow heat exchangers in that a significant portion of their pressure drop is from dynamic loss (orifice Δp) which is independent of viscosity. The actual cold start characteristics will be system-dependent, i.e., dependent on loop inventory, pump pressure/flowrate curve, etc., but dynamic-loss devices will perform better than viscous-loss devices such as those employing tubing.

ADIABATIC PRESSURE DROP
(Does not include QD pressure drop)
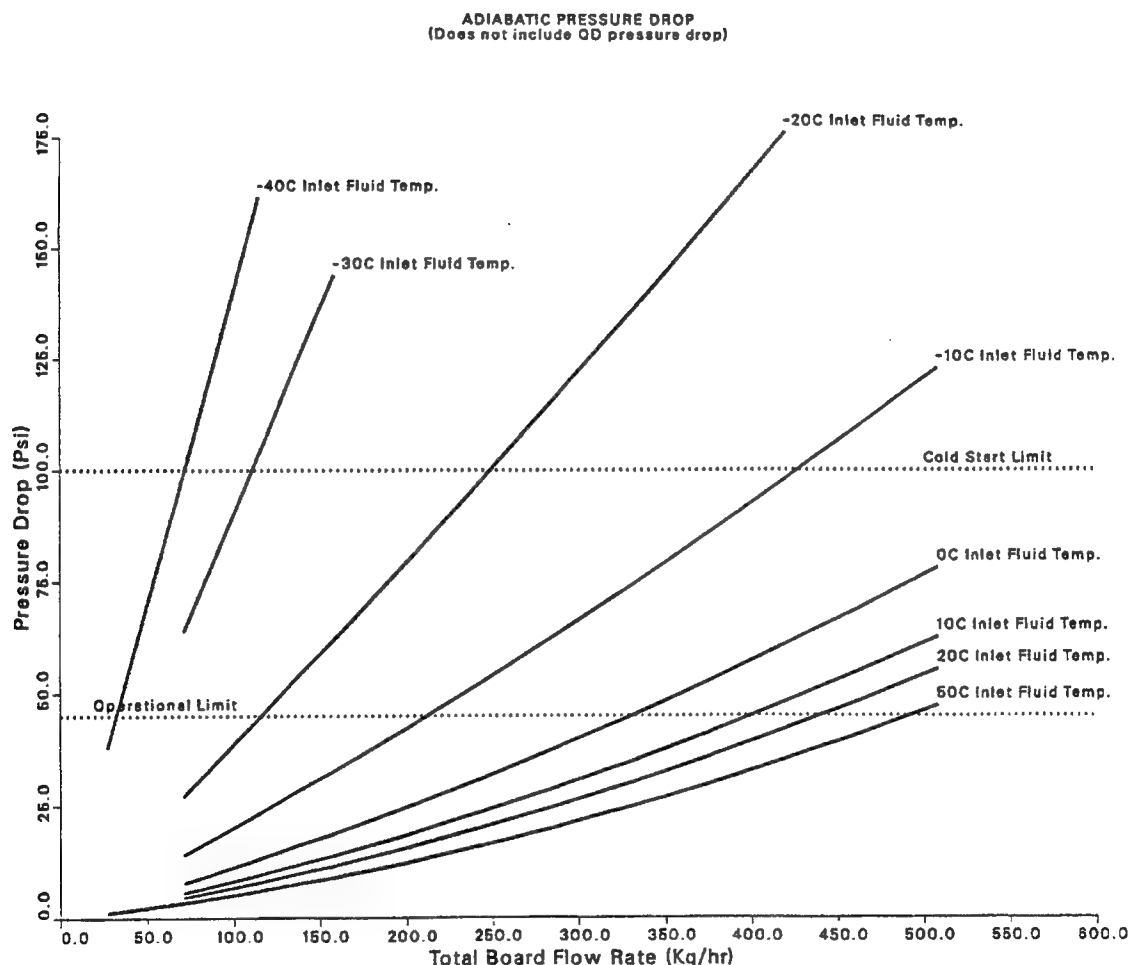
Figure 12. Predicted Hydraulic Performance of HFHE

25

3.6 Design Operating Point

The thermal requirement of removing 100 W/cm2 heat flux while maintaining 90 °C junction temperature can be met with 30 °C coolant at a flow rate of 452 kg/hr, 20 °C coolant temperature at a flow rate of 214 kg/hr, 10 °C coolant temperature at a flow rate of 135 kg/hr, and 0 °C coolant temperature at a flow rate of 106 kg/hr. TOGW results (see Appendices C and D) indicate that TOGW is equally minimized with either 10 °C or 20 °C coolant. Because warmer coolant is easier to pump, 20 °C coolant was selected as the design point. The design point flow rate is therefore 214 kg/hr (1.2 gallons per minute (gpm)).

3.7 Mechanical Analysis

A stress analysis was performed to ensure that the design could meet proof pressure requirements with appropriate factors of safety. The design was analyzed with the header-frame modeled as a 0.254 cm (0.100 in) thick solid aluminum plate as back support. This rigid support element eliminated deflection of the back cover of the CHIC insert as a concern. Two critical areas of stress were identified:

a. The top cover plates over the large mustache-shaped headers represent a zone which will first undergo permanent deflection at 1775 kPa (257 psi) internal pressure using conservative mechanical property data and a factor of safety (FOS) of 1.5. In this area, the design was taken as acceptable.

b. The manifold divider separates the lower and upper regions of the mustache-shaped manifold into an inlet feed flow header and a collector channel for the spent exhaust fluid. This manifold divider, formed by Plate E, therefore has the CHIC pressure drop as a pressure differential across it. Initially, Plate E was designed to be 0.010 cm (0.004 in) thick, but analysis showed that permanent deflection would first occur at a pressure differential of 42.8 kPa (6.2 psi), with a FOS of 1.5 again using conservative material property data. The CHIC pressure drop at full design flow was 12 psi, but could be considerably higher under cold start conditions. Therefore, this design feature required modification. To increase the strength of the manifold separator, the thickness of Plate E was increased to 0.038 cm (0.015 in). This increased the predicted yield pressure of Plate E to 602 kPa (87.2 psi) based on a FOS of 1.5 and conservative material property data.

3.8 Reliability Analysis

A top-level reliability analysis was performed to analyze failure rates of critical components (see Table 11). Failure rate of HFHE plates is expected to be less than that of the QDs which are already a part of existing flow-through modules. Therefore, reliability of the HFHE was deemed sufficient.

Table 11

Top-Level Reliability Analysis

Item	Quantity	Failure Rate*	Basis
HX Plate	1	1.4×10^{-6}	Better Than L-1011 and DC-10 Refrigerator HXs
QD Male Half	2	4.25×10^{-6}	Aeroquip Analysis
QD Female Half	2	4.25×10^{-6}	Aeroquip Analysis
Wedge Locks	2	1.0×10^{-6}	Estimated
Viton Gasket	1	0.6×10^{-7}	E&E Data Series
Total	--	2.05×10^{-5}	MTBF = 48,876

Notes: 1) Reliability of production design would be higher
2) Failure modes - liquid leakage, flow blockage (i.e., denting)
3) Aeroquip reliability numbers are estimates - believed to be conservative
*Failures/Flt.Hr.

3.9 Design to Cost Analysis

A top-level cost analysis of the options presented in the preliminary design trade study resulted in the following observations and conclusions:

Material

Aluminum alloy is available at reasonable cost. Copper is more expensive and difficult to handle. Thin laminations bend and scratch easily.

Bonding

For aluminum vacuum brazing, several stacks can be vacuum brazed at one time. Direct labor hours will be fairly low. Both copper and aluminum require acid etch after chemical photoetch to clean the surface. Copper requires several intermediate steps prior to assembly whereas the aluminum surface is more tolerant to the atmosphere.

Based on these preliminary results, it was concluded that an aluminum alloy HFHE may be less expensive in a production environment than a copper alloy HFHE.

SECTION 4

FABRICATION AND CHECKOUT

4.1 Fabrication

The HFHE was constructed by diffusion bonding a stack of 24 copper alloy laminates to form the high intensity cooling surface which was then bolted with gasket interface to an aluminum header-frame. The header frame is fully compatible with the newer model liquid cooled SEM-E size modules developed under the AAAPT (reference [2]) program. The copper alloy insert is depicted in Figure 9. The header-frame is shown in Figure 8. The insert/header-frame assembly is shown in Figure 5.

4.1.1 Copper Alloy CHIC Laminations

Lamination drawings and stacking order are shown in Appendix E. Eight different types of laminations were used to comprise the 24-plate stack. The laminations were produced from zirconium copper alloy CDA 15100, using material from stock thicknesses of 0.004 and 0.015 inches (0.010 and 0.038 cm).

Since the incremental cost of the copper alloy was small and some risk was involved in the photochemical etching and diffusion bonding processes, a total of ten sets of laminates was produced. Five of these laminate sets were diffusion bonded, and the remaining five stored for possible future use.

The final drawings of the laminations at 6 X scale were sent to Mechtronics, the photo-etch vendor. This size print was optically reduced to the actual size necessary for the photomask. The large size (6 X) was required to provide the required resolution on the small features, e.g., the 0.020 cm (0.008 in) diameter orifices. The features and size of the transmitted art were selected in cooperation with Mechtronics so that the drawings did not have to be redrawn or dimensioned, thereby saving costs. One of the interesting features of the drawings was that all etched holes had to be internally shaded to guarantee complete etching. Because the orifices were drawn as circles with finite line width, some manual touch-up was needed to guarantee all orifices were internally shaded.

One of the C* laminations was inadvertently produced to a preliminary version of the drawing, which was slightly different than the final C* drawing. The version of the C* lamination used in each unit is noted below and in Figure E.10.

Figure E.10 shows the stacking order for a number of HFHE diffusion bond trials and builds. The following HFHE stacks can be or were produced, using various combinations of old (large C*) and new (small C*) laminations:

- Perfect Units (#1 and #2) - contain all new C* and are thermally and hydraulically ideal. Unit #2 was diffusion bonded and was used in the tests. Unit #1 was not bonded.

- Thermal Units (#3 and #4) - contain an old C* lamination on the target side of the manifold divider. The old C* and new C* plates are fully compatible in this

28

location, but the old C* will be cantilevered into the manifold flow area slightly. These units should be hydraulically and thermally equivalent to the #1 and #2 units. Both of these stacks were bonded. Unit #3 was later sectioned for metallurgical inspection and scrapped. Unit #4 has an additional bottom cover plate G, for a total of 25 plates.

- Pressure units (#5 and #6) - contain only C-type orifice plates with no "flipped" offset orifice plates, C*. Since the orifice holes are aligned, these units will have lower thermal performance. The pressure drop of these units should be slightly less because the flow does not have to laterally jog at each impingement/orifice plate. The proof, burst and leak performance should be identical to the top units. Unit #6 was bonded.

- Bonding builds (#7, #8, and #9) - contain old C* laminations. With the old lamination, there is a short circuit flow path between the inlet and outlet flow manifolds. However, the bonding results should be representative because the same number and type of plates were used. The proof, burst, and leak performance should be identical to the "perfect" units. None of these units were bonded.

- Practice Stack (#10) - is a collection of the extra laminations of each type. Enough laminations were used to give the correct stack height. This unit was only suitable for metallurgical bond testing. This was the first stack bonded.

4.1.2 Diffusion Bonding of Laminations

Diffusion bonding of the zirconium copper laminations was performed after the laminations were cleaned and stacked. REFRAC Systems initiated this process with a series of parametric diffusion bonding tests to identify required values of critical bonding parameters, namely bonding pressure, temperature, and time.

Special fixtures were required for high temperature diffusion bonding. Large and very rigid blocks of TZ Molybdenum were used as the top and bottom platens in the furnace. This metal has excellent strength at temperatures in excess of 816 °C (1500° F). Between these platens and the working piece were placed thin sheets of a refractory ceramic to provide surface smoothness, flatness, and to act as a release surface for the copper laminations. The laminations were cleaned in a pickle solution of 10% concentration HCl / 90% concentration H_2O for two minutes, followed by a water- and isopropyl alcohol-rinse. A vacuum level of 10^{-4} torr was used. All furnace operations were performed in full conformance with MIL-H-6875 "H" procedures.

The initial bonding run was a practice stack (#10). A corner of this stack was sectioned to inspect interior bonds. Because results were encouraging, but not perfect, a second furnace lot was selected with a higher bond temperature which had some "good" stacks. The second furnace run had two stacks, #2, which was a perfect set, and #3, which was deemed only "good" because of the inclusion of an old C* lamination. A third furnace run included #4, another "good" stack, with an additional backplate, and #6, which could be used for proof, burst or leak test. Since an acceptable heat exchanger (#2) was fabricated during this sequence, no further units were bonded.

4.1.3 Header-Frame

The header-frame is shown in Figure 8. The header-frame design was modified to reduce pressure drop. The Lockhart Industries, Inc. (LII) ultra-thin liquid cooled module is currently 0.254 cm (0.100 in) thick in the working zone. This thickness consists of a 0.152 cm (0.060 in) thick heat exchanger core layer sandwiched between

two 0.051 cm (0.020 in) thick cover places. Lockhart modified this construction to be 0.381 cm (0.150 in) thick. The core thickness was increased from 0.152 to 0.279 cm (0.060 to 0.110 in) in order to reduce pressure drop. The internal passage flow cross sectional area was specified to be not less than 0.232 cm^2.

Another minor modification to the LII header-frame design was made. To improve mechanical strength and sealing pressure capability, a support rib was added along the centerline of the connector channel internal to the header frame. This rib minimized deflection of the unsupported cover skin over the internal flow passage.

4.1.4 Quick Disconnects

An attempt was made to enhance design realism by adding liquid quick disconnects (QDs) to the HFHE coolant inlet and outlet ports. Valveless models of these QDs were supplied at no cost from Aeroquip. The plan was to test the HFHE mounted in a Lockhart test stand which has mating ports for these QDs; however, the test stand was not purchased. Therefore, the QDs were removed and standard pipe fittings were used in their place.

4.2 Checkout Tests

Three checkout tests of the heat exchanger were performed: leak check, proof pressure, and pressure drop. Table 12 shows the test methods and pass/fail criteria.

Table 12

Checkout Test Methodology and Pass/Fail Criteria

TEST	METHOD	PASS CRITERION
Leak Check	Pressurize to 552 kPa (80) psig with argon for five minutes while submerged in water.	No bubbles detected.
Proof Pressure	Pressurize to 1034 kPa (gage) (150 psig) with argon for one minute while submerged in water.	No deformation detected after pressurization. No leaks detected on subsequent leak test.
Pressure Drop	Flow filtered tap water. Flow rate measured with graduated cylinder & stop watch, Δp with gage.	Δp within -20% / +50% of predicted value.*

* Scaled to PAO from tests with tap water.

A test fixture was fabricated (Figure 13) to simulate the header-frame. It was bolted to the copper insert and sealed with a rubber gasket.

The first test unit (#10) was received and assembled into the test fixture. The test fixture, shown in Figure 13, was modified for testing this first unit. A second aluminum plate and rubber gasket were used on the side of the HFHE facing away

from the inlet/outlet ports. At 552 kPa (85 psi) gage pressure with argon, there was visual leakage of gas at several locations, with the worst leakage occurring at the corner near the component part identification letter. Vacuum grease and additional torque reduced the leakage, but it still occurred near the inlet and outlet ports. It was difficult to determine whether leakage occurred from the gaskets or the laminations. After this indication of leaks, it was decided to increase the bond temperature for subsequent units.

HIGH FLUX HEAT EXCHANGER TEST FIXTURE
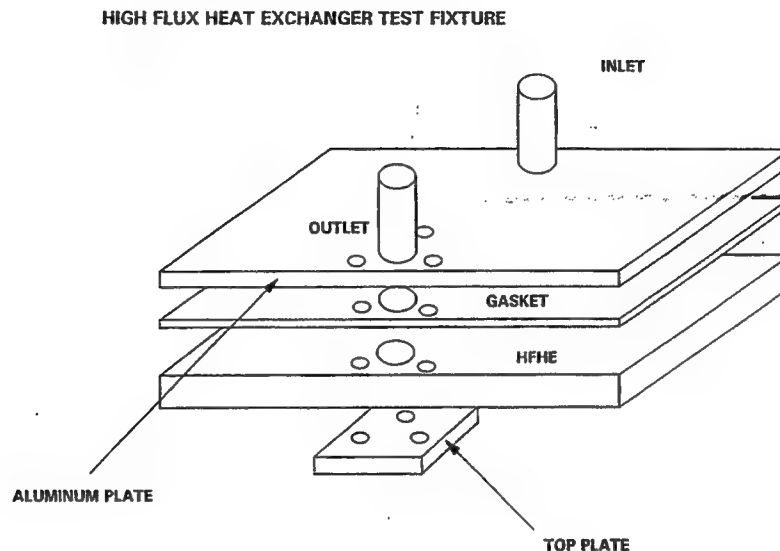
Figure 13. Checkout Test Fixture

The next unit to be tested was #3. Initial testing in the same test configuration as described above for Unit #10 indicated leakage from bolt holes and edges. To eliminate questions of leakage from the gasket assembly, the fixture was modified to adhesively bond the fixture to the HFHE with RTV and no gasket. This unit was then tested at 552 kPa (80 psi) gage pressure with argon; no leaks occurred at the inlet and outlet, but pin-point sized bubbles issued from the slot corner. The pressure was increased to the proof pressure of 1034 kPa (150 psig) for three minutes and then reduced to 552 kPa (80 psig). Various spots on the HFHE were measured before and after the proof pressure test and the thicknesses changed by less than 0.00025 cm (0.0001 in) in all cases. Small bubbles were still issuing from the corner. Although it was felt that PAO would not leak, it was decided to metallurgically inspect this unit by sectioning and polishing. Slight delamination was evident between two layers at this location.

The next unit to be tested, #2, was tested as depicted in Figure 13 to give a better simulation of the HFHE design, where the aluminum plate represented the header-frame. A leak test was performed with argon at 552 kPa (80 psig) for six minutes. No leaks were evident except at the fixture/plate interface which was not HFHE related. On the basis of this test the unit was deemed acceptable from a leak test standpoint. A flow check was then performed on the unit using water. This was performed per the description in Table 12 using two flow rates. The purpose of the pressure drop test was to verify that there were no significant internal manufacturing defects, as determined by comparing measured and predicted pressure drop. Measured pressure drops are summarized in Table 13, along with predicted HFHE pressure drop. The

31

comparison shows no gross differences in pressure drop, and Unit #2 was therefore deemed as having passed checkout testing. The measured pressure drops shown in Table 13 are of limited accuracy (but considered sufficient for the intent of the test) because of approximate methods used to correct for line and discharge losses, and should not be used to judge the accuracy of the predicted values. Having passed checkout testing, Unit #2 was used for thermal performance testing documented in Sections 5 and 6.

Table 13

Check-out Test Results - Pressure Drop

Water Flow Rate kg/hr	gpm*	Measured Δp (including lines, discharge Δp)		Measured HFHE Δp (estimated line, discharge Δp removed)		Predicted HFHE Δp (no lines, discharge)	
		kPa	psi	kPa	psi	kPa	psi
341	1.5	131	19	110	16	98	14
455	2.0	200	29	163	23	138	20

* Gallons per minute

SECTION 5

PERFORMANCE TEST DESCRIPTION

5.1 Performance Test Requirements

Heat exchanger design and performance requirements, given in Table 1, state that in addition to 100 W/cm^2 heat flux capability at twenty locations each 1.0 cm^2 in size, the remaining 180 cm^2 of module surface area must be capable of removing 1.0 W/cm^2 heat flux. This lower heat flux condition was verified through analysis (see Section 3.4.2) in order to minimize schedule impact and cost. The remaining testing requirements are shown in Table 14.

Table 14

Heat Exchanger Testing Requirements

Steady-State Local Heat Flux Capability	100 W/cm^2
Steady-State Total Module Heat Flux Capability	2000 W
Transient Heat Flux Capability	Ramp-up from 0 to 100 W/cm^2 in several seconds
Maximum junction temperature	90 °C
Minimum coolant temperature	0 °C
Maximum module pressure drop	311 kPa (45 psi)

5.2 Test Objectives and Success Criteria

Table 15 summarizes the test objectives, criteria for measuring success, and significance of the results.

Table 15

Test Objectives and Success Criteria

OBJECTIVE	SUCCESS CRITERION	SIGNIFICANCE
Demonstrate 100 W/cm^2 heat flux capability while maintaining 90 °C junction temperature.	100 W/cm^2 heat flux with maximum 50 °C ΔT between heat exchanger and coolant.	First demonstration of 100 W/cm^2 heat flux capability using PAO.
Demonstrate 2000 W total module heat flux capability.	Verify 100 W flux capability at several of the 20 cooling sites.	First demonstration of 2000 W module cooling capability.
Demonstrate feasibility of systems integration.	Attain performance objectives using coolant supply temperature, flowrate, and pressure drop which could reasonably be supplied by a fighter aircraft ECS, in a SEM-E format heat exchanger.	Provides design realism.
Obtain data for comparison to analytical predictions.	Obtain repeatable data by minimizing error sources. Obtain correlation or follow correct trends.	Basic data for low-Re multiple-jet flows. Reduces risk associated with further development.

Objective #1: 100 W/cm^2 Local Heat Flux Capability

The first objective was to demonstrate local cooling capability of 100 W/cm^2 while maintaining 90 °C device junction temperature. The HFHE must operate with a minimum coolant temperature of 0 °C (based on aircraft environmental control subsystem (ECS) capabilities), and thus is limited to a maximum ΔT of 90 °C from junction to coolant. Because a copper heater was used to simulate real devices, there was no junction temperature to measure. Heat exchanger wall temperature was instead used as a requirement, and was limited to 50 °C as discussed in Section 2.1. Thus, the success criterion in Table 15 shows a maximum allowable ΔT from coolant to heat exchanger wall of 50 °C. The significance of accomplishing this first objective is the first practical demonstration of 100 W/cm^2 heat flux capability by a heat exchanger using PAO.

<u>Objective #2: 2000 W Module Heat Load</u>

The second objective was to demonstrate 2000 W total module heat flux capability. This was achieved by demonstrating the capability of cooling twenty 100 W sites on the module. Since only one heat source was available, simultaneous heating of all twenty sites was not possible. Therefore, the 100 W heat source was moved to several different locations one at a time. Since all sites are cooled in parallel, it was assumed that demonstration of module total heat flux capability is independent of the method of heat application (i.e., simultaneous vs. sequential).

Success was measured by the ability of the heat exchanger to maintain a maximum 50 °C heat exchanger wall temperature at all locations tested. The significance of meeting this objective is the demonstration of a flow-through module total heat flux level four to five times that currently achievable with PAO-cooled flow-through modules. Achieving such an increase in cooling capacity does not come without attendant increases in coolant flow rate and pressure drop and heat exchanger thickness. The elevated operating conditions must be acceptable from an aircraft systems standpoint, and are the subject of the next objective.

<u>Objective #3: Demonstration of Integration Feasibility</u>

The third objective was to demonstrate feasibility of integrating the heat exchanger into a fighter aircraft ECS. This objective was achieved by meeting required thermal performance while minimizing aircraft Take-Off Gross Weight (TOGW) impact. Appendix C includes estimates of the sensitivity of TOGW to coolant supply temperature, flow rate, and pressure drop. Reasonable limits for HFHE operation were selected as 0 °C minimum coolant supply temperature, 690 kPa (100 psi) maximum pressure drop across the HFHE, and 1000 kg/hr (5.5 gallons per minute (gpm)) maximum coolant flow rate.

<u>Objective #4: Data for Prediction Assessment</u>

The fourth objective was to gather test data for assessment of analytical methods. The analytical code which was developed by Sundstrand and used to design the HFHE had not been validated for the low jet Reynolds numbers projected using PAO.

5.3 Test System Description

5.3.1 <u>Test Article</u>

The HFHE test article is described in Section 3.

5.3.2 <u>Laboratory Flow Loop</u>

A schematic of the laboratory test system is shown in Figure 14. A photograph is presented in Appendix I. A brief description of each component is given below. The heat source is described in the following subsection.
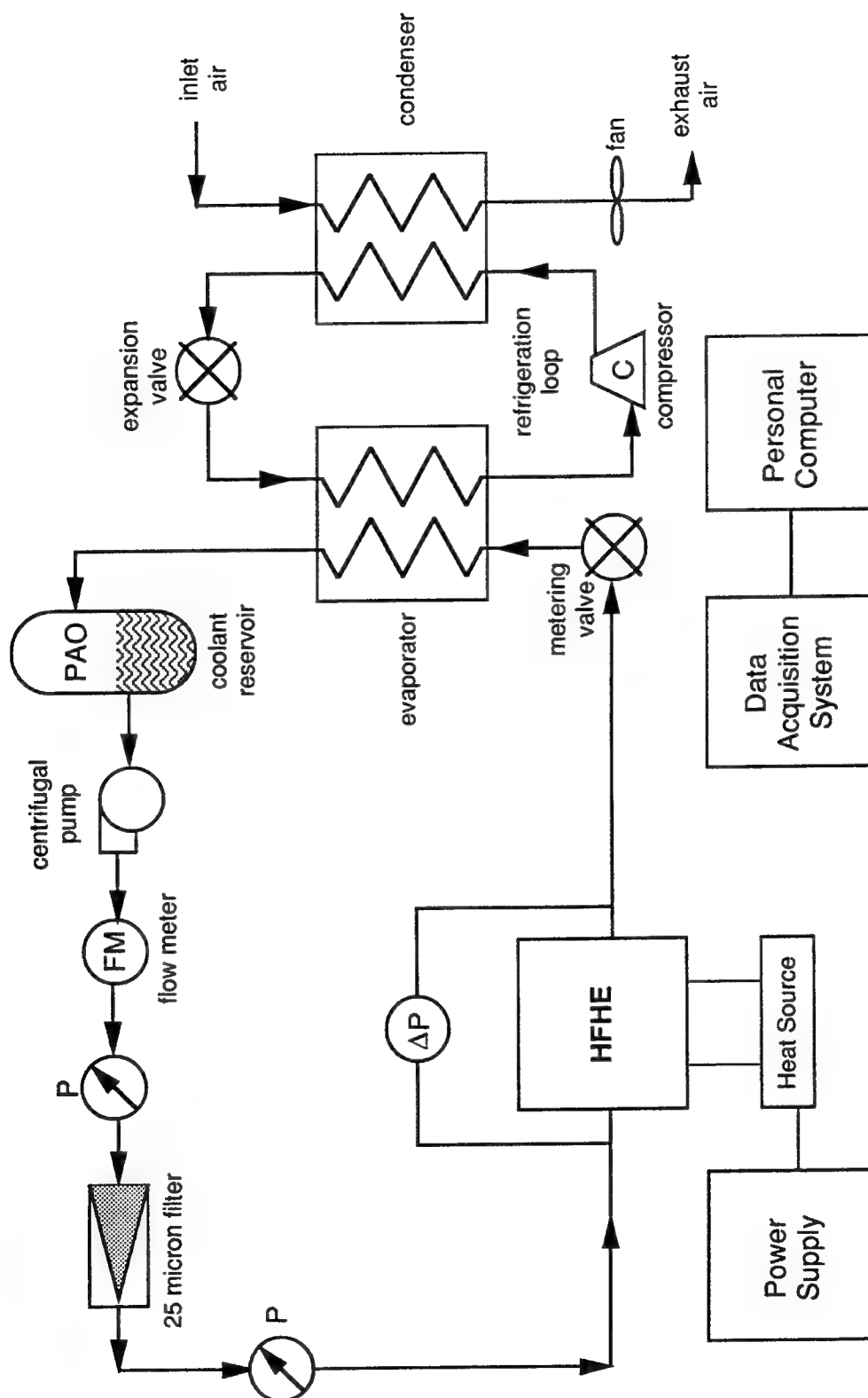
Figure 14. Laboratory Flow Loop.

Chiller: The chiller for this test was an FTS Systems, Inc. RC-100C-032 Recirculating Cooler, which was capable of 0-715 kg/hr (0-4 gpm) at 0-552 kPa (0-80 psi). The chiller included a centrifugal pump, coolant reservoir, refrigeration loop, and temperature controller. The RC-100 had both a cooling mode and a heating mode, allowing control of the coolant temperature well beyond the 0°C to 40°C range required for these tests.

Filter: A 20-micron filter (HYCON, Inc., MFC80-20BN/2) was used to remove particulates that could clog the small coolant passages in the HFHE.

Flow Meter: A Micromotion™ DS25 flow meter provided an analog output that was monitored by the data acquisition system. This flow meter was calibrated for flow rates from 0-900 kg/hr (0-5 gpm).

Metering Valve: A metering valve was used to control flow rate.

Visual Pressure Gauge: A visual pressure gauge was used to monitor pressure drop across the filter. High pressure drop would indicate the filter needed to be cleaned. (As it turned out, after 22 hours of testing, no significant increase in fliter Δp was noted). This data was not recorded.

Differential Pressure Transducer: A Validyne™ 350 pressure transducer provided pressure drop measurement from 0-850 kPa (0-125 psi).

Power Supply: An HP 6012B power supply was used to drive the heaters during the test.

Data Acquisition System: An HP 9000 system with data storage capability was used. This system consists of an HP3852 Data Acquisition System, capable of handling 120 data channels, along with an HP350 Personal Computer for controlling the power supplies and data acquisition system. The HP350 monitor screen was capable of displaying up to 120 data channels simultaneously.

5.3.3 Heat Source

A single heat source was used, having a 1.0 cm x 1.0 cm footprint. This type of "heat flux amplifier" approach, used previously to test CHIC and microchannel coolers (reference [10]), is shown in Figure 15. A photograph of the amplifier is included in Appendix I. It reduces the heat conduction area from 40.3 cm^2 at the location of the heaters to 1.0 cm^2 at the heat transfer transfer interface with the HFHE. Thus, low heat flux heating elements produce a high heat flux at the amplifier/HFHE interface. The amplifier was machined from high-conductivity copper so that a uniform heat flux was obtained at the base.

Heat flux was determined with the thermocouple (T/C) arrangement shown in Figure 16. There were eight T/Cs in each of three planes in the constant cross-sectional area "neck" of the amplifier. The T/Cs were 36 gage type T (copper-constantan). A 0.5 mm diameter hole was drilled 0.5 mm deep at each T/C location. The T/C bead was peened into each hole. A hole was also drilled to the center of each plane, and a T/C was covered with Ecco-Bond 56C epoxy and inserted. The other T/Cs were also bonded with epoxy and their leads secured with Kapton tape. The ninth temperature in each plane was extrapolated during the data reduction process. The
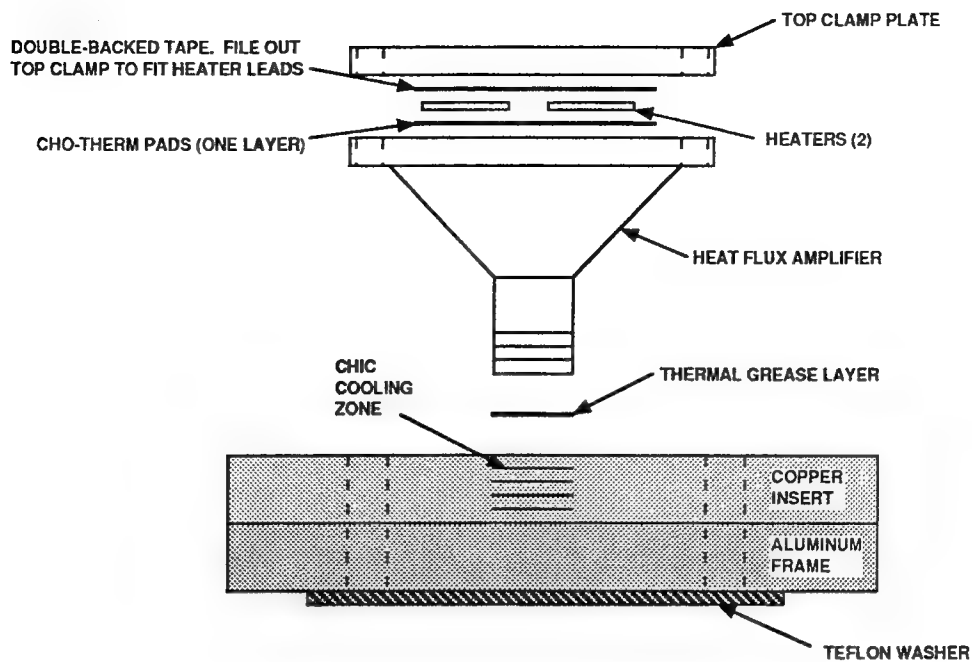
Figure 15. Heat Flux Amplifier
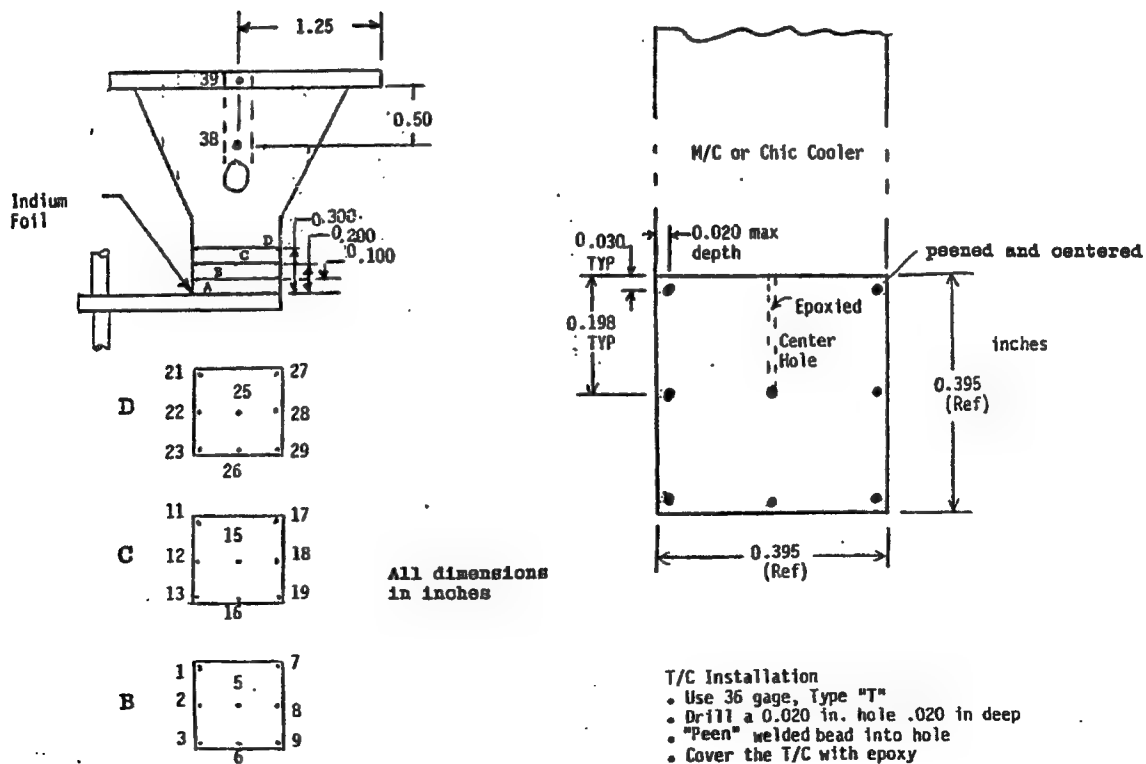
Figure 16. Heat Flux Amplifier Thermocouple Locations

measured temperatures at Planes B, C, and D were extrapolated to predict the temperature at Plane A, which is the interface with the HFHE.

Thermal grease was applied at the amplifier/HFHE interface to provide good thermal contact. The amplifier was bolted to the HFHE with a contact pressure up to an estimated 4800 kPa (700 psi), based on an approximate bolt torque/force relationship of $F = 4 \cdot T/(k \cdot D)$, where F = force carried by bolt, T = torque applied to bolt, $k = 0.2$, D = bolt diameter (0.35 cm), and the constant "4" used because there were four bolts used to secure the amplifier to the HFHE.

Two thick-film ceramic resistance heaters, wired in parallel, were used to supply heat to the large face of the amplifier. Cho-Therm (Type 1671) pads were inserted between the heaters and the copper surface to enhance thermal contact to prevent heater burnout. Thermal contact was also enhanced with pressure applied to the heaters from a top clamp plate.

The heat flux amplifier and HFHE were covered with blanket-type insulation to reduce undesired heat loss.

For test #24, the pulsed heating test, a thick-film resistance heater was used in place of the amplifier to provide better control of transient heat flux. This heater is described in Section 5.4.1.

5.3.4 Instrumentation and Data Collection

Table 16 summarizes the instrumentation used for the tests. The 26 thermocouples (T/Cs) used on the amplifier are shown in Figure 16, and are described in Section 5.3. The locations of the pressure gage and flowmeter are shown in Figure 14.

Table 16

List of Instrumentation

TYPE	MEASUREMENT OF	QUANTITY
Thermocouple	Amplifier Temperature	26
Thermocouple	Resistance Heater Temp.	1
Thermocouple	HFHE Wall	8
Thermocouple	Coolant Inlet Temp.	1
Thermocouple	Coolant Outlet Temp.	1
Flowmeter	Coolant Flow Rate	1
Pressure Transducer	HFHE Δp	1
Current Meter	Heater Current	1
Voltmeter	Heater Voltage	1

Measurement of heat exchanger wall temperature at the location of heat input is important because all thermal performance correlations are tied to it. Measurement is difficult because the heat flux amplifier covers the HFHE wall at that point. The solution was to cut a 0.051 cm deep channel in the HFHE wall under the amplifier for placement of a T/C. This solution involved some risk because the wall is only 0.076 cm thick. Therefore, this action was not implemented until the final CHIC location (Site "D" in Figure 9) was tested. For the tests which preceded the use of this embedded T/C (at Sites "A", "B", and "C"), wall temperature was estimated by placing two T/Cs on the HFHE surface adjacent to the amplifier. Surface T/C layout at Site "D" is shown in Figure 17.
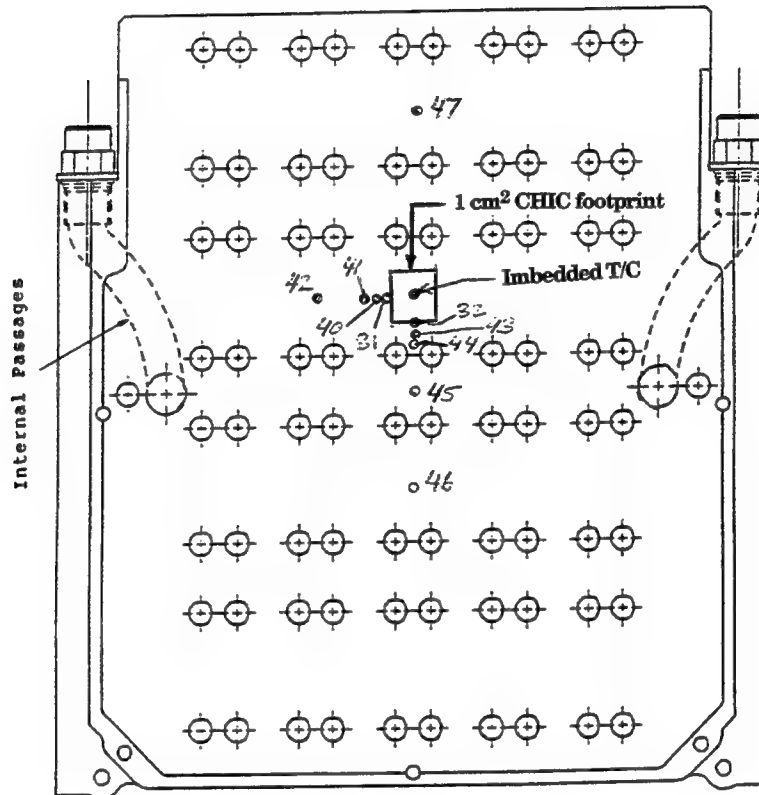
Figure 17. Surface Thermocouple Locations, Site "D"

All thermocouple, pressure transducer, flowmeter, and heater inputs were monitored by a Hewlett Packard Model 3852 data acquisition system. This system was run by a personal computer and stored data directly on the VAX computer. Data manipulation was performed by the acquisition system, which also displayed the data and calculated parameters on a single screen in real time.

Heat flux was determined from the measured temperature gradient in the constant cross-sectional area portion of the amplifier. Two checks were made on heat flux: one from the voltage/current product, "Heater Power", and another from the measured temperature rise of the coolant "Q-Check".

5.4 Test Conditions and Procedures

5.4.1 Test Matrix

The test matrix, shown in Table 17, subjected the HFHE to 24 tests required to meet testing requirements, plus an additional 11 tests to acquire data to complete flow rate and coolant temperature correlations. Table 18 summarizes in matrix form the correspondance between key steady state tests and flow rate / coolant temperature conditions.

Tests 1-5 (Hydraulic Checkout)

The first set of tests evaluated the sensitivity of flow rate to pressure drop without heat applied. Runs were made at the design condition coolant temperature of 20 °C. Test #5 is a repeat of Test #1. Drift in measurements between tests could signify such things as surface aging (scale deposits, etc.), heat exchanger permanent deformation, or instrumentation drifting from calibration.

Tests 6-11 (Thermal Checkout and Max. Heat Flux Test)

The second test segment consisted of checking out the heating system and gradually increasing heat flux to the peak level of 100 W/cm^2. In Test #6, a small heat flux (nominally 10 W/cm^2) was applied. Significant heat flow nonuniformity, heat loss, thermal resistance, or high heater temperature in Test #6 would indicate a problem with the heating system or attachment method. Any problems would be corrected before proceeding to tests with higher heat fluxes. Test #11 was a repeat of Test #4 to verify repeatability.

Tests 12-15 (Failure Mode Tests)

The purpose of these tests was to evaluate degradation in thermal performance of the heat exchanger due to failures in the cooling system. *Heat exchanger failure modes*, such as clogging and leakage, could result in permanent damage to the heat exchanger and were not tested. Therefore, only *system failure modes* were tested. Two system "failures" were simulated: a) reduced coolant supply pressure (and thus reduced flow rate), and b) increased coolant supply temperature.

These tests were conducted by maintaining a heat exchanger wall temperature of 50 °C (simulating 90 °C junction temperature as explained earlier) and measuring maximum heat flux.

Tests 16-18 (Low Temperature Tests)

The purpose of these tests was to study the performance of the HFHE with low temperature coolant. The viscosity of PAO is well known to increase rapidly as temperature is reduced.

Tests 19-21 (AAAPT Design Conditions)

These tests subjected the HFHE to similar coolant temperature and module pressure drops as flow-through modules developed under the Air Force AAAPT (reference [2]) program. The objective was to demonstrate what, if any, gains in

41

Table 17

Test Matrix

TEST #	Q (W/cm^2)	FLOW RATE kg/hr	gpm	COOLANT TEMP. (°C)	PREDICTED ΔP (psi) **	TEST PURPOSE
			REQUIRED TESTS			
1	0	54	0.30	20	4.4	Hydraulic Checkout
2	0	108	0.60	20	9.1	Hydraulic Checkout
3	0	161	0.90	20	14.8	Hydraulic Checkout
4	0	215	1.20	20	21.6	Hydraulic Checkout
5	0	54	0.30	20	4.4	Repeat of Test 1
6	10	215	1.20	20	21.6	Thermal Checkout
7	25	215	1.20	20	21.6	25% Max. Q
8	50	215	1.20	20	21.6	50% Max. Q
9	75	215	1.20	20	21.6	75% Max. Q
10	100	~215*	~1.20*	20	21.6	Max. Q Test
11	0	215	1.20	20	21.6	Repeat of Test 4
12	<100 *	161	0.90	20	14.8	Reduced Flow rate Test
13	<100 *	108	0.60	20	9.1	Reduced Flow rate Test
14	<100 *	215	1.20	30	20.0	Increased Coolant Temp.
15	<100 *	215	1.20	40	18.4	Increased Coolant Temp.
16	0	108	0.60	0	15.1	Low Temp. Test
17	50	108	0.60	0	15.1	Low Temp. Test
18	100	108	0.60	0	15.1	Low Temp. Test
19	<100*	23*	0.13*	23	2***	AAAPT condition
20	<100*	56*	0.31*	23	5***	AAAPT condition
21	<100*	115*	0.64*	23	10***	AAAPT condition
22	0	215	1.20	20	21.6	Repeat of Test 4
23	100	~215*	~1.20*	20	21.6	Repeat of Test 10
24	100	215	1.20	20	21.6	Pulsed Heat Load
			ADDITIONAL TESTS TO COMPLETE CORRELATIONS			
25	100	54	0.30	20	4.4	Rth and Δp vs. Flow Rate and Coolant Temperature.
26	100	54	0.30	10		"
27	100	108	0.60	10		"
28	100	161	0.90	10		"
29	100	215	1.20	10		"
30	100	54	0.30	30		"
31	100	108	0.60	30		"
32	100	161	0.90	30		"
33	100	54	0.30	40		"
34	100	108	0.60	40		"
35	100	161	0.90	40		"

* A test result, not a controlled parameter.

** Pressure drop in CHIC + Header Frame is predicted based on specified flow rate, using ref. [11] predictions multiplied by 1.25 to account for ratio of measured-to-predicted Δp observed during checkout tests.

*** For Tests 17-19, Δp is specified and flow rate is predicted.

Table 18

Matrix of Flow Rates and Coolant Temperatures Tested

FLOW RATE		COOLANT TEMPERATURE (°C)				
kg/hr	gpm	0	10	20	30	40
54	0.3		Test #26	#25	#30	#33
108	0.6	#18	#27	#13	#31	#34
161	0.9		#28	#12	#32	#35
215	1.2		#29	#10	#14	#15

thermal performance could be realized by employing a CHIC cooler over a AAAPT flow-through module *under the same operating conditions.* It is emphasized that the HFHE was optimized for a higher pressure drop than the AAAPT condition, so that measured performance is not totally indicative of its true capability. Coolant supply temperature on fighter aircraft which will use AAAPT flow-through modules was estimated at 23 °C. Module pressure drop is uncertain, so three pressure drops were tested, covering the expected range.

Test 24 (Pulsed Heat Load)

This test measured the performance of the heat exchanger under transient thermal conditions. Heat flux was applied from zero to 100 W in several seconds, while coolant flow rate and inlet temperature were held constant. The temperature response of the heat exchanger was measured.

The variable which needed to be controlled in this test was heat flux vs. time at the heat source/HFHE interface. The heat flux amplifier was ill-suited to provide transient heat flux because of the significant thermal lag between the location of heat flux control (the resistance heaters) and the amplifier/HFHE interface. Therefore, the amplifier was removed and a high-power thick film ceramic heater, provided free of charge from Mini-Systems, Inc. (Mini-Systems MSR-26) of 1.0 cm^2 footprint was used in its place. Heat flux was determined by the voltage-current product. The ceramic heater was secured to the HFHE surface by placing the amplifier on top of the ceramic heater with an insulator placed between, and bolting the amplifier to the HFHE to provide contact pressure. Thermal grease was applied at the ceramic heater/HFHE interface. A photograph of the installed resistance heater, with amplifier removed, is provided in Appendix I.

Tests 25-35

These tests are designed to complete the correlations which were developed analytically for this heat exchanger.

5.4.2 **Procedures**

Steady-State Tests

For each test, the coolant flow rate and temperature were first increased to their specified values. After a steady-state condition was reached (defined by coolant temperature rate of change of less than 2 °C/hr in accordance with MIL-STD-810E, and flow rate maintained as constant as the system would allow), HFHE pressure drop was measured. Power was then applied to the resistance heaters up to the heat flux specified for the particular test. A steady-state condition was reached (defined as the point where all thermocouple readings changed by less than 2 °C/hr), after which all temperature, pressure, power, and flow rate data were recorded. After data recording was complete, power to the resistance heaters was switched off completely, and the coolant continued to flow until all temperatures registered within 5 °C of coolant temperature.

Transient Test

For Test #24, after steady-state flow rate and coolant temperature were achieved, power was increased manually with dial control from zero to approximately 100 W in several seconds, then truncated. Data was recorded approximately once per second throughout the period of power application and cooldown. In order to achieve a one sample-per-second data rate, the number of channels being monitored had to be minimized. Therefore, steady-state flow rate, pressure drop, and coolant temperature were recorded prior to and after power application, but not during it. During power application, only current, voltage, resistance heater temperature, imbedded wall temperature, and one surface temperature were measured.

Movement of Heat Flux Amplifier

The heat flux amplifier was moved to four different CHIC locations (designated in Figure 9) to verify consistent performance among different cooling sites. Tests 1 through 23 were all performed at site "A". The amplifier was then moved to site "B", and Test 10 was repeated. The amplifier was then moved to site "C" and Test 10 was repeated. The amplifier was then moved to Site "D", and all tests in the test matrix were performed.

SECTION 6

PERFORMANCE TEST RESULTS AND COMPARISON TO PREDICTIONS

The following section presents test results and comparisons to predictions.

6.1 Hydraulic Test Results

Figure 18 shows measured versus predicted HFHE pressure drop (Δp) as a function of flow rate and coolant temperature. Predicted pressure drops through the HFHE are from the Sundstrand analytical model and were made well in advance of the test. Appendix G shows raw pressure drop data which included HFHE and supply/return line pressure drop, and calculations to extract the HFHE portion of the total Δp. Measured Δp's compare well to prediction at lower flow rates, but are about 30% higher than predicted at the design flow rate of 215 kg/hr (1.2 gpm). This difference is perhaps attributal to greater turbulence developed at the higher flow rates than was predicted, but this was not pursued in this study.

These results were invariant over a testing period of 28 days, which included approximately 22 hours of flowing coolant. There was no evidence of clogging.

6.2 Thermal Test Results

6.2.1 Heat Loss

Originally, twenty heat sources were planned to be used for simultaneous heating of the twenty CHICs. In the interest of cost savings, only a single heat source was used, which was moved to several different CHIC locations to verify consistent thermal performance. Because each CHIC received coolant in parallel, it was felt that the objective of demonstrating 2000 W module cooling capacity could be accomplished by heating only one CHIC at a time.

A problem with this approach was that heat was conducted from the CHIC being heated to neighboring CHICs which were not heated. Had all twenty CHICs been heated equally, the lines of symmetry dividing adjacent CHICs would have represented adiabatic boundaries. When only one CHIC was heated, some of the heat was conducted away to neighboring CHICs. Thus, apparent thermal performance of the CHIC was greater than true performance. Calculation of heat conducted away was therefore required so that it could be subtracted from the incident heat to calculate true thermal performance.
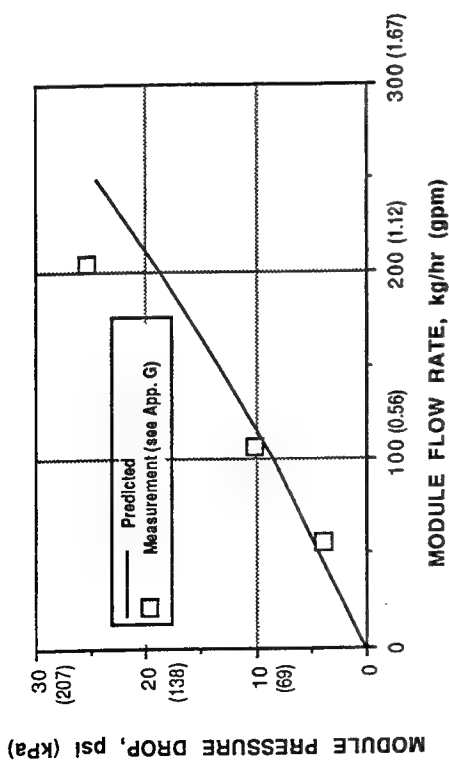
45

(a) 10 °C Coolant Temperature
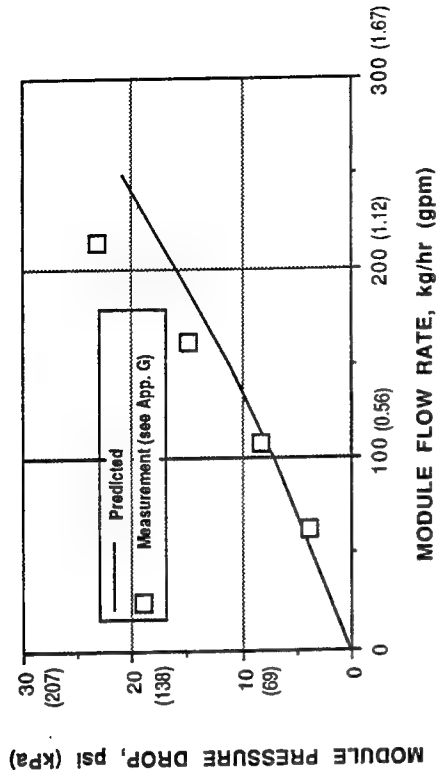
(b) 20 °C Coolant Temperature
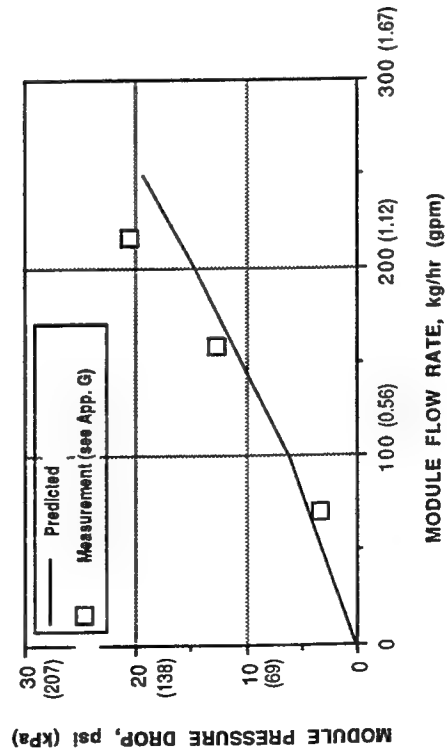
(c) 30 °C Coolant Temperature

(d) 40 °C Coolant Temperature

Figure 18. Measured vs. Predicted Pressure Drop

Note: Measured pressure drops are "corrected" by subtracting supply/return line Δp from raw data (see App. G).

46

Conduction heat loss was estimated by attaching thermocouples to the suface of the HFHE at varying distances from the heat source in order to measure surface temperature gradient. Conduction from the CHIC could then be calculated using Fourier's Law of heat conduction in radial coordinates. Conduction heat loss calculations are shown in Appendix H, Section H.1.1. It amounts to approximately 10% of incident heat flux at the design condition of 215 kg/hr (1.2 gallons per minute (gpm)) flow rate and 20 °C coolant temperature.

6.2.2 Thermal Resistance

Thermal resistance was calculated, after correcting for conduction heat loss as discussed above, by:

$$R_{wf} = \frac{T_w - T_f}{Q/A_{net}} \qquad (2)$$

where: R_{wf} = Wall-to-fluid thermal resistance
T_w = wall temperature at CHIC location
T_f = fluid (coolant) supply temperature
Q/A_{net} = net heat flux to CHIC

Calculations of thermal resistance are shown in Appendix H, and are plotted in Figure 19.

Measured thermal resistance is consistently below predicted values. This may be because the most conservative correlation was used for the predictions. At the design flow rate of 215 kg/hr (1.2 gpm), measured thermal resistance is only slightly lower than prediction. As flow rate is reduced, however, the deviation increases. It is interesting that the dependence of thermal resistance on flow rate is much lower than predicted. This result may shift the optimum design point toward a lower flow rate, where the benefit of reduced demands on the ECS may more than offset a slight degradation in thermal performance. Further discussion of these results is given in the following subsections.

6.2.3 Heat Flux Capability

The maximum heat flux level demonstrated in these tests is shown in Table 19 along with HFHE operating conditions. The 100 W/cm^2 objective was met in test while operating within pressure drop and coolant temperature limitations specified in Table 1. Appendix H, Section H.1.4 provides the calculations involved in determining the net heat flux, "Q-net", after accounting for heat losses.
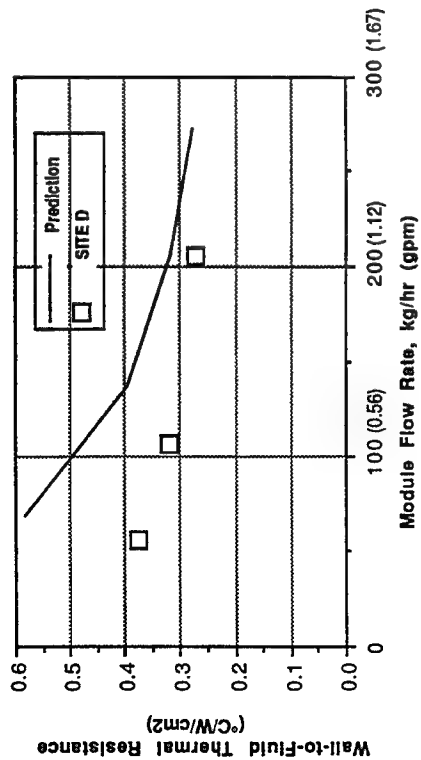
47

(a) 10 °C Coolant Temperature
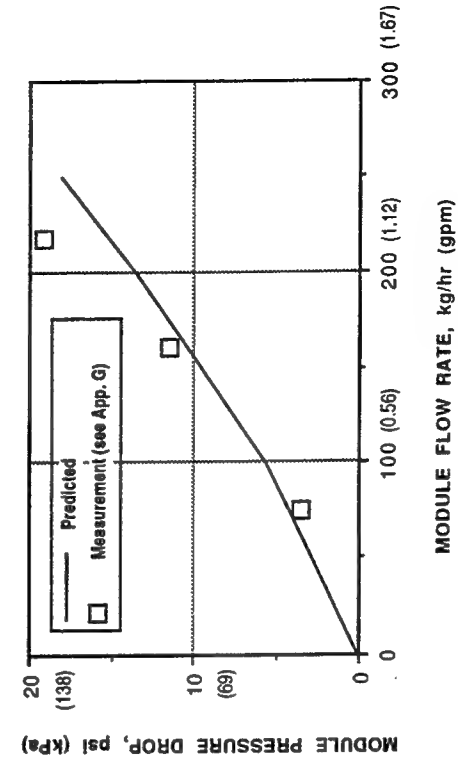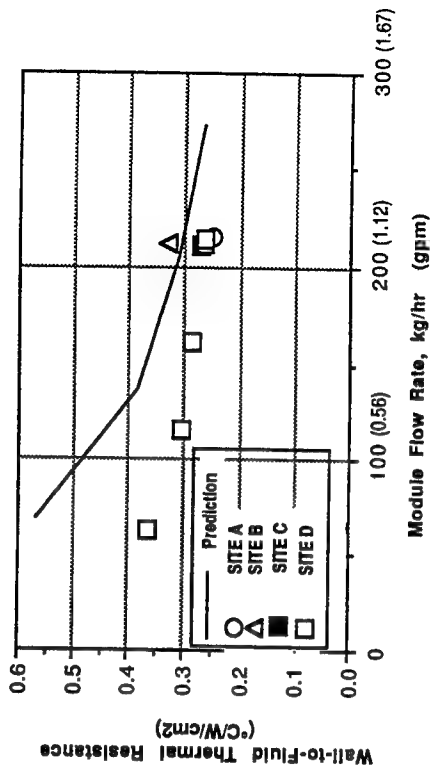
(b) 20 °C Coolant Temperature
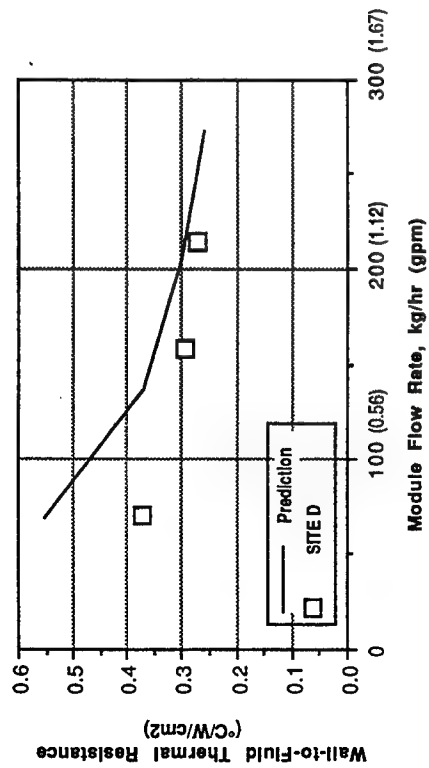
(c) 30 °C Coolant Temperature
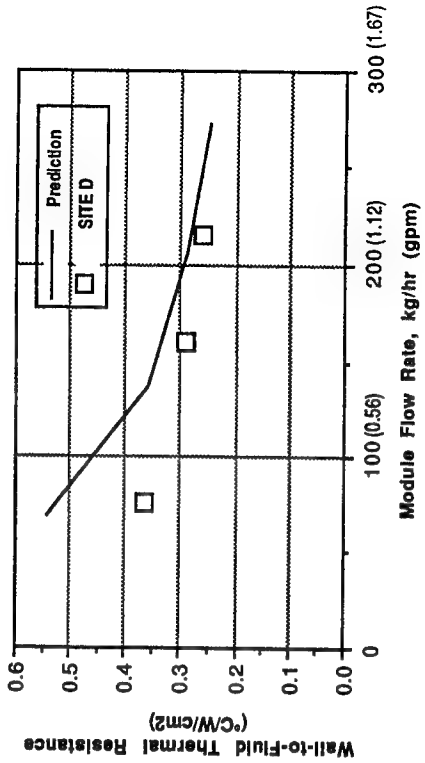
(d) 40 °C Coolant Temperature

Figure 19. Measured vs. Predicted Thermal Resistance

48

Table 19

HFHE Maximum Measured Heat Flux Level

CHIC SITE	FLOW RATE		Δp*		COOLANT TEMP. (°C)	WALL TEMP. (°C)	Q-net (W/cm²)
	kg/hr	gpm	kPa	psi			
D	211	1.18	131	19.0	18.80	45.95	106.8
Limits			310	45.0	0	50	

* Pressure drop through HFHE assembly (supply/return line Δp subtracted from raw data per method described in Appendix G).

6.2.4 Failure Mode Test Results

The maximum heat flux capability of the HFHE may be estimated by extrapolating the results shown in Table 19 to limit operating conditions. Coolant temperature is reduced to 0 °C and HFHE pressure drop is increased to 311 kPa (45 psi). At such conditions, flow rate is predicted to be 329 kg/hr (1.84 gpm) based on Figure 12. From Figure 10, for a flow rate of 329 kg/hr and coolant temperature of 0 °C, wall-to-fluid thermal resistance is 0.270 °C/(W/cm2). Thus, using equation (1):

$$ Q = \frac{\Delta T}{R_{cw} + R_{wf}} = \frac{90\ °C - 0\ °C}{0.4 + 0.27\ °C/(W/cm^2)} = 134\ W/cm^2 $$

Reduced Flow

The thermal performance of the HFHE under conditions of reduced flow rate is of interest in assessing impact of off-design operating conditions on electronics temperature and reliability. Design conditions are 215 kg/hr (1.2 gpm) flow rate and 20 °C coolant temperature. Figure 19b shows the effect of flow rate on wall-to-fluid thermal resistance at 20 °C. Near the design flow rate, measurement is in fairly good agreement with prediction. As flow rate is reduced, thermal resistance rises more slowly than predicted. The relative "flatness" of the thermal resistance curve with flow rate indicates tolerance in heat exchanger performance to flow rate reduction.

Increased Coolant Temperature

Thermal performance with increased coolant temperature is likewise of interest. Figure 19 shows that at the design flow rate of 215 kg/hr (1.2 gpm), measured thermal resistance is essentially independent of coolant temperature (this effect is also shown in Figure 21). A thermal benefit of operating with higher coolant temperature is increased flow due to viscosity reduction. Increased flow in turn leads to reduced thermal resistance. In fact, thermal resistance drops by about 0.03 °C/(W/cm²) as

49

coolant temperature increases from 20 °C to 40 °C. However, this gain in thermal performance, resulting in a 3 °C smaller wall-to-fluid ΔT, is not nearly enough to counterbalance the simple effect of increased heat sink temperature of 20 °C. As coolant temperature increases, junction temperature will increase, at just a slightly lesser rate.

6.2.5 Low-Temperature Performance

Six tests were performed at a nominal 10 °C coolant temperature (test I.D.'s 54-59). The results of these tests are plotted in Figures 18a (pressure drop data) and 19a (thermal resistance data). The measured pressure drop is in good agreement with predictions at lower flow rates, and about 33% higher than predictions at the highest flow rate tested. Figures 20 and 21 plot Δp and R_{wf} for a fixed flow rate, as a function of coolant temperature, and show that increases in pressure drop and thermal resistance remain gradual as coolant temperature is reduced to 10 °C.

The test matrix (Table 12) specified 0 °C coolant temperature tests. One test (test I.D. 43) nearly achieved this with 1.78 °C coolant, but the pump failed, either from the increased coolant viscosity or its bearings freezing up. Pressure drop and thermal resistance obtained before this test was truncated indicated that performance was as expected, with no sudden change in thermal or hydraulic performance occurring at this temperature.

FLOW RATE = 108 kg/hr (0.6 gpm)
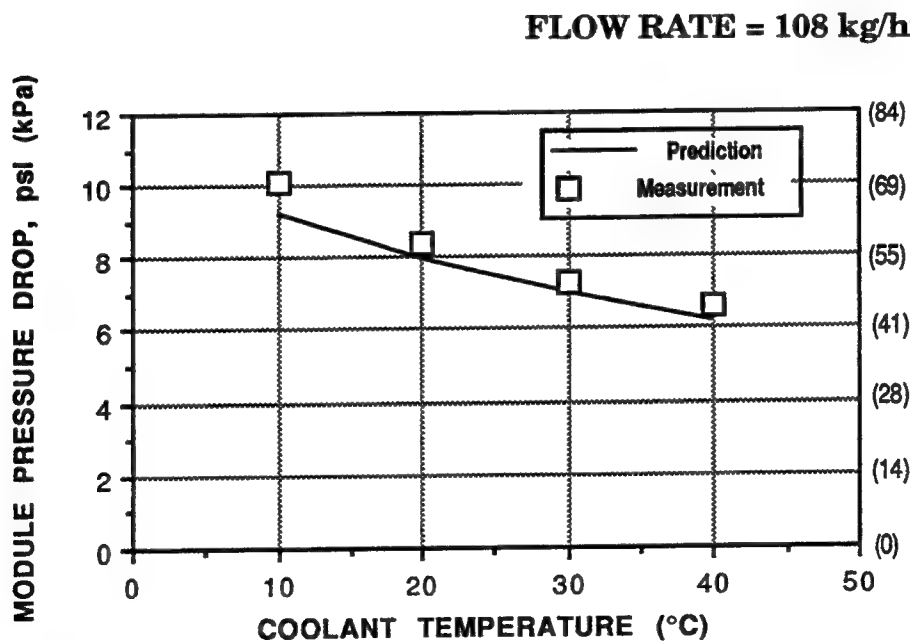
Figure 20. HFHE Pressure Drop as a Function of Coolant Temperature

50
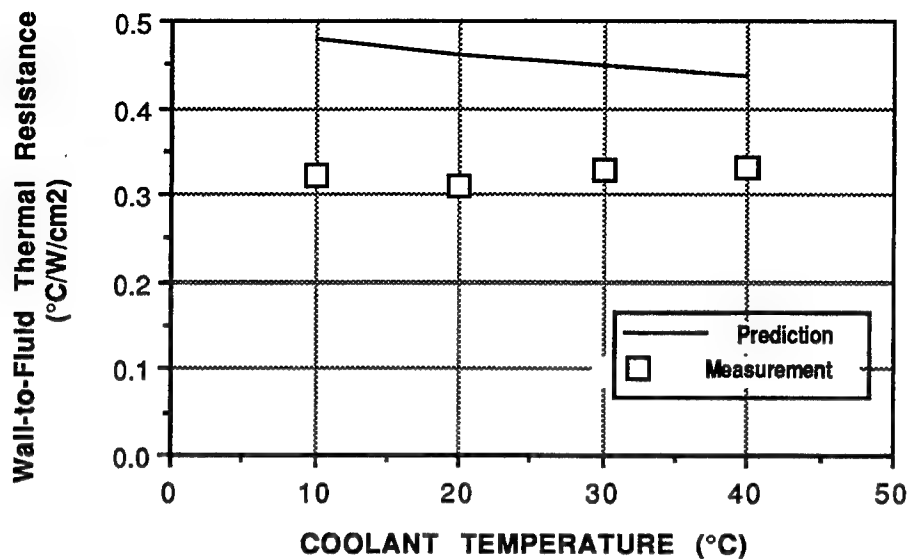
Figure 21.   Wall-to-Fluid Thermal Resistance as a Function of Coolant Temperature

6.2.6 Performance Under AAAPT Conditions

The Air Force Advanced Aircraft Avionics Packaging Technology (AAAPT) program design conditions, as specified in the Test Matrix, are 23 °C coolant temperature and 14 to 69 kPa (2 to 10 psi) module pressure drop (*these conditions are somewhat uncertain to the investigators, especially pressure drop, and represent best guesses*). Low flow rate results obtained for 20 °C coolant temperature (Figures 18a and 19a) may be used to infer AAAPT performance. Measured pressure drops at low flow (Figure 18a) agree well with prediction. At the lower limit AAAPT pressure drop, 14 kPa, predicted module flow rate is 28 kg/hr (0.16 gpm). At the upper limit, 69 kPa, predicted flow rate is 135 kg/hr (0.75 gpm). Applying these two flow rates to Figure 19a, and extrapolating measured thermal resistance values, values of R_{wf} are obtained as 0.43 and 0.28 °C/(W/cm^2) at the lower and upper AAAPT pressure drop limits, respectively. These thermal resistances are believed to be significantly lower than the resistances obtained in the present AAAPT flow-through module. Thus, CHIC technology may present an opportunity to increase local heat flux capability for such modules.

6.2.7 Uniformity of Thermal Performance

The heat flux amplifier was positioned at four different CHIC locations on the module (sites "A", "B", "C", and "D" in Figure 9) to verify consistent thermal performance. Figure 19b plots thermal resistance results obtained at the four sites, for the nominal design operating point (20 °C / 215 kg/hr). Thermal resistances, in units of °C/(W/cm^2), were obtained as follows: Site "A", 0.249; Site "B", 0.307; Site

51

"C", 0.260; and Site "D", 0.255. It is interesting to note that there is a correlation between thermal resistance and location of each CHIC on the HFHE. Site "B" is a corner CHIC and therefore has least access to lose heat to neighboring CHICs. It also demonstrates the highest thermal resistance. Sites "A" and "D" have more neighboring CHICs and have the lowest thermal resistance. Thus, the variation in thermal resistance may be due more to heat loss than to specific thermal performance. The average value is 0.281 $°C/(W/cm^2)$, the maximum deviation from average is +19%, and the average deviation, 9%.

SECTION 7

CONCLUSIONS

A heat exchanger was designed, fabricated, and tested which conforms in lateral dimensions to SEM-E packaging format, uses PAO coolant, operates within constraints imposed by fighter aircraft applications, and demonstrates 100 W/cm^2 local heat flux capability while maintaining 90 °C junction temeprature. In addition, the capability to handle a total module heat load of 2000 W was also shown. Higher heat fluxes are possible if the heat exchanger is operated at higher flow rate or lower coolant temperature while still being within the bounds provided by a fighter aircraft environmental control system. Constructing the HFHE to SEM-E size was a goal of this program but not a requirement. Heat exchanger thickness slightly exceeds SEM-E specification, the result of selecting the lowest-cost assembly procedure. No obstacles from a thermal performance standpoint nor significant costs should be incurred to reduce thickness to SEM-E requirements.

Cost

The heat exchanger was designed for minimum prototype cost and as a result was constructed from copper alloy and the laminates were diffusion bonded. In production, the lowest-cost approach would probably be a vacuum brazed aluminum heat exchanger. The supplier of the vacuum brazed aluminum flow-through SEM-E module for the F-22 program was involved in this program.

System Impact

The heat exchanger was designed to minimize impact on other aircraft systems. The standard aircraft coolant (PAO) is used, and heat exchanger operating conditions were designed to minimize take-off gross weight penalty to a notional advanced fighter aircraft.

Heat Flux Capability

The 2000 W module heat load capability represents a four- to five-fold increase in SEM-E flow-through module heat flux capability using PAO. Non-SEM-E applications such as electronic power conditioners can also use the HFHE design. Increased capability comes with attendant increases in heat exchanger thickness, flow rate and pressure drop, and/or reduction in coolant supply temperature. However, these conditions are within the operating range of typical aircraft environmental control systems.

SECTION 8

REFERENCES

1. E. M. Flynn and M. J. Mackowski, "High Flux Heat Exchanger - Interim Report," WL-TR-93-2027, January, 1993.

2. Advanced Aircraft Avionics Packaging Technology (AAAPT) Program, U. S. Air Force Contract Number F33615-89-C-1110.

3. T. J. Bland, R.E. Niggemann, and M. B. Parekh, "A Compact High Intensity Cooler (CHIC)," SAE Paper No. 831127, July 1983.

4. T. J. Bland, M. P. Ciaccio, R. S. Downing, and W. G. Smith, "The Development of Advanced Cooling Methods for High-Power Electronics," SAE Paper No. 901962, October 1990.

5. M. G. Grote, R. E. Hendron, H. W. Kipp, and J. R. Lapinski, "Test Results of Wafer Thin Coolers at Heat Fluxes from 5 to 125 W/cm^2," SAE Paper #880997, 18th Intersociety Conference on Environmental Systems, July 11-13, 1988.

6. MIL-C-87252, "Military Specification - Coolant Fluid, Hydrolytically Stable, Dielectric," 2 November 1988.

7. "Mini-Task 19, "Feasibility of Replacing Coolanol with PAO Coolant in F-15 Radar Liquid Cooling System," McAIR Internal Memo, November 1989.

8. ROYCO 602 Product Bulletin and Material Safety Data Sheet, November 1987.

9. Hughes Aircraft Company Report No. 2001-D, "F-15 R&M PAO Coolant Study," March 1988.

10. R. E. Hendron, et al., "Stackable Wafer Thin Coolers for High Power Laser Diode Arrays," *Laser Diode Technology and Applications*, Proc. SPIE 1219, 1990.

11. Sundstrand Aerospace, "High Flux Heat Exchanger Critical Design Review," Informal Report, 22 January 1993.

12. T. J. Bland, M. P. Ciaccio, R. S. Downing, and W. G. Smith, "The Development of Advanced Cooling Methods for Power Electronics," Sundstrand Publication *Technology News*, Winter 1991.

13. D. E. Metzger, et al, "Heat Transfer Characteristics for Inline and Staggered Arrays of Circular Jets with Crossflow of Spent Air," J. Heat Transfer, vol. 101, No. 3, August, 1979.

14. Computer Aided Environmental Control System Analysis (CAECS) Users Manual, McDonnell Douglas Report No. A8073, Rev. B, October 1987.

APPENDIX A

CHIC OPERATING PRINCIPALS

At low power densities for electronics equipment, air cooling is the preferred approach due to its simplicity, leakage tolerance, and reliability. However, with higher heat fluxes, liquid cooling becomes more and more attractive. Although liquid cooling can introduce increased complexity, with the need for an intermediate aircraft cooling loop and associated penalty of additional temperature drops, it can result in greatly increased flexibility in packaging and the ability to handle higher heat fluxes at tolerable temperature levels. The higher heat transfer characteristics of liquids as compared to gases are due to their higher thermal conductivities and densities. Leakage and handling considerations lead to the selection of liquid coolants that are non-toxic, non-corrosive, and are adequate dielectrics. Single-phase liquid-cooled systems are attitude-insensitive like air cooling systems, but often offer increased thermal capacitance, minimizing the effect of thermal transients during overload conditions.

Jet impingement cooling is one of the most effective mechanisms for achieving high heat transfer coefficients. The "classical" jet impingement process (see Figure A.1) for a single jet can be divided into three zones: the relatively small diameter stagnation zone, the turning region, and the wall jet region. For an array of circular jets, a fourth region occurs, the jet interaction zone. Heat transfer rates in the stagnation and turning regions are primarily functions of inlet jet velocity and upstream turbulence level. For jets formed by a slot, the peak heat transfer coefficient occurs at the stagnation centerline at most jet Reynolds numbers, whereas for circular jets the peak value occurs just outside the diameter of the jet. A secondary peak due to the transition to turbulence in the wall jet is observed for jet Reynolds numbers greater than 2500. The very high heat transfer rates in the inner two zones results from the extremely thin boundary layers due to the negative pressure gradient. High heat transfer rates are maintained in the jet interaction zone due to the increased turbulence of mixing. Studies at Sundstrand have shown that for the same fluid power consumption, a multiplicity of small jets (jet array) is more effective in cooling an area than a single large jet. Further enhancement of cooling performance can be achieved using extended surface areas.

The total coldplate-to-fluid conductance is given by the equation:

$$G_{th} = 1 / R_{th} = \eta h A_t \qquad (3)$$

In Equation 3, A_t is the total wetted surface area and η is its efficiency. As can be seen by equation 3, thermal resistance is minimized by maximizing the surface area and fin effectiveness as well as the heat transfer coefficient. Using a multiplicity of thin lamination plates that are vigorously scrubbed by high heat transfer coolant jets and in close proximity to the heat source is a way to meet all these objectives. If the plates are thin, a greater surface area density per unit volume can be achieved leading to higher fin efficiencies resulting from the shorter conduction path lengths. The patented CHIC concept, using the combination of liquid jet impingement with arrays of jets and the surface enhancement of multiple plates provides an excellent approach to the high flux cooling problem.
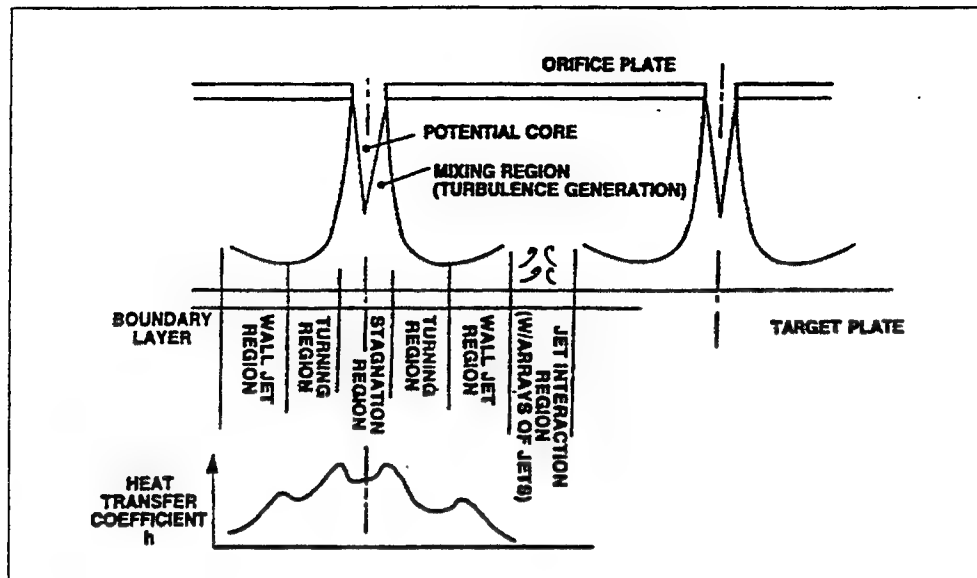
Figure A.1 Jet Impingement Heat Transfer

Figure A.2 shows the basic operating principle of the CHIC. The heat exchange structure is comprised of a stack of orifice plates separated by spacer plates which have cut-outs in the region of the jet orifice arrays. The hole pattern on alternate orifice plates is offset so that jets issuing from one plate are targeted midway between holes on the next layer. Within the stack of laminations, the fluid flows towards the heat source via a series of jets that impinge on successive orifice plates followed by lateral flow rearrangements, until the final impingement layer, adjacent to the heat source, is reached. Within this final jet impingement layer, lateral drainage of the coolant causes a cross-flow effect on the impingement process. The cross-flow degrades the jet impingement heat transfer process but improves the convective coefficient on the side walls and suction side of the last orifice plate. The net effect of the cross-flow in this last layer can either be positive or negative depending on the orifice pitch and jet-to-target spacing.

Experimental studies with free jets show that peak heat transfer coefficients occur with jet throw-to-target spacings of five to seven jet diameters ($z/d = 5$ to 7); however, to optimize the entire heat transfer, much tighter jet-to-target spacings are preferred. Tighter target spacing decreases the conduction distances, increasing fin efficiency perpendicular to the heat addition surface and bringing more heat transfer surface into close proximity of the heat source. Typical values of z/d in the 0.5 to 2.0 range have been selected. Very tight orifice plate spacing, although not ideal for target plate heat transfer coefficient, does improve heat transfer coefficient on the anti-target plate. Studies using CFD modeling and experimental investigations that Sundstrand has funded at the University of Wisconsin-Milwaukee have shown that the anti-target heat transfer coefficient can be nearly as high as the target plate coefficient.
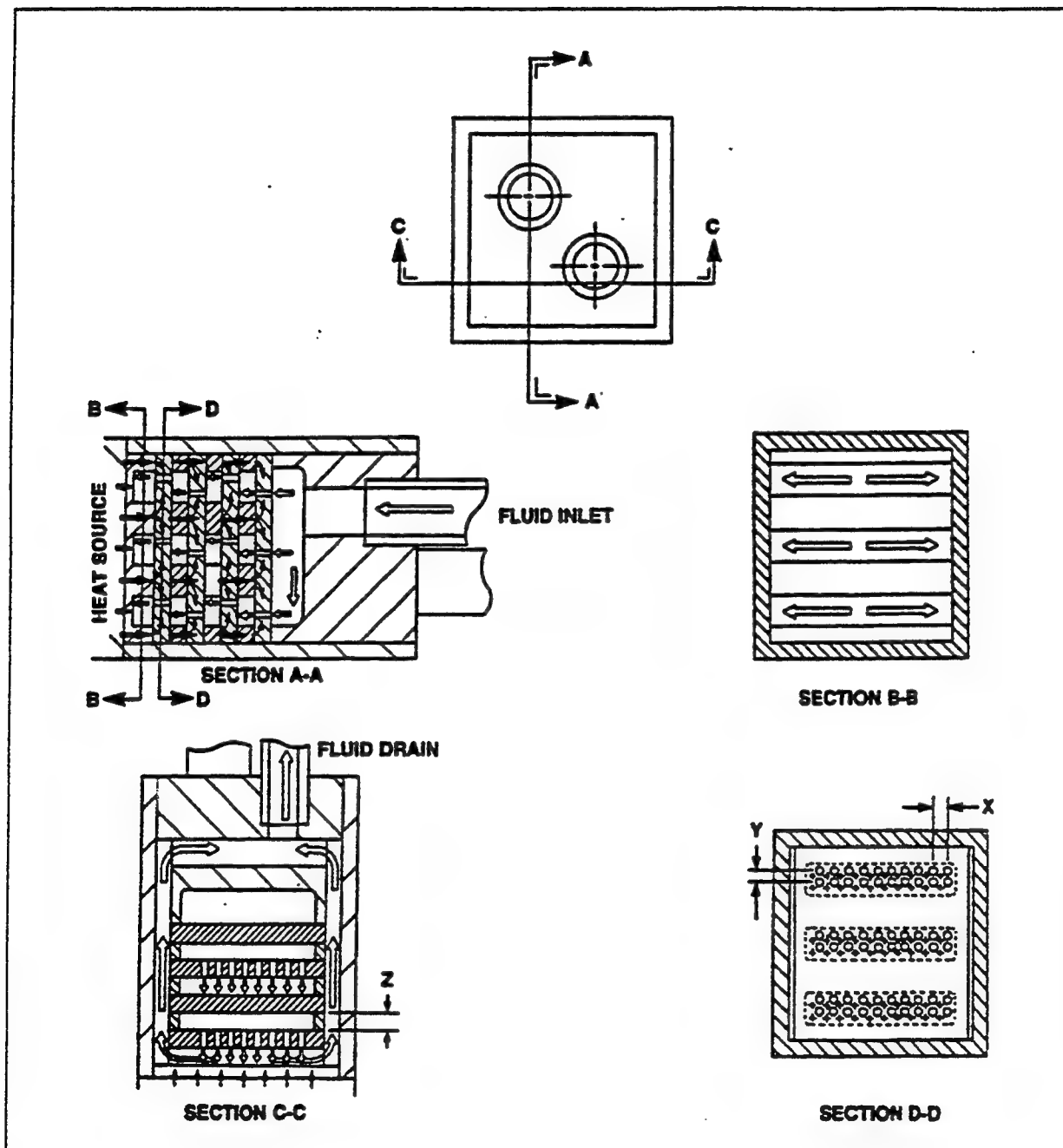
Figure A.2 CHIC Operating Principle (Shown with Single Device)

57

APPENDIX B

CHIC EXPERIENCE AND DATABASE FOR THERMAL PREDICTIONS

In 1984, Sundstrand was faced with the challenging thermal problem of cooling a one-centimeter square laser diode array to within 1°C of isothermality at a heat flux of 50 W/cm^2. A trade study of cooling techniques led to the development of the first CHIC. Since that time, many CHICs have been fabricated in a variety of sizes and shapes (Figure B.1), mostly constructed by the diffusion bonding of copper laminates. The photo-chemical etching process used to generate hydraulic passages in the laminations can be applied to most configuration drawings, making the process easy to customize for any heat source geometry.
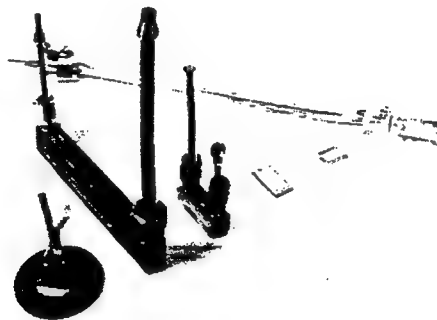
Figure B.1 CHIC Devices

CHIC devices built in copper have been tested with thermal resistances as low as 0.05 °C/(W/cm^2). The high heat flux capability of a 1.0 cm by 2.8 cm copper CHIC was tested with a heat flux of 2.67 kW/cm^2 using water as the coolant [4], [12]. The coolant flow rate and temperature rise were 250 kg/hr and 20°C, respectively. Testing was conducted at the Kirtland Air Force Base Weapons Lab in Albuquerque, New Mexico using an electron beam as the heat source. The beam was programmed to provide a specified heat flux over a controlled footprint by rapidly scanning the test area. It was planned to increase the input heat flux to 4.0 kW/cm^2, but the stainless steel support fixture began to melt from beam overshoot at the higher heat fluxes.

Sundstrand has also integrated CHIC technology with power transistors in an effort to increase semiconductor operating power levels and improve reliability [12]. This was accomplished by repackaging bipolar "hockey-puck" type devices so they became an integral part of the CHIC package with its associated fluid manifolding. The device, shown in Figure B.2, is a hermetically sealed package consisting of a central CHIC core with power diodes mounted on each side. The unit was designed for liquid cooling with integrated design features making the assembly electrically correct. The repacked units have roughly one third the weight and one half the volume of the state-of-the-art flow through coolers. The integrally cooled CHIC semiconductors also showed a four-to-one improvement in junction-to-case thermal resistance.

Normalized	ICS	SOA
Weight (Lb.)	.44	1.0
Volume (In³)	.35	1.0
$R_{J\text{-}OIL}$ (Degree C/Watt)	.23	1.0
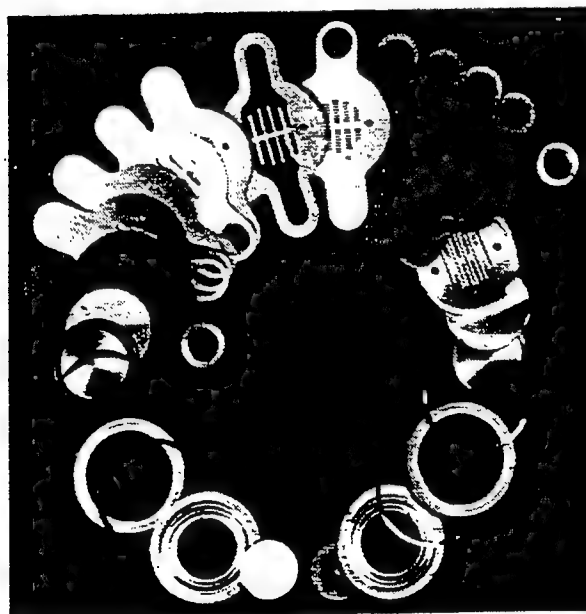
Figure B.2 Integrally Cooled Devices

Most recently, Sundstrand has extended the CHIC cooling concept beyond the single device level to the cold plane of a high power density inverter board. The aluminum module was designed for two-sided cooling with six IGBTs mounted on each surface, each dissipating 100W. The low power density controller circuit board that used conventional printed wiring board technology with printed circuits was included in the design along with the high power IGBT switch layer with its large copper bus bars for the high current conductors. In this design, shown in Figures B.3 and B.4, the cold plate, including CHIC components, was constructed from aluminum, using double-etched laminations to reduce the number of parts and braze joints. All necessary flow headering as well as CHIC features were designed and included into the laminations. This design focused on achieving uniform, high intensity cooling at twelve IGBT footprints, without providing any other low density cooling locations. However, a mixture of high- and low-density cooling patterns could be easily accommodated with the photo-chemical etch fabrication process. The IR&D program High Flux Cold Plane was performance-tested using an ethylene glycol/water mixture as the coolant and electric foil heaters to simulate power transistors. Electric heaters were used in lieu of power transistors because they provided a more controlled heat flux. The measured thermal resistance at the CHIC locations was in the range of 0.2 to 0.3 °C/(W/cm^2), depending on flow rate and, to a lesser degree, location on the coldplate. Flow distribution was not totally uniform between the parallel cooling flow paths, partially due to excess braze melt causing some flow blockage. The experiences of designing, building and testing this developmental cold plate are directly applicable to the current HFHE contract.

Most of the experiments reported in the open literature on jet impingement cooling have used air as the coolant. Primarily motivated by gas turbine cooling applications, heat transfer coefficient as a function of geometrical parameters and jet Reynolds number has been correlated for arrays of air jets. Because open literature heat transfer coefficients were not available on the tighter geometries and for the liquids appropriate to CHIC applications, Sundstrand has collected overall performance data on various designs in an effort to extend the basic impingement heat transfer correlations to the new geometries and flow regimes with liquid coolants. Fundamental research on both single-phase and two-phase impingement cooling arrays was carried out for a four year period with the University of Wisconsin-Milwaukee. Proprietary correlations were developed which further increase the predictability of new designs. Most of the data taken to date has been on moderate to high Reynolds numbers, those above 500. The smaller feature sizes required for the HFHE application in combination with the high viscosity of the selected HFHE coolant (poly alpha olefin (PAO)) have resulted in low Reynolds numbers. Therefore, there was some design risk due to the lack of heat transfer data in a similar hydraulic flow regime for a similar geometry.

Impingement heat transfer is correlated in terms of the jet Nusselt number, Nu. This is defined by:

$$Nu = hd/k \qquad (4)$$

where   h = Heat transfer coefficient
                                d = Orifice hole diameter
                                k = Fluid thermal conductivity.
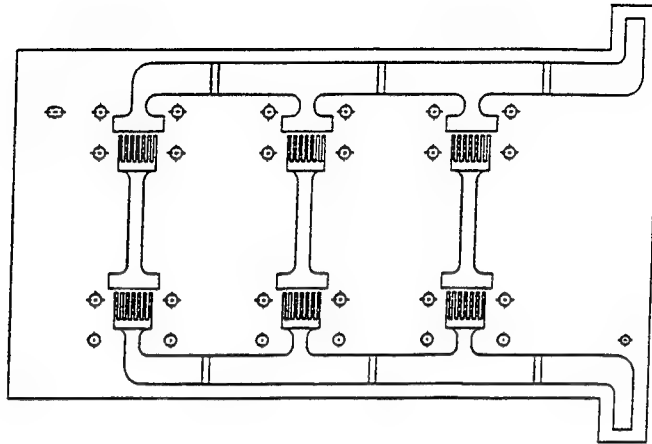
Figure B.3 Lamination Structure of High Heat Flux CHIC Cold Plane

RP43719
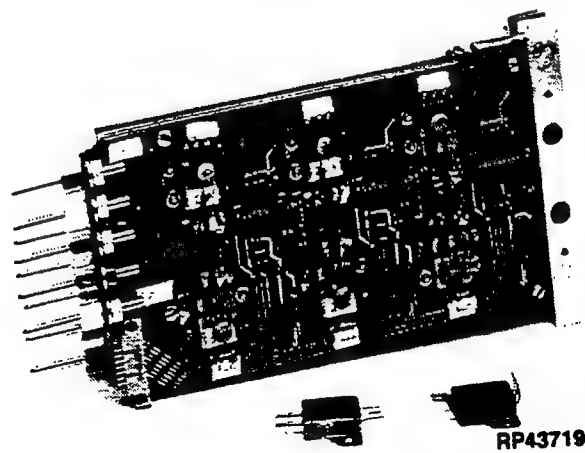
Figure B.4 Power Conversion Module Mounted to CHIC Cold Plane

61

The impingement Nusselt number depends on jet Reynolds number, fluid properties and orifice plate geometry, including hole diameter and pitch.

Three impingement correlations are plotted on log-log plots in Figure B.5 with Prandlt numbers ranging from 0.7 to 132. The selected Prandtl numbers of 0.7, 6.0, 28.0, and 132 correspond to the fluids and conditions on which the data is based and our present design. These are, respectively: air in the range 21-38 °C; liquid R11 and R113 in the range 4-26 °C; MIL-L-7808 oil at 121 °C; and PAO at 10 °C.

These predictions are made for a square hole distribution with a hole pitch to diameter ratio of four and a plate spacing to hole diameter ratio of two. The range of test data used in the correlations is also plotted. In general, correlation 1 estimates lowest Nusselt number, correlation 3 gives highest Nusselt number and correlation 2 is in the middle. Correlation 1 is from the open literature [13] and was tested with air; correlation 2 was developed by Sundstrand and the University of Wisconsin using Freon data; and correlation 3 was developed by Sundstrand using a variety of geometries with oil.

The air impingement test Reynolds numbers ranged from 2000 to 70000.

Data for multiple jet impingement of both R-11 and R-113 are plotted on correlation 2 in the Pr=6 plot. The R-113 experimentation at the University of Wisconsin gave detailed local heat transfer performance, whereas the heat transfer coefficients must be derived from the CHIC device performance on the R-11 experiments. Data sets in Reynolds numbers in the ranges of 9000 to 90000 (R-113) and 400 to 1600 (R-11) are included.

The Pr=28 plot shows Nusselt number for MIL-L-7808 oil impingement for the three correlations. The tested Reynolds number ranges from 700 to 14000. These test data has been used to develop correlation 3.

The Pr=136 plot shows predicted Nusselt number with PAO impingement using the three correlations. The design point is also shown. The most conservative correlation was selected to design and estimate the performance of the HFHE.
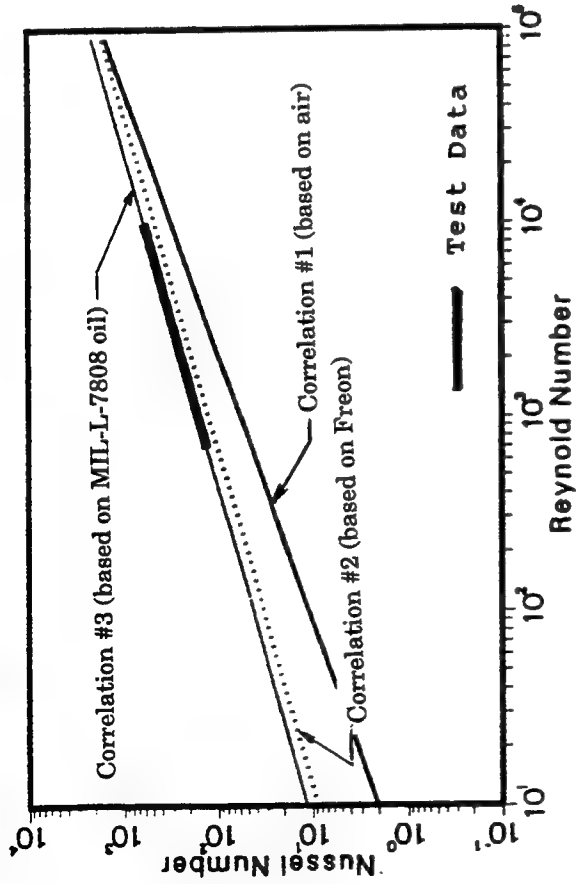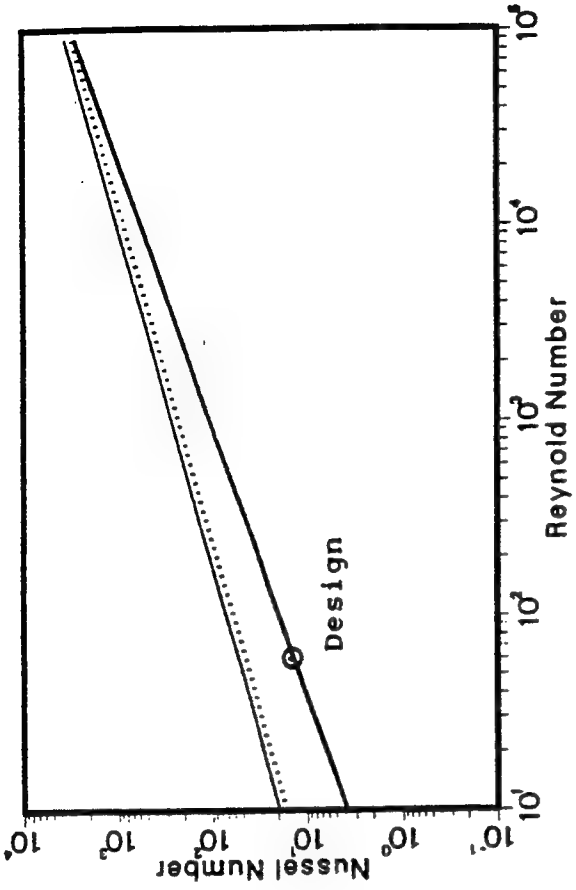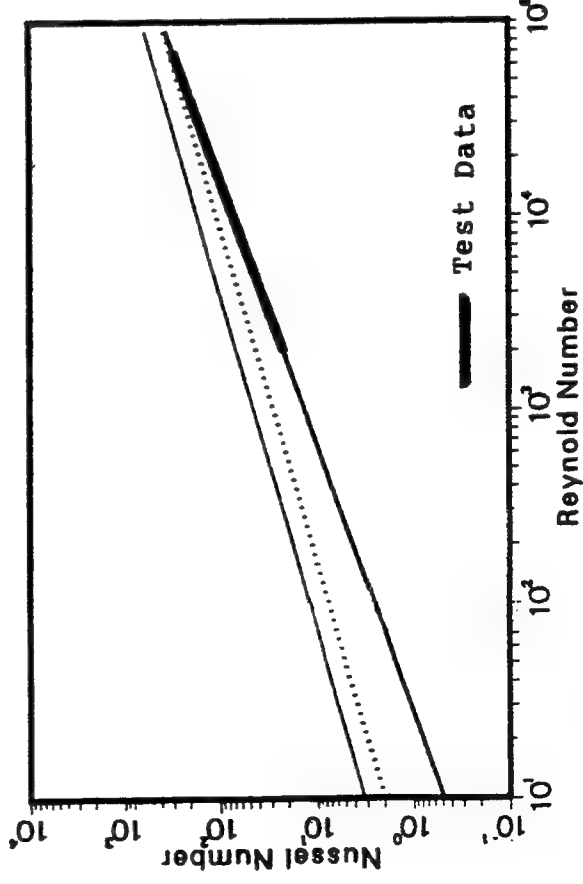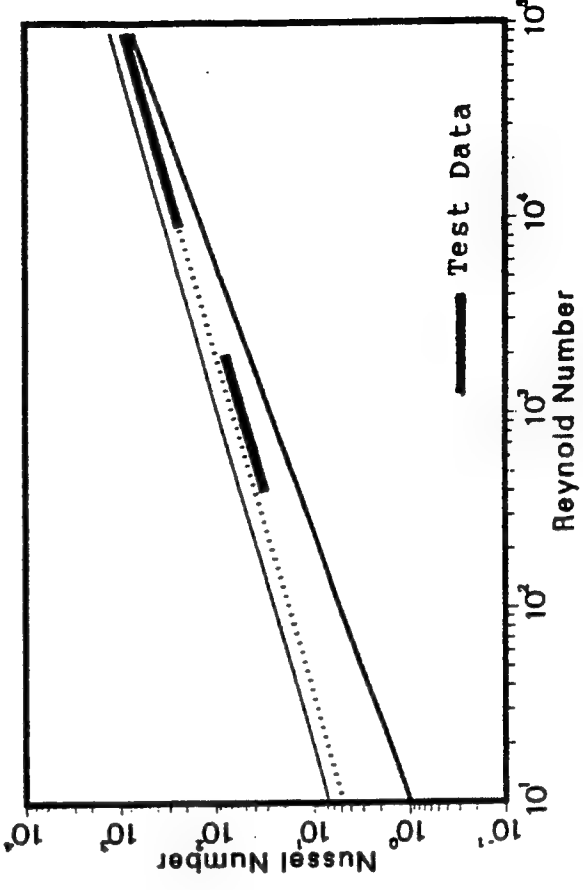
Figure B-5 : Impingement Nusselt Number vs Reynold & Prandtl number

63

APPENDIX C

TAKE-OFF GROSS WEIGHT SENSITIVITY TO HEAT EXCHANGER FIXED WEIGHT AND OPERATING CONDITIONS

In the preliminary design phase, the impact of heat exchanger design parameters on The sensitivity of fighter aircraft TOGW to HFHE operating parameters was estimated for an advanced fighter in its baseline mission role. A vapor cycle system was assumed as the intermediate cooling loop for transporting heat from the HFHE loop to the aircraft fuel heat sink. The analysis was performed using the McDonnell Douglas Computer-Aided Environmental Control System (CAECS) [14] software. CAECS computes steady-state flow rate, pressure drop, temperature, and enthalpy at each location in the system. It then computes component weight and power requirements based upon flow conditions. TOGW penalty is calulated by multiplying applicable penalty factors (for a representative advanced fighter aircraft) by weight, power, and ram air flow rate from CAECS.

The calculated sensitivities of TOGW to coolant flow rate, pressure drop, supply temperature, and fixed weight of the HFHE, are shown in Figures C.1 through C.4, for the case of a 2 kW total heat load. The results are expressed in terms of ΔTOGW from an assumed baseline condition. The results indicate that TOGW is most sensitive to coolant supply temperature and coolant flow rate, and less sensitive to HFHE weight and pressure drop. These results were used in conjunction with the results from Appendix D.
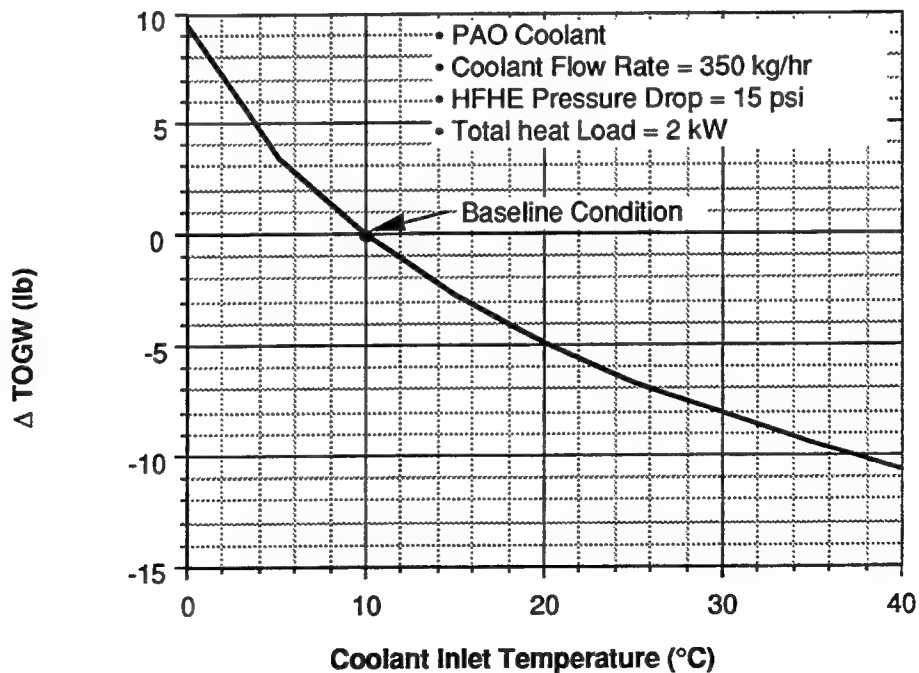
Figure C.1. Sensitivity of Aircraft Take-Off Gross Weight to Coolant Supply Temperature.
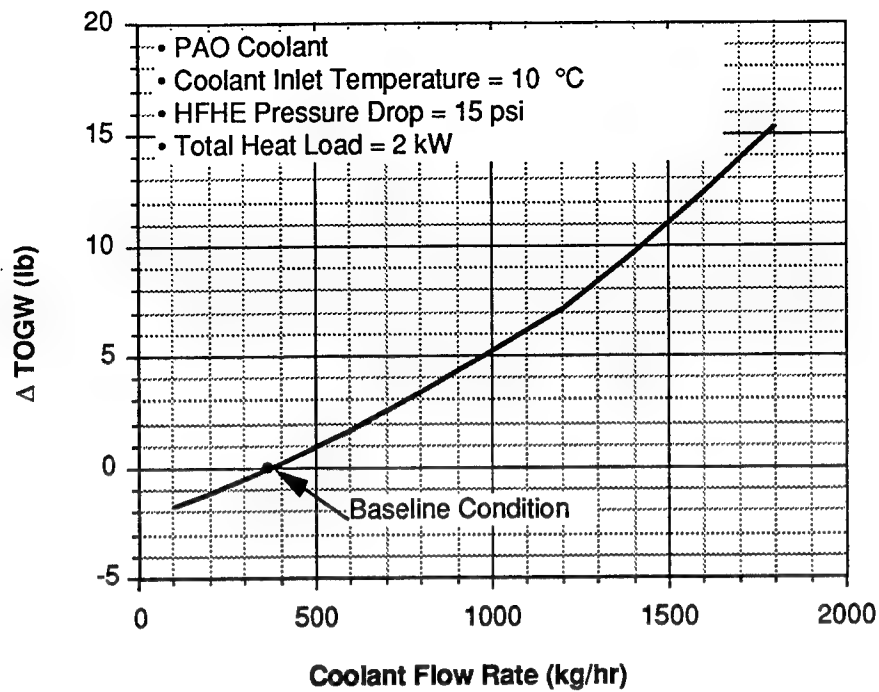
Figure C.2. Sensitivity of Aircraft Take-Off Gross Weight to Coolant Flow Rate.
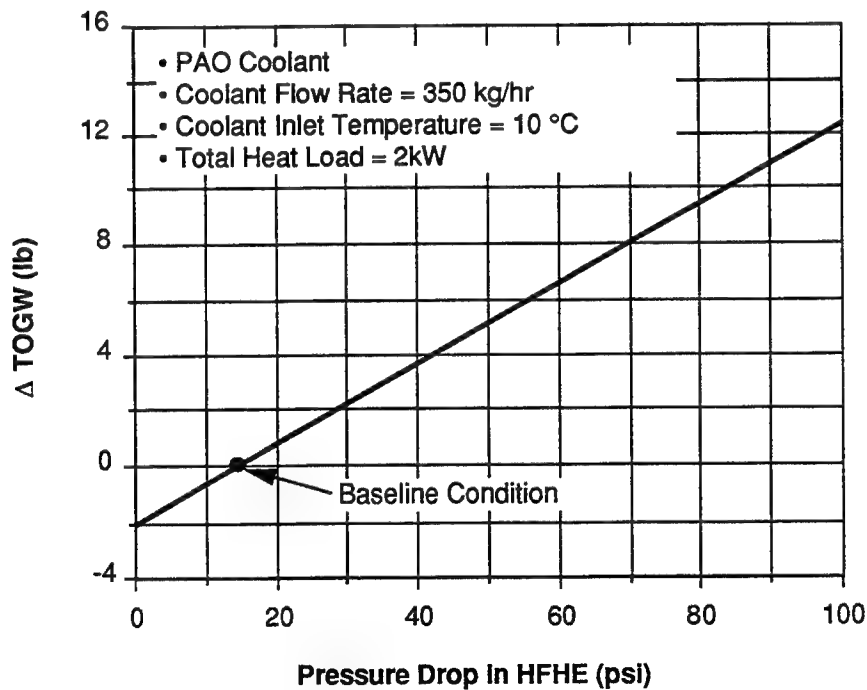
Figure C.3. Sensitivity of Aircraft Take-Off Gross Weight to HFHE Pressure Drop.
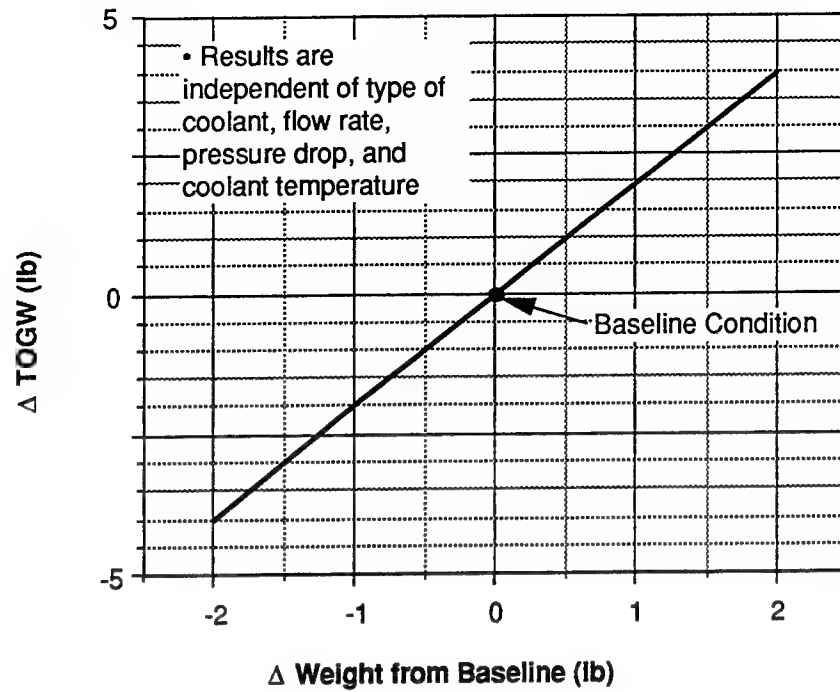
Figure C.4. Sensitivity of Aircraft Take-Off Gross Weight to HFHE Structural and Contained Coolant Weight.

APPENDIX D

IMPACT OF HEAT EXCHANGER DESIGN PARAMETERS ON FIGHTER AIRCRAFT TAKE-OFF GROSS WEIGHT

This appendix documents the procedure used in the preliminary design to estimate the sensitivity of aircraft TOGW to the following heat exchanger design parameters:

1. Heat exchanger material (copper vs. aluminum)
2. Flow configuration (one, two, or four CHICs receiving coolant in series)
3. Flow rate (150 to 1100 kg/hr)
4. Number of orifice plates (four to nine)
5. Orifice plate thickness (0.010, 0.015, and 0.020 cm)
6. Orifice spacing

TOGW sensitivities were determined by first calculating sensitivity of heat exchanger weight, flow rate, pressure drop, and required coolant supply temperature to the six design parameters listed above, then applying the results of Appendix C to obtain TOGW sensitivities. A discussion of these results is given in Section 2.5.

Method of Calculating TOGW Sensitivity to Design Parameters

1. Select a set of design parameters (items 1 through 6 above).

2. Given the requirement of 100 W/cm^2 heat flux, 2000 W total module heat load, and maximum module wall temperature of 50 °C, calculate required coolant supply temperature using the Sundstrand correlations shown in App. B.

3. Use Sundstrand hydraulic model to calculate module Δp.

4. Calculate module weight, assuming solid block of material (copper or aluminum) in SEM-E size.

5. Using flow rate, coolant supply temperature, Δp, and heat exchanger weight, apply the results of Appendix C to calculate relative TOGW penalty. Assume fifteen 2000-W SEM-E modules.

Assumptions

The following assumptions were used to complete the TOGW portion of the preliminary design:

> 1) HFHE module volume was taken as constant for all designs, regardless of the number of orifice plates. A solid volume of 14.94 cm wide by 15.60 cm long by 0.254 cm thick was assumed.

2) A coolant Δp of 15 psi was allocated for the QDs, the headers, and distribution plumbing within the module. This assumption is poor because Δp will vary with flow rate, but a detailed knowledge of this variance was not known at the time of preliminary design.

3) The number of holes per CHIC orifice plate was kept constant and the hole diameter was varied which is reflected in x, y (ratio of hole pitch to hole diameter). A square impingement pattern was assumed ($x = y$).

4) A minimum plate thickness of 0.010 cm was considered. For fabrication considerations, orifice diameter was kept larger than plate thickness, and no less than 0.012 cm.

Results

Figures D.1 through D.13 show predicted aircraft TOGW sensitivity to CHIC design parameters. The ΔTOGWs shown are relative to an assumed baseline condition (which was chosen as a reference point for this preliminary design-phase study but differed from the final detailed design) as follows:

> CHIC material: copper
> Flow distribution: four CHICs in series (five in parallel)
> Module flow rate: 135 kg/hr
> Orifice pitch-to-diameter ratio (x,y) = 1.8
> Number of orifice plates: three
> Plate thickness: 0.010 cm (0.004 in)

Copper CHIC, Four CHICs in Series

Figures D.1, D.2, and D.3 show TOGW sensitivity to design parameters for the case of copper CHICs with four CHIC locations receiving coolant in series (or five in parallel).

Figure D.1 shows the sensitivity of TOGW to flow rate, orifice hole structure, and plate thickness. TOGW is fairly sensitive to hole structure at high flow rates. At the flow rate of minimum ΔTOGW (~ 300 kg/hr), however, hole structure has only a small impact on TOGW. TOGW is virtually unaffected by plate thickness. This result is due to high fin efficiency resulting from the use of a high thermal conductivity material.

Figure D.2 indicates that TOGW is fairly sensitive to the number of orifice plates, but at the flow rate which gives minimum TOGW, it is less sensitive. Pressure drop increases with the number of orifice plates as would be expected. As mentioned in Section 2.7 however, pressure drop will actually *decrease* with number of plates because the flow area in the manifold regions increases and reduces manifold Δp at a faster rate than orice Δp increases. This effect is not shown in Figure D.2 which was generated early in the preliminary design, but is shown in Figures X, Y, and Z.

Figure D.3 shows the contributions toward TOGW penalty by the four heat exchanger parameters (flow rate, pressure drop, coolant supply temperature, and fixed weight) for the specific design of four orifice plates and four CHICs cooled in series. As

flow rate is increased from zero, thermal performance improves rapidly which results in a higher allowable coolant supply temperature. Although the contribution toward TOGW from flow rate and pressure drop increases, the benefit of increased coolant supply temperature outweighs these two penalties and the net TOGW falls. A minimum is reached at a flow rate of about 250 kg/hr. At flow rates greater than this value, penalties incurred by high flow rate and pressure drop outweigh the benefit of higher coolant supply temperature, and net TOGW increases. Thus, this design would be optimized from a TOGW standpoint at a flow rate of 250 kg/hr.

Copper CHIC, Two CHICs in Series

Figures D.4, D.5, and D.6 are similar to Figures D1, D.2, and D.3, but apply to the case on two CHICs cooled in series (ten in parallel). This design incurs a lower pressure drop than the four-in-series design, and slightly lower TOGW penalty. In addition, system warm-up time under a cold start condition is reduced due to the reduced hydraulic resistance in the flow loop.

Copper CHIC, 1 CHIC in Series

Figures D.7, D.8, and D.9 are similar to Figures D1, D.2, and D.3, but apply to the case on all twenty CHICs cooled in parallel (one in series). This design incurs the lowest pressure drop, and lowest TOGW penalty. In addition, system warm-up time under a cold start condition will be minimized due to the reduced hydraulic resistance in the flow loop.

Aluminum CHIC

Figures D.10, D.11, and D.12 summarize TOGW penalty contributors for aluminum CHICs for four, two, and one CHIC cooled in series, respectively. They may be compared to Figures D.3, D.6, and D.9 for copper CHICs.

Overall Comparison

Figure D.13 compares the total TOGW penalty for all six designs studied - three copper and three aluminum, each material with one, two, and four CHICs cooled in series. The all-in-parallel copper design incurs the lowest TOGW penalty. TOGWs incurred by copper designs are five to twelve kg lower than those incurred by aluminum designs. The copper design also incurs the lowest thermal resistance in a cold-start scenario. Based on these two considerations, this design is optimal.

ΔTOGW based on cooling
fifteen 2000-W modules
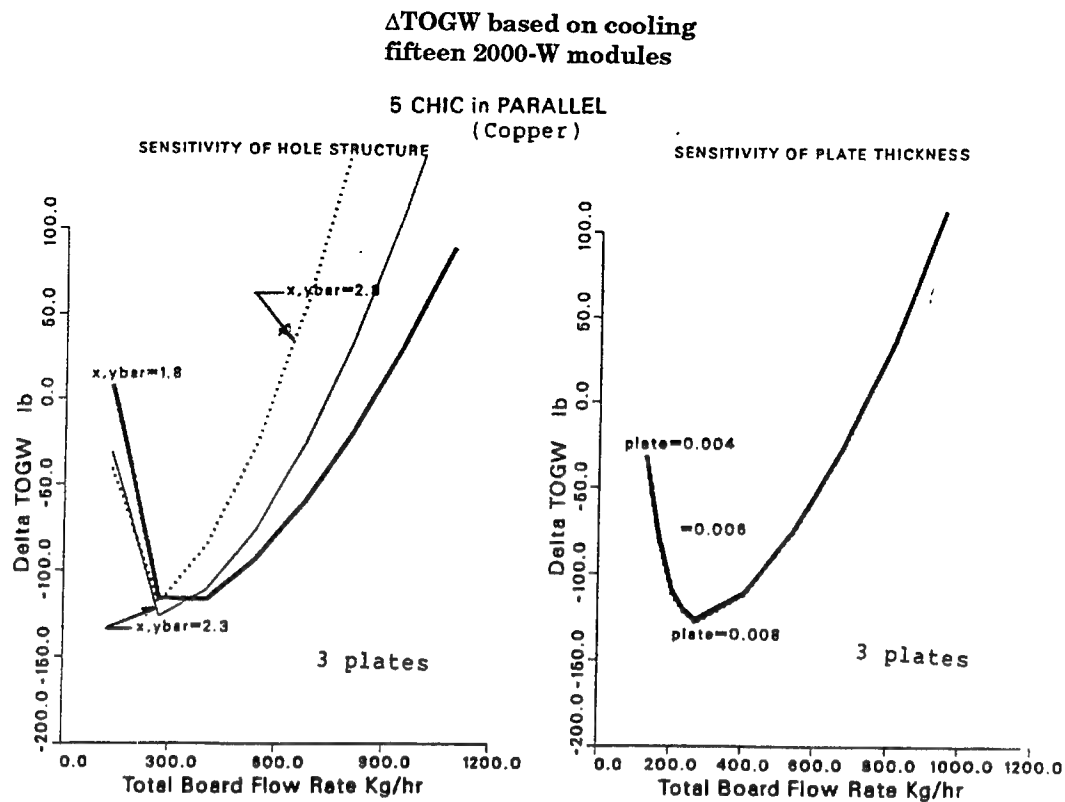
Figure D.1. TOGW Sensitivity to Hole Structure and Plate Thickness, Five
Copper CHICs in Parallel
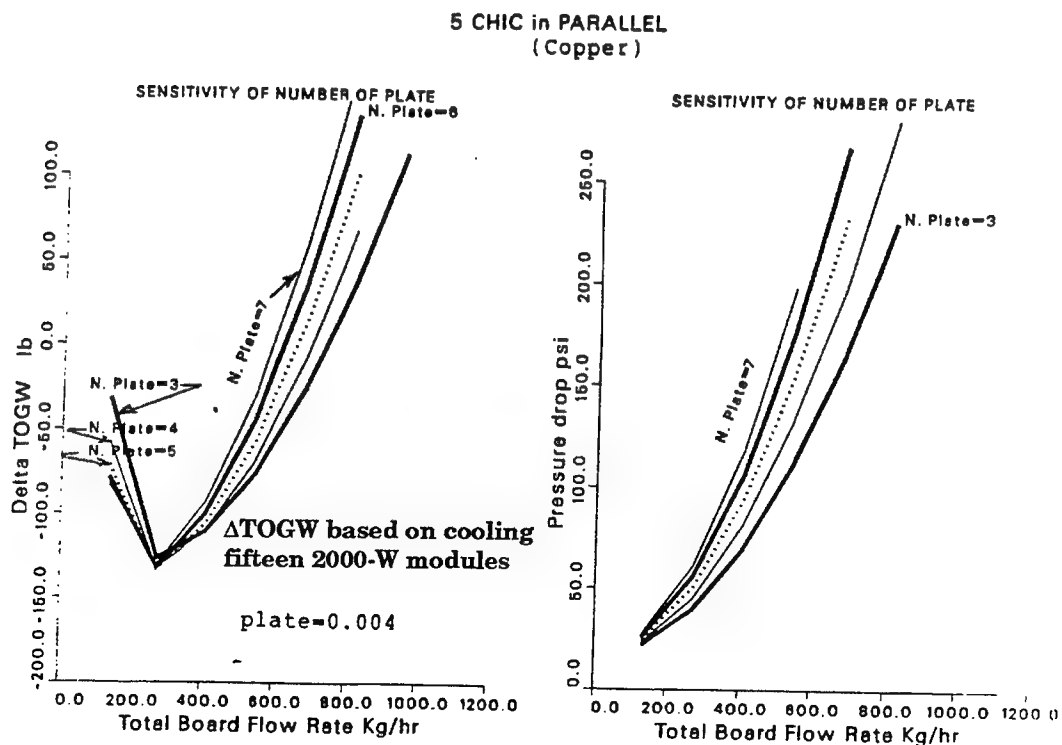
Figure D.2. TOGW and Pressure Drop Sensitivity to Number of Plates, Five
Copper CHICs in Parallel

70
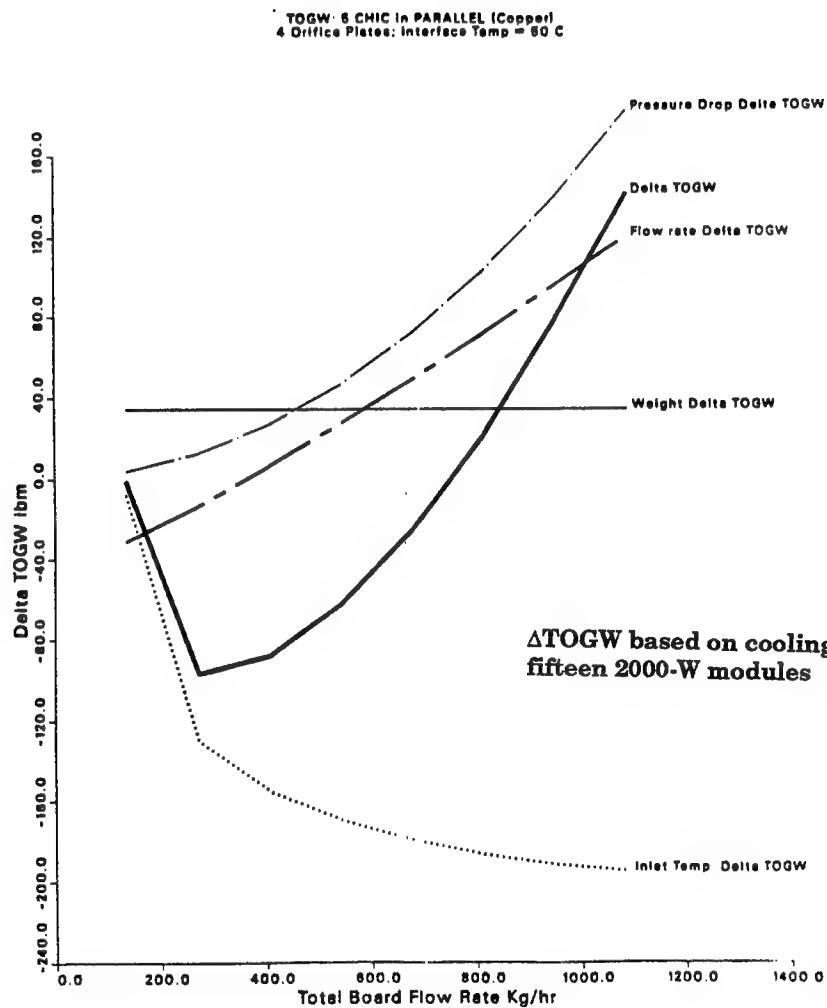
Figure D.3. TOGW Sensitivity Summary, Five Copper CHICs in Parallel

71

ΔTOGW based on cooling
fifteen 2000-W modules

10 CHIC in PARALLEL
(copper)

SENSITIVITY OF HOLE STRUCTURE

SENSITIVITY OF PLATE THICKNESS
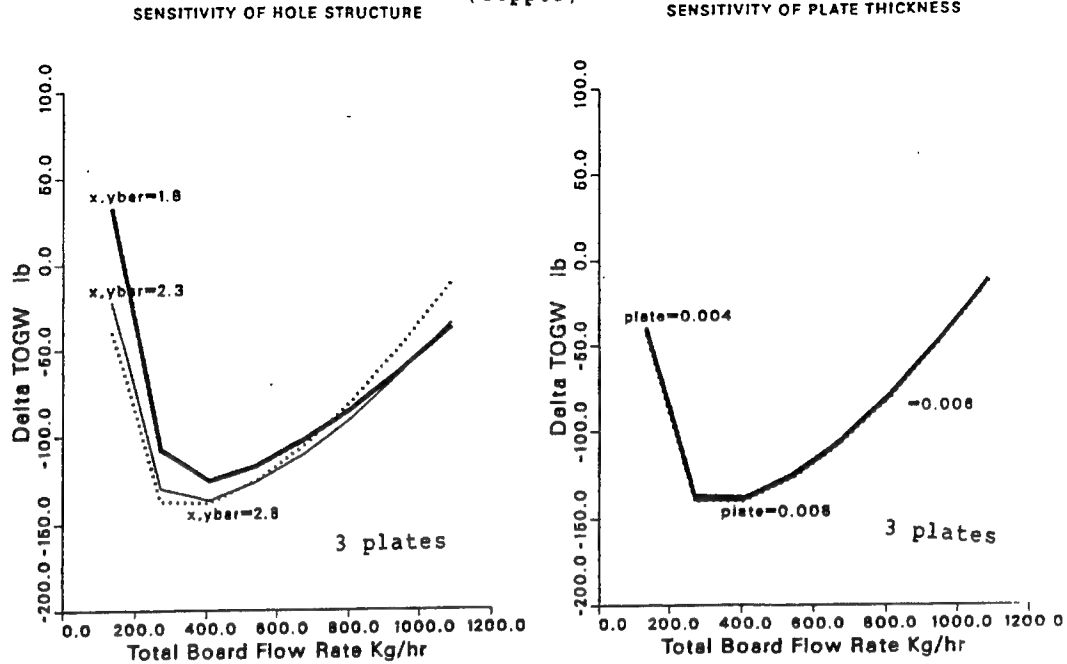
Figure D.4. TOGW Sensitivity to Hole Structure and Plate Thickness, Ten Copper CHICs in Parallel

10 CHIC in PARALLEL
(copper)

SENSITIVITY OF NUMBER OF PLATE

SENSITIVITY OF NUMBER OF PLATE
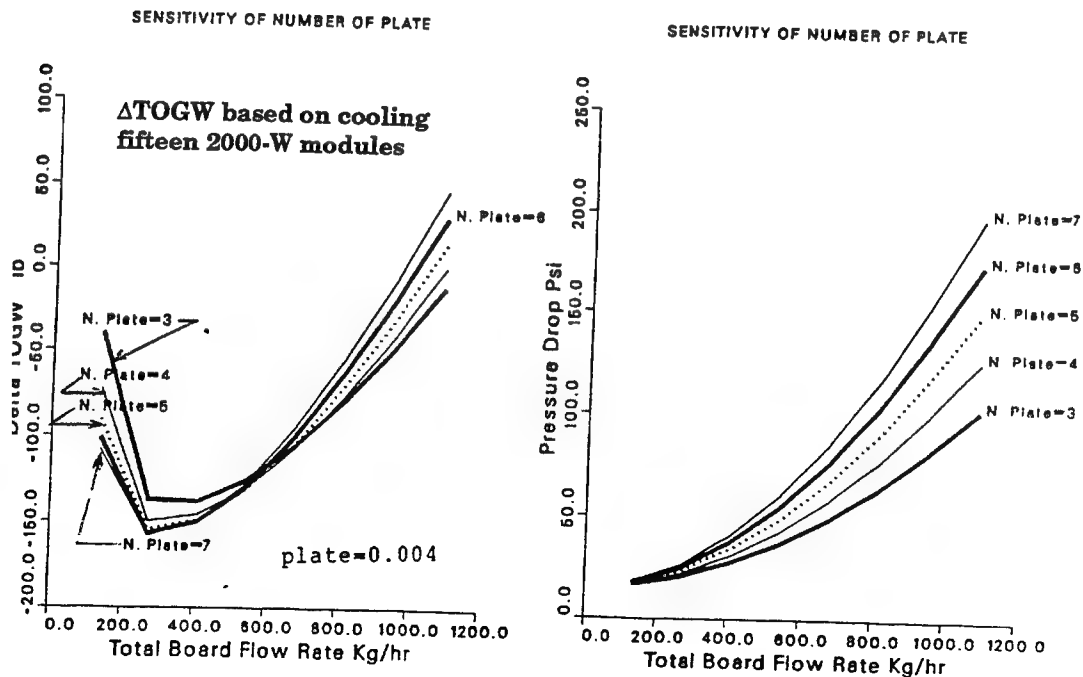
Figure D.5. TOGW and Pressure Drop Sensitivity to Number of Plates, Ten Copper CHICs in Parallel

72
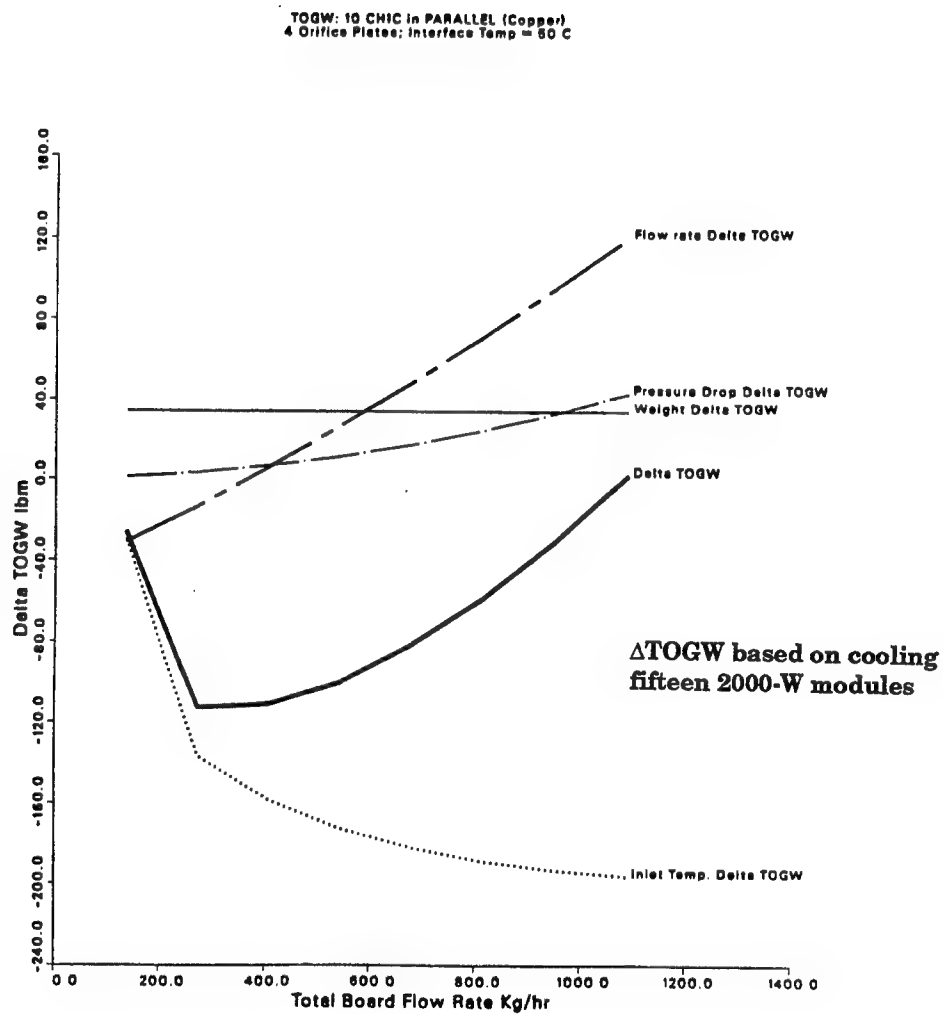
Figure D.6. TOGW Sensitivity Summary, Ten Copper CHICs in Parallel

ΔTOGW based on cooling fifteen 2000-W modules

20 CHIC in PARALLEL
(Copper)

SENSITIVITY OF HOLE STRUCTURE

SENSITIVITY OF PLATE THICKNESS
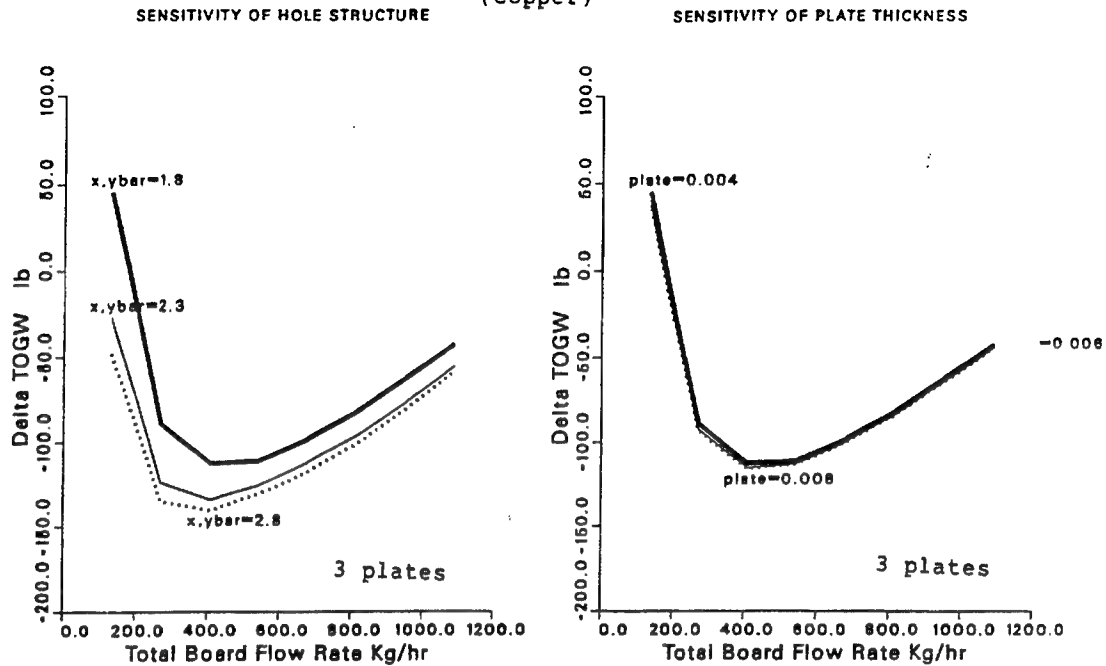
Figure D.7. TOGW Sensitivity to Hole Structure and Plate Thickness, Twenty Copper CHICs in Parallel

20 CHIC in PARALLEL
(Copper)

SENSITIVITY OF NUMBER OF PLATE

SENSITIVITY OF NUMBER OF PLATE
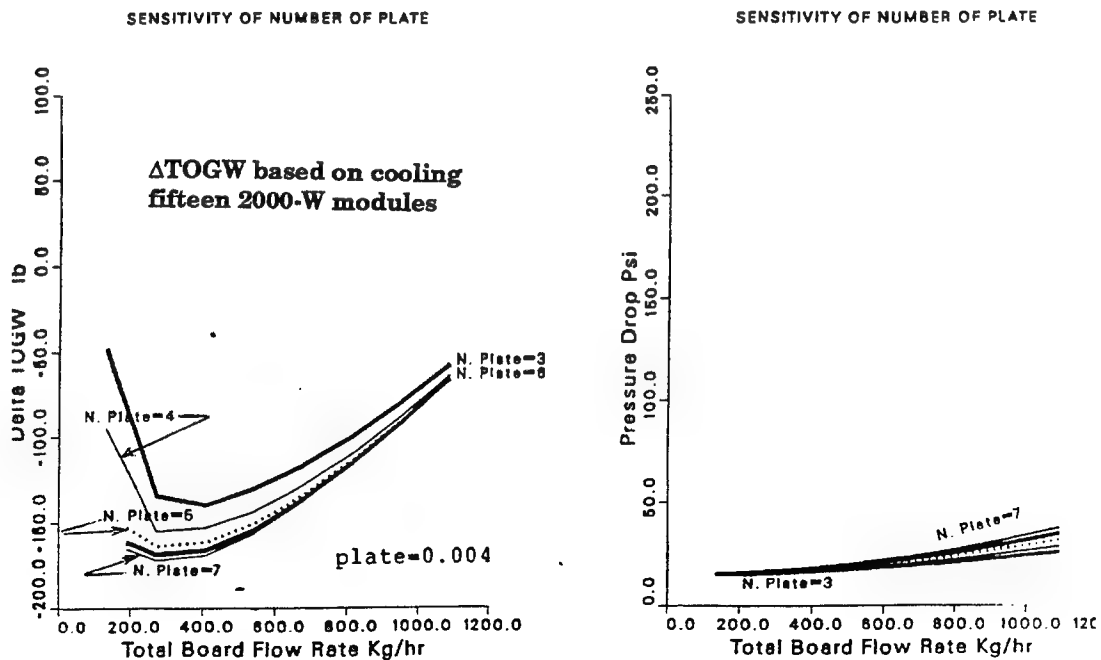
Figure D.8. TOGW and Pressure Drop Sensitivity to Number of Plates, Twenty Copper CHICs in Parallel

74
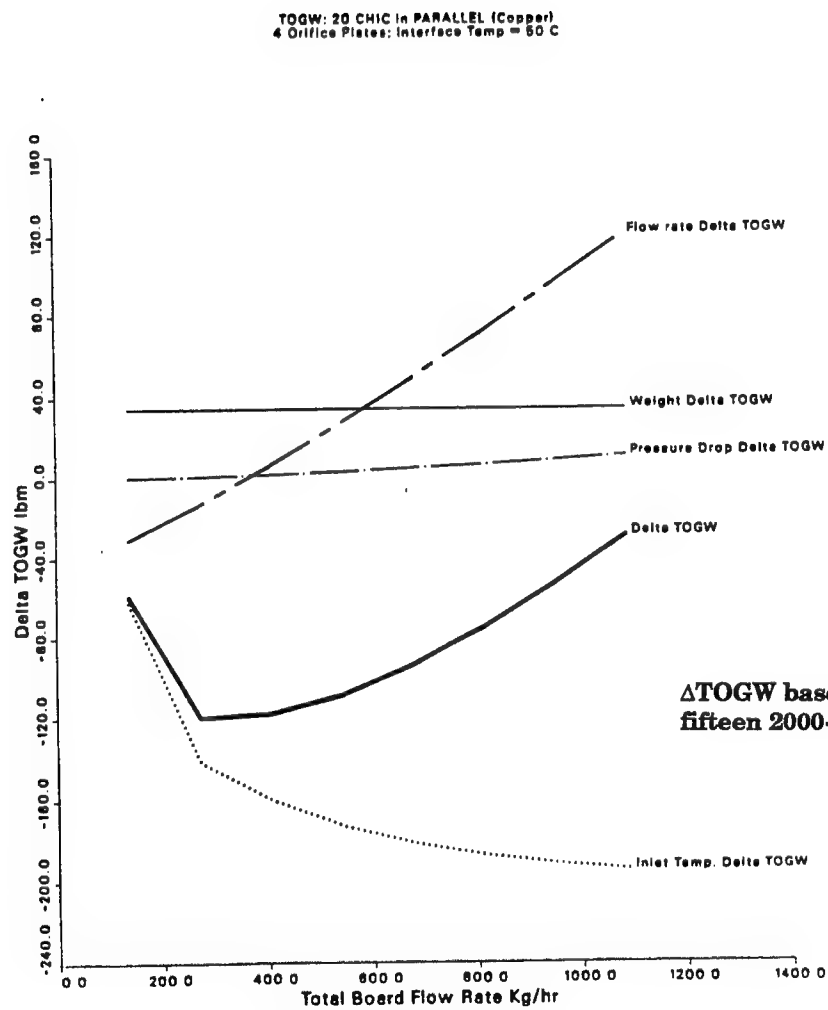
Figure D.9. TOGW Sensitivity Summary, Twenty Copper CHICs in Parallel
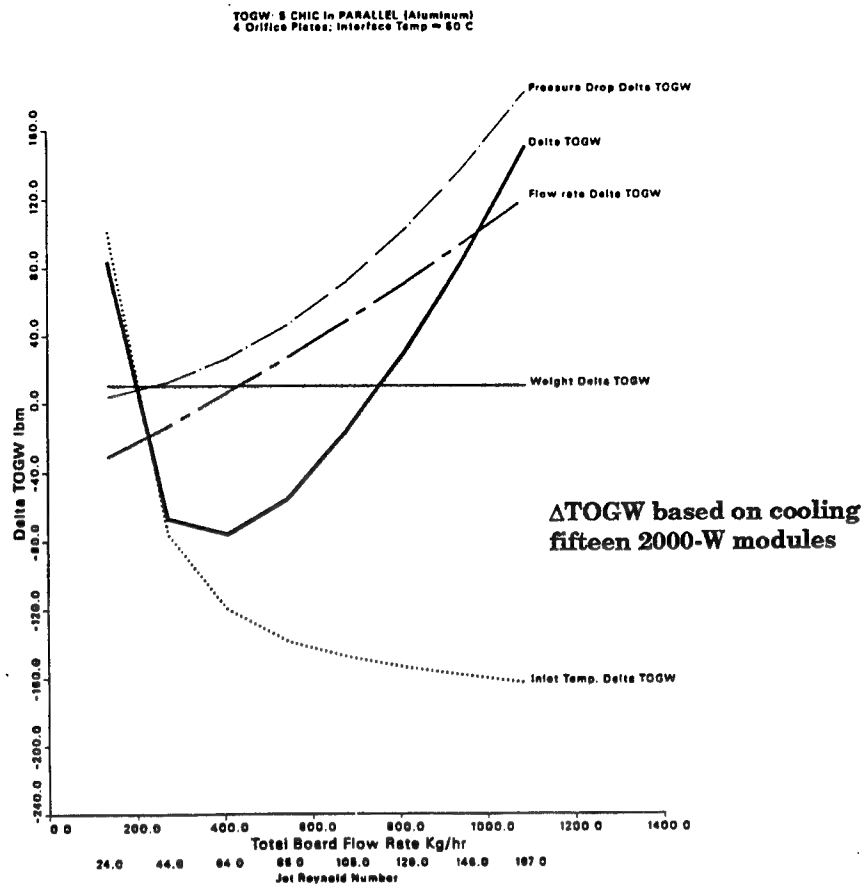
Figure D.10. TOGW Sensitivity Summary, Five Aluminum CHICs in Parallel
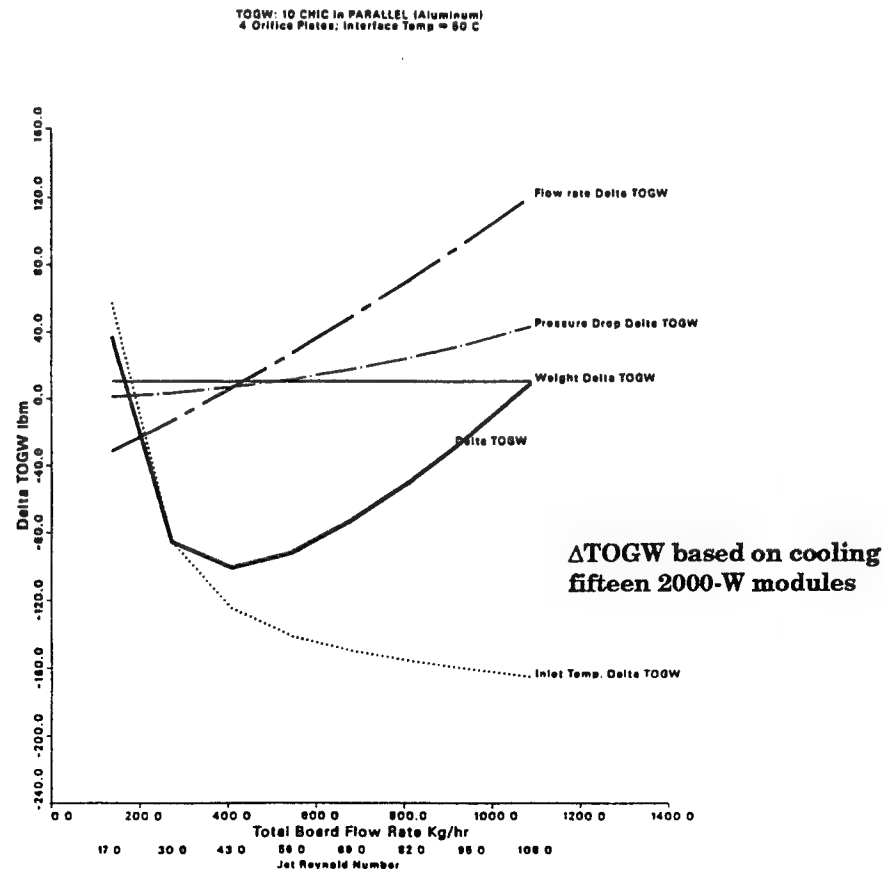
Figure D.11. TOGW Sensitivity Summary, Ten Aluminum CHICs in Parallel
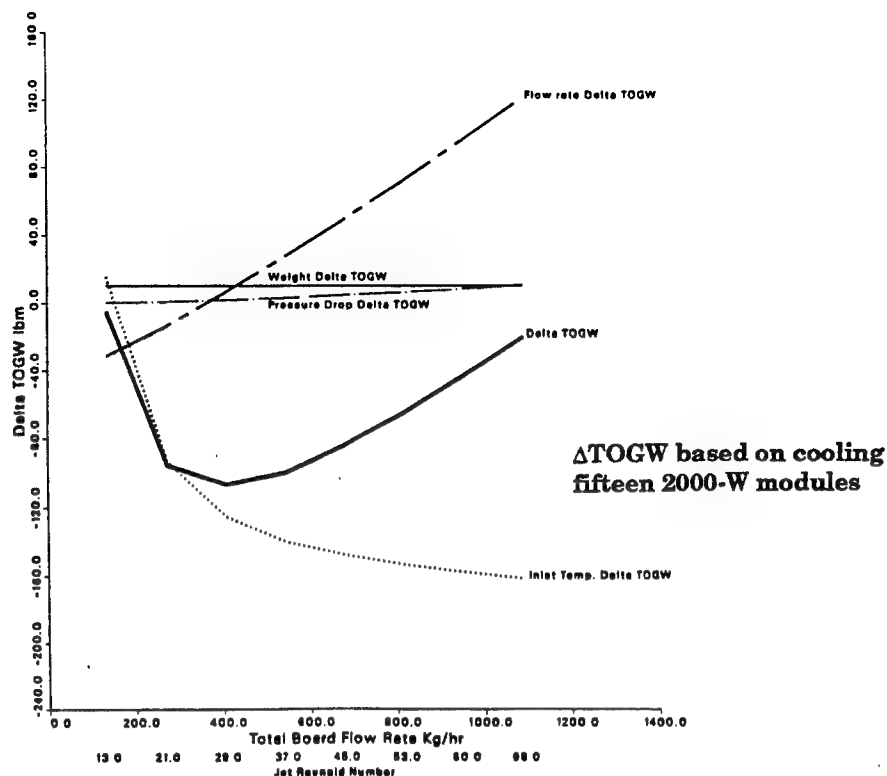
Figure D.12 TOGW Sensitivity Summary, Twenty Aluminum CHICs in Parallel
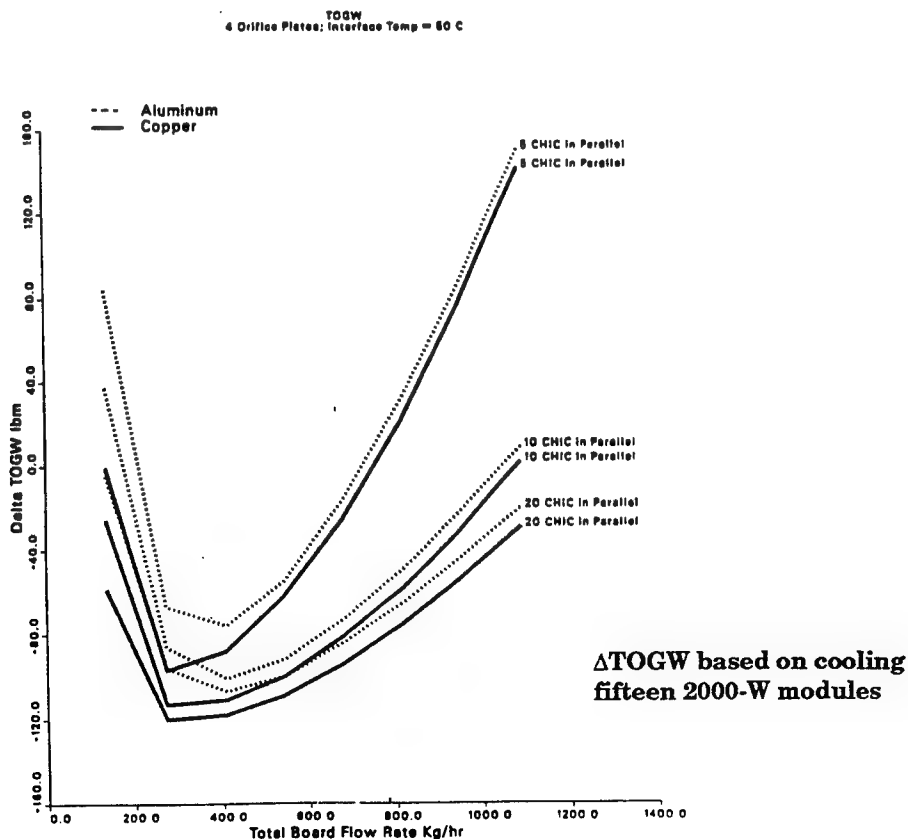
Figure D.13. TOGW Sensitivity Summary, Copper vs. Aluminum

APPENDIX E

LAMINATE DRAWINGS AND STACKING ORDER

Plate Number	Plate Type	Description	Thickness	
			cm	in
1	A	Target	0.038	0.015
2	A	Target	0.038	0.015
3	B	Target Spacer	0.038	0.015
4	C	Orifice	0.010	0.004
5	D	Spacer	0.010	0.004
6	C*	Orifice (Flipped)	0.010	0.004
7	D	Spacer	0.010	0.004
8	C	Orifice	0.010	0.004
9	E	Spacer/Manifold Divider	0.038	0.015
10	C*	Orifice (Flipped)	0.010	0.004
11	D	Spacer	0.010	0.004
12	C	Orifice	0.010	0.004
13	D	Spacer	0.010	0.004
14	C*	Orifice (Flipped)	0.010	0.004
15	D	Spacer	0.010	0.004
16	C	Orifice	0.010	0.004
17	D	Spacer	0.010	0.004
18	C*	Orifice (Flipped)	0.010	0.004
19	D	Spacer	0.010	0.004
20	C	Orifice	0.010	0.004
21	F	Distributor	0.038	0.015
22	F	Distributor	0.038	0.015
23	F	Distributor	0.038	0.015
24	G	Back Cover	0.038	0.015
		TOTAL	0.467	0.184

Figure E.1 CHIC Plate Stacking Order, Unit #2
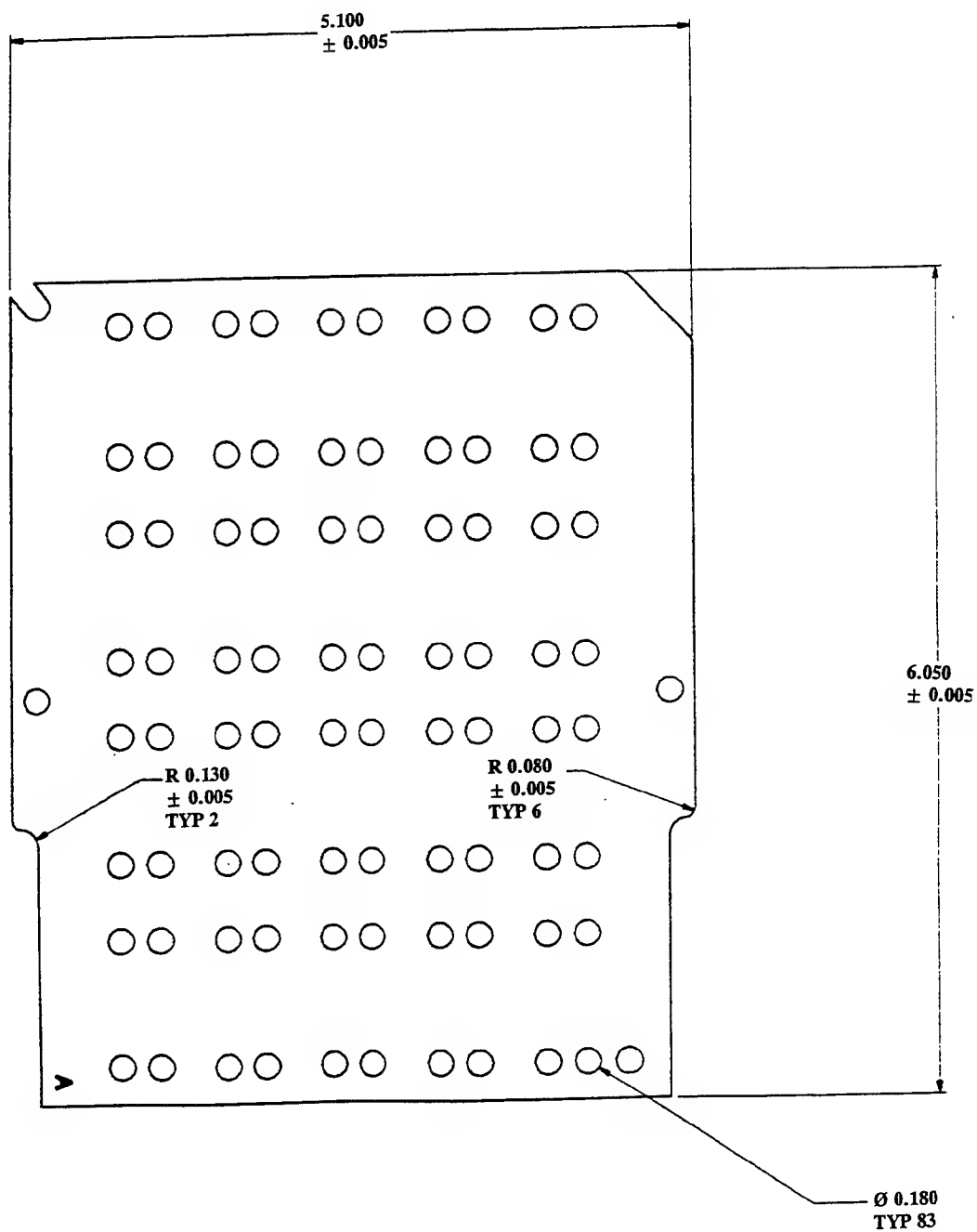
Figure E.2 Plate "A" , Target Plate.

5.100
± 0.005

6.050
± 0.005
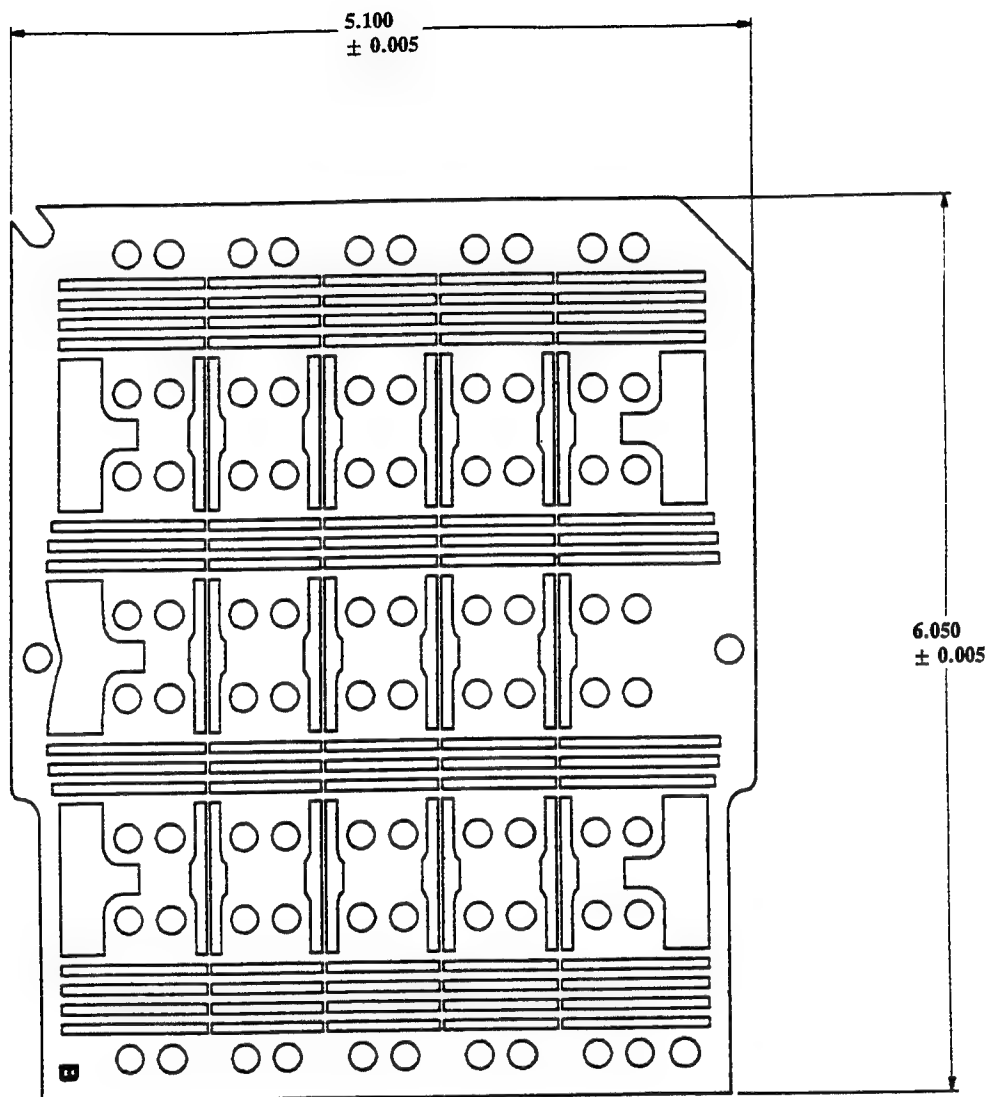
Thickness = 0.015 in.
Dimensions in inches

Figure E.3 Plate "B" , Target Spacer.

5.100
± 0.005

6.050
± 0.005

Ø 0.187
0.180
TYP
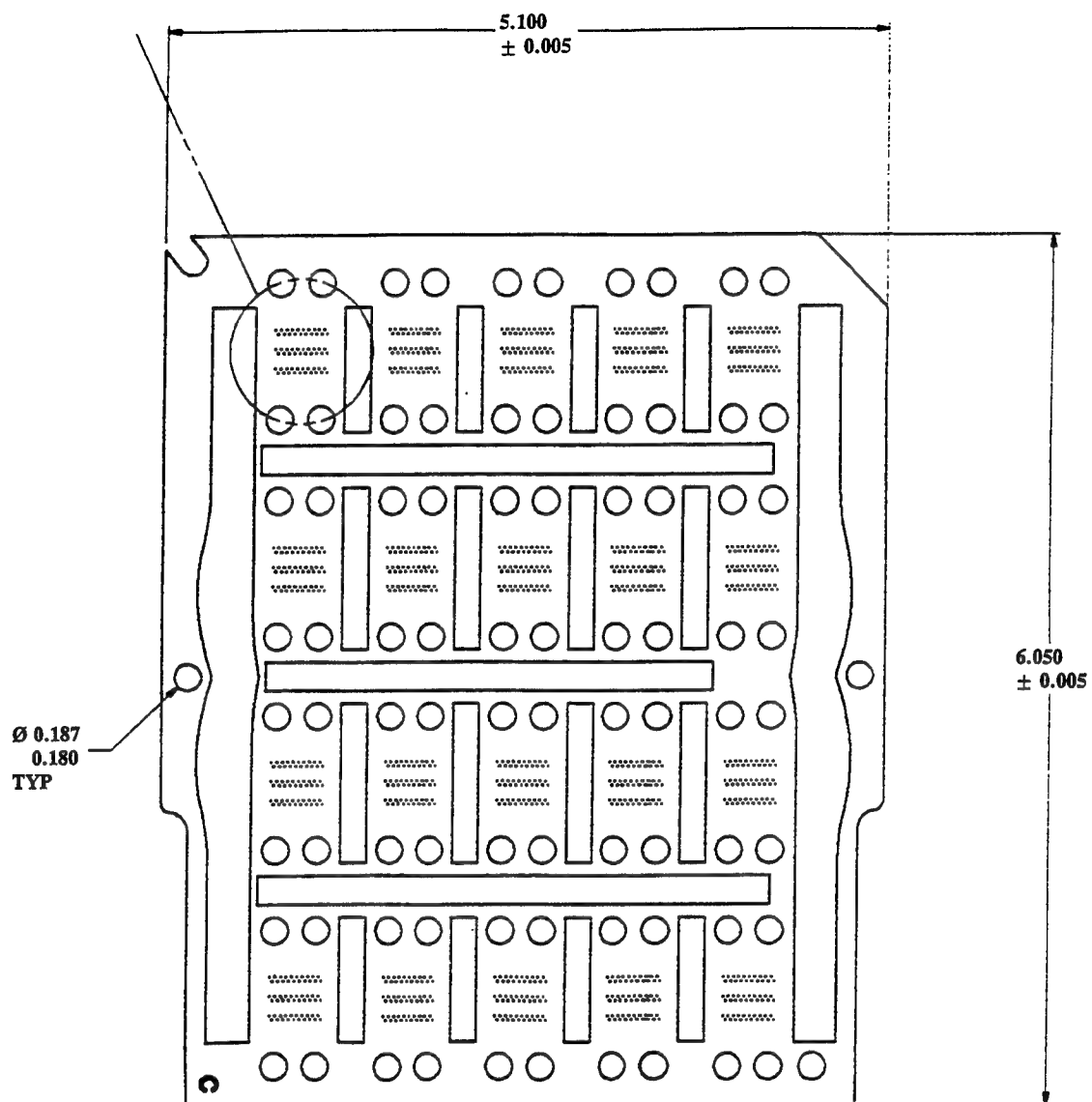
Thickness = 0.004 in.
Dimensions in inches

Figure E.4 Plate "C" , Orifice Plate.

82

5.100
± 0.005

6.050
± 0.005

Ø .187
.180
TYP
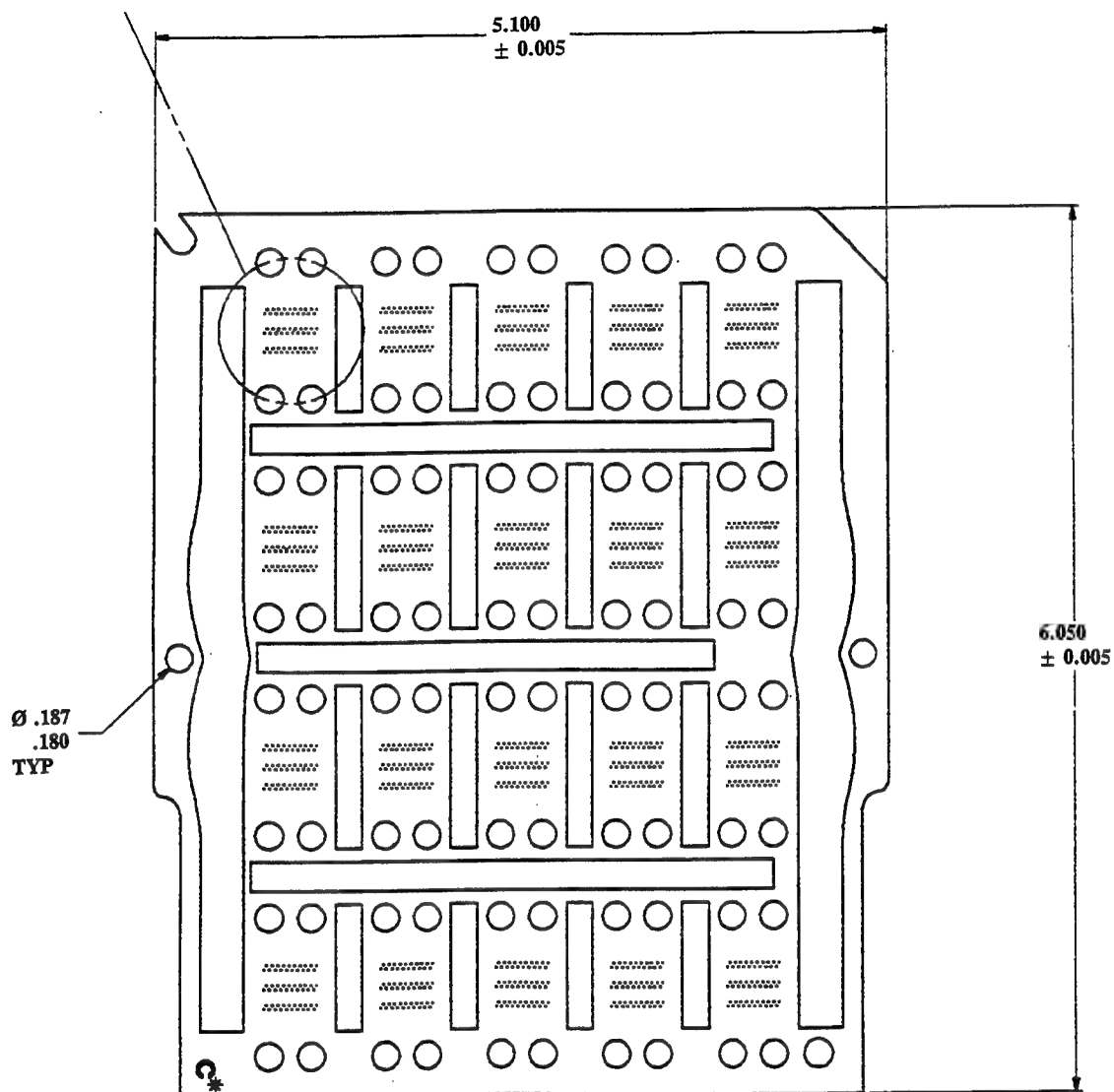
Thickness = 0.004 in.
Dimensions in inches

Figure E.5 Plate "C*" , Orifice Plate, Orifices Staggered Relative to Plate "C"

5.100
± 0.005

6.050
± 0.005

Ø .187
.180
TYP
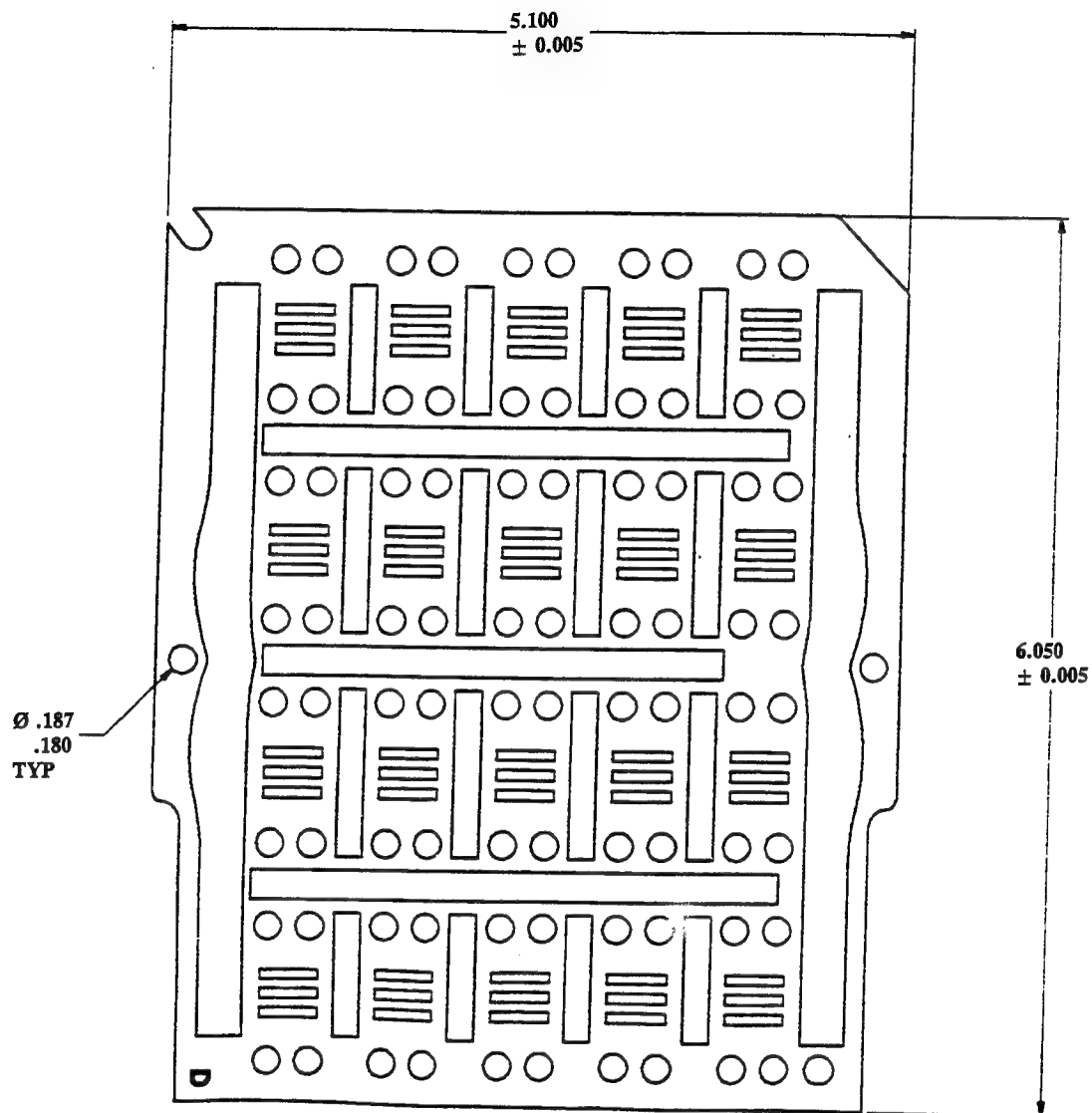
Thickness = 0.004 in.
Dimensions in inches

Figure E.6 Plate "D" , Spacer Plate.

5.100
± 0.005

6.050
± 0.005

Ø .187
.180
TYP
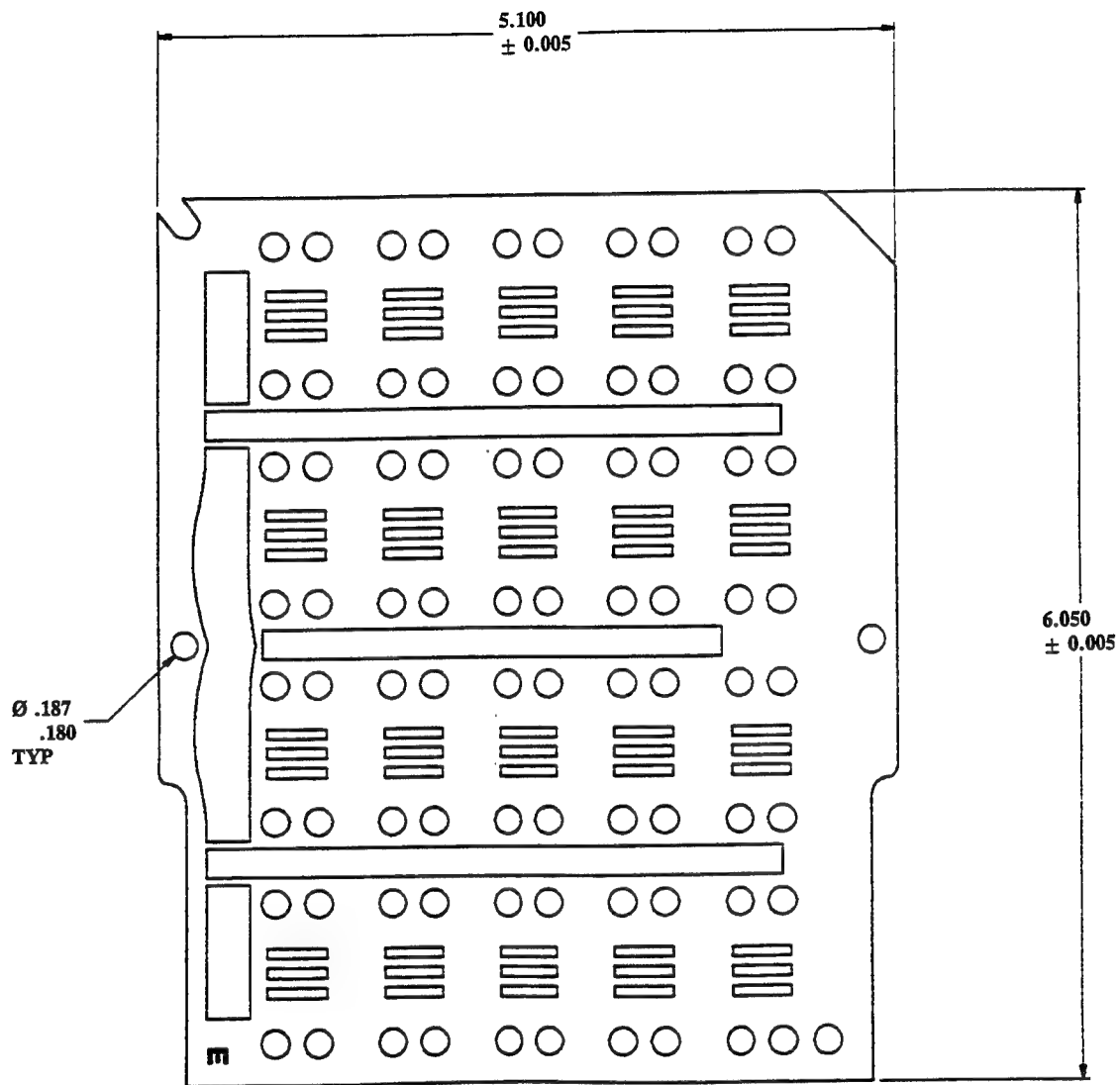
Thickness = 0.015 in.
Dimensions in inches

Figure E.7 Plate "E" , Spacer/Manifold Divider Plate.

85

5.100
± 0.005

6.050
± 0.005

Ø .187
.180
TYP
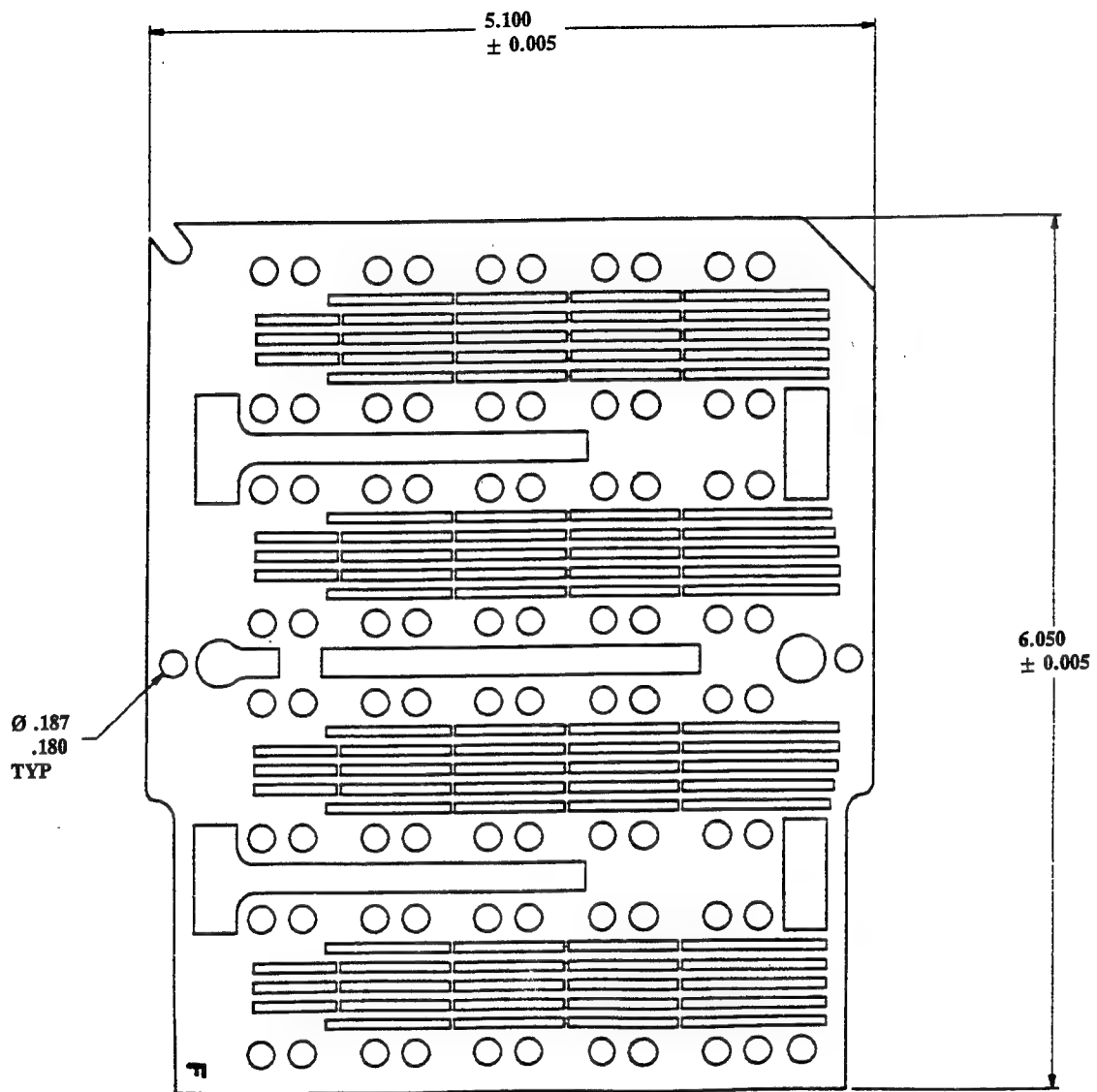
Thickness = 0.015 in.
Dimensions in inches

Figure E.8 Plate "F" , Distributor Plate.

5.100
± 0.005

6.050
± 0.005
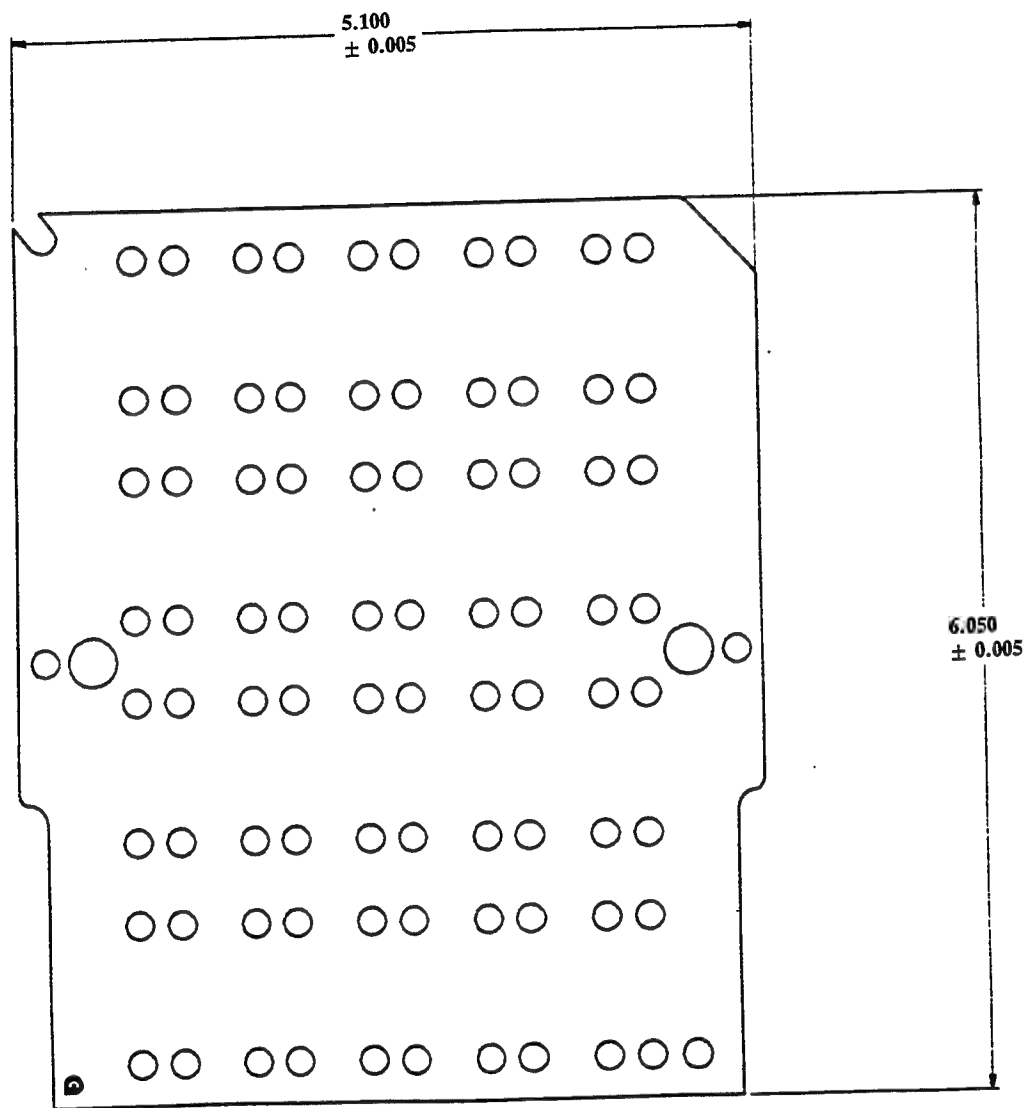
Thickness = 0.015 in.
Dimensions in inches

Figure E.9 Plate "G" , Back Cover.

HFHE PLATE STACKING ORDER

PERFECT Builds (#1 & 2) — Best Units

Plate No.	Plate Type	Thickness (Inch)	Description
Top	A	0.015	Target
2	A	0.015	Target
3	B	0.015	Target Spacer
4	C	0.004	Orifice
5	D	0.004	Spacer
6	C*small	0.004	Flipped Orifice
7	D	0.004	Spacer
8	C	0.004	Orifice
9	E	0.015	Manifold Divider / Spacer
10	C*small	0.004	Flipped Orifice
11	D	0.004	Spacer
12	C	0.004	Orifice
13	D	0.004	Spacer
14	C*small	0.004	Flipped Orifice
15	D	0.004	Spacer
16	C	0.004	Orifice
17	D	0.004	Spacer
18	C*small	0.004	Flipped Orifice
19	D	0.004	Spacer
20	C	0.004	Orifice
21	F	0.015	Distributor
22	F	0.015	Distributor
23	F	0.015	Distributor
24	G	0.015	Additional Bottom Cover on #1
Bottom 25	G	0.015	Bottom Cover
TOTALs		0.199 or 0.184	

A	4
B	2
C	10
C*small	8
C*BIG	0
D	14
E	2
F	6
G	3
Total	49

THERMAL Builds (#3 & 4) — Very Good

Plate No.	Plate Type	Thickness (Inch)
Top	A	0.015
2	A	0.015
3	B	0.015
4	C	0.004
5	D	0.004
6	C*BIG	0.004
7	D	0.004
8	C	0.004
9	E	0.015
10	C*small	0.004
11	D	0.004
12	C	0.004
13	D	0.004
14	C*small	0.004
15	D	0.004
16	C	0.004
17	D	0.004
18	C*small	0.004
19	D	0.004
20	C	0.004
21	F	0.015
22	F	0.015
23	F	0.015
24	G	0.015 on #4 only
Bottom 25	G	0.015
TOTALs		0.199 or 0.184

A	4
B	2
C	10
C*small	6
C*BIG	2
D	14
E	2
F	6
G	3
Total	49

PRESSURE Builds (#5 & 6) — Good Units

Plate No.	Plate Type	Thickness (Inch)
Top	A	0.015
2	A	0.015
3	B	0.015
4	C	0.004
5	D	0.004
6	C	0.004
7	D	0.004
8	C	0.004
9	E	0.015
10	C	0.004
11	D	0.004
12	C	0.004
13	D	0.004
14	C	0.004
15	D	0.004
16	C	0.004
17	D	0.004
18	C	0.004
19	D	0.004
20	C	0.004
21	F	0.015
22	F	0.015
23	F	0.015
Bottom 24	G	0.015
TOTALs		0.184

A	4
B	2
C	18
C*small	0
C*BIG	0
D	14
E	2
F	6
G	2
Total	48

BONDING Builds (#7, 8 & 9) — Proof and Leak ONLY

Plate No.	Plate Type	Thickness (Inch)
Top	A	0.015
2	A	0.015
3	B	0.015
4	C*BIG	0.004
5	D	0.004
6	C*BIG	0.004
7	D	0.004
8	C*BIG	0.004
9	E	0.015
10	C*BIG	0.004
11	D	0.004
12	C*BIG	0.004
13	D	0.004
14	C*BIG	0.004
15	D	0.004
16	C*BIG	0.004
17	D	0.004
18	C*BIG	0.004
19	D	0.004
20	C*BIG	0.004
21	F	0.015
22	F	0.015
23	F	0.015
Bottom 24	G	0.015 --Note
TOTALs		0.184 or 0.169

A	6
B	3
C	0
C*small	0
C*BIG	27
D	21
E	3
F	9
G	1
Total	70

PRACTICE STACK (#10) — Bonding ONLY

Plate No.	Plate Type	Thickness (Inch)
Top	A	0.015
2	A	0.015
3	4 x C	0.016
4	C	0.004
5	C	0.004
6	C*BIG	0.004
7	D	0.004
8	C*BIG	0.004
9	4 X C*BIG	0.015
10	C*BIG	0.004
11	D	0.004
12	C*BIG	0.004
13	D	0.004
14	C*BIG	0.004
15	D	0.004
16	C*BIG	0.004
17	D	0.004
18	C*BIG	0.004
19	D	0.004
20	C*BIG	0.004
21	3XC*BIG	0.012
22	F	0.015
23	F	0.015
Bottom 24	G	0.015
TOTALs		0.192

	TOTALs	Delivered
A	2	20
B	0	9
C	6	44
C*small	0	14
C*BIG	15	44
D	6	69
E	0	9
F	2	29
G	1	10
Total	32	248

-- Note : Units #8 and #9 do not have plate G

||| NOTE: Units must be Stacked from bottom to top with letter designator visible to Stacker

Figure E.10 Plate Stacking Order for All Units

Units #2, 3, 4, 6, and 10 were bonded.

APPENDIX F

SUMMARY OF PERFORMANCE TEST DATA

Table F.1 summarizes important test data from each steady-state test conducted. This does not include all data gathered, such as surface temperature measurements, amplifier temperature profiles, and so on, but only the most essential data. Each test conducted was assigned a unique test I.D. number, so that the full raw data set (not included in this report) can be readily referenced if necessary.

Table F.1

Summary of Test Data

TEST ID*	TEST NO.**	TEST SITE	COOLANT SUPPLY TEMP. (°C)	COOLANT FLOW RATE (gpm)***	AMPLIFIER HEAT FLUX (W)	Δp HFHE + supply / return lines (psi)
1	1	A	20.00	0.35	0	5.55
2	1	A	20.13	0.35	0	5.83
3	2	A	20.43	0.60	0	11.94
4	2	A	20.05	0.60	0	11.91
5	2	A	20.08	0.60	0	12.40
6	3	A	20.29	0.90	0	21.65
7	3	A	19.46	0.89	0	21.54
8	3	A	20.34	0.90	0	21.43
9	4	A	19.64	1.19	0	34.00
10	4	A	20.83	1.20	0	33.86
11	4	A	19.62	1.19	0	33.73
12	5	A	20.40	0.35	0	5.49
13	5	A	20.54	0.35	0	5.81
14	6	A	19.91	0.59	9.17	11.70
15	7	A	20.22	0.60	21.69	11.97
16	7	A	20.15	0.59	21.81	11.83
17	7	A	21.87	0.59	21.87	11.49
18	7	A	19.35	0.59	24.06	11.83
19	8	A	19.12	0.89	47.21	21.14
20	8	A	19.61	0.89	46.79	21.37
21	8	A	19.96	0.89	46.26	21.47
22	8	A	20.08	1.19	45.62	33.43
23	8	A	19.34	1.16	44.19	32.36
24	9	A	20.06	1.19	67.00	33.67
25	9	A	19.40	1.19	68.54	33.87
26	9	A	20.08	1.19	67.24	33.39
27	9	A	19.53	1.20	64.50	33.95
28	10	A	20.29	1.22	98.63	34.86
29	10	A	19.36	1.22	100.24	35.04
30	11	A	20.93	1.20	0	33.29
31	12	A	19.47	0.89	75.60	21.18

32	12	A	19.72	0.89	76.03	21.04
33	12	A	19.09	1.20	78.82	33.94
34	12	A	20.27	1.20	76.92	33.55
35	13	A	19.75	0.60	72.26	11.82
36	13	A	20.12	0.60	71.26	11.62
37	13	A	20.26	0.35	66.85	5.89
38	13	A	20.24	0.35	67.41	5.48
39	14	A	30.28	1.23	50.56	31.68
40	15	A	39.30	1.22	48.07	29.50
41	15	A	40.51	1.21	24.17	28.40
42	15	A	39.40	1.21	24.74	28.64
43	16	A	1.78	0.57	86.52	17.28
44	20	A	22.98	0.36	60.89	5.57
45	20	A	22.98	0.36	60.61	6.06
46	21	A	22.90	0.62	65.53	12.11
47	21	A	22.82	0.63	65.59	11.81
48	8	B	19.45	1.15	44.76	32.24
49	8	B	19.33	1.15	44.71	31.97
50	9	B	19.63	1.19	79.38	33.56
51	9	B	19.64	1.18	63.23	33.29
52	25	C	20.11	0.34	54.60	6.12
53	9	C	19.72	1.17	57.4	32.71
54	26	D	10.87	0.31	51.75	5.92
55	26	D	10.87	0.31	51.85	6.09
56	27	D	10.15	0.59	53.15	14.22
57	27	D	9.90	0.59	53.53	14.46
58	29	D	9.00	1.14	56.44	36.89
59	29	D	9.70	1.13	54.46	36.26
60	13	D	20.01	0.64	45.47	12.56
61	21	D	20.03	0.64	45.35	12.83
62	30	D	30.55	0.39	49.38	5.35
63	30	D	30.80	0.39	49.34	5.17
64	32	D	31.80	0.88	49.19	18.58
65	32	D	30.80	0.88	50.78	18.24
66	14	D	30.95	1.19	49.65	29.77
67	14	D	31.37	1.19	50.12	30.03
68	33	D	40.59	0.42	44.63	5.96
69	33	D	40.59	0.41	44.83	5.27
70	35	D	41.36	0.89	46.39	17.52
71	35	D	41.41	0.89	46.24	17.16
72	15	D	41.46	1.20	45.55	28.38
73	15	D	39.62	1.20	47.52	28.38
74	25	D	20.36	0.35	78.73	6.18
75	25	D	20.29	0.35	78.60	5.71
76	13	D	19.87	0.64	76.83	12.70
77	13	D	19.70	0.63	77.22	13.02
78	12	D	20.25	0.90	79.41	21.47
79	12	D	19.56	0.89	80.57	21.45
80	12	D	20.53	0.90	79.92	21.24
81	9	D	20.25	1.19	82.13	32.83
82	9	D	19.80	1.18	82.01	33.10
83	10	D	20.24	1.19	101.0	33.03
84	10	D	20.37	1.19	100.6	32.97

85	10	D	19.54	1.18	118.61	33.20
86	10	D	18.80	1.18	118.94	33.62

* A unique Test I.D. number was assigned to each test conducted.
** Refer to Table 17 for Test Number.
*** Gallons per minute

Table F.2 summarizes important test data from each transient test conducted. This does not include all data gathered, such as surface temperature measurements, but only the most essential data. Each test conducted was assigned a unique test I.D. number, so that the full raw data set (not included in this report) can be readily referenced if necessary.

Table F.2

Summary of Transient Test Data

TEST I.D. *	TEST SITE	COOLANT SUPPLY TEMP. (°C)	COOLANT FLOW RATE (gpm)	MAXIMUM HEAT FLUX (W)	PERIOD OF HEAT FLUX RAMP-UP (Sec)	Δp (HFHE + supply / return lines (psi)
87	D	20.75	1.20	24.0	S.S.	33.40
88	D	20.07	1.20	71.2	7	33.48
89	D	20.49	1.20	108.9	6	33.67
90	D	19.06	1.20	60	7	33.80
91	D	20.08	1.20	57	4	33.66
92	D	19.22	0.35	59	7	5.87
93	D	20.19	1.20	87	7	33.57
94	D	19.89	1.20	114	5	33.71
95	D	19.83	1.20	122	3.5	33.84
96	D	20.32	1.20	137	3	33.45
97	D	20.18	1.20	94	9	33.64
98	D	19.34	1.20	60	8	33.74

* A unique Test I.D. number was assigned to each test conducted.

APPENDIX G

PRESSURE DROP DATA AND DATA REDUCTION

Three steps were taken to derive pressure drop (Δp) across the HFHE:

I. Obtain raw pressure drop test data, which included Δp across HFHE plus 50 cm (20 in) of 4.65 mm (0.183 in) inner diameter supply/return copper tubing.

II. Measure pressure drop through copper tubing separately.

III. Subtract Δp associated with tubing from raw data Δp to obtain Δp solely through HFHE.

This method introduces some error because pipe entrance lengths, velocity profiles, and pipe turns between the two conditions (with HFHE in flow loop versus without) differ. However, using actual tubing pressure drop measurements, albeit with some error introduced, was deemed more reliable than using analytically derived Δp's of a complex flow configuration.

Step I. Raw Pressure Drop Data

Figure G.1 shows the test configuration and pressure measurement port locations. Pressure drop measurement includes the HFHE (copper insert plus aluminum header-frame), 50 cm (20 in) of 4.65 mm (0.183 in) inner diameter copper tubing, and several low-pressure-drop Swagelock ^{TM} fittings. The following tables group Δp measurement by coolant supply temperature:
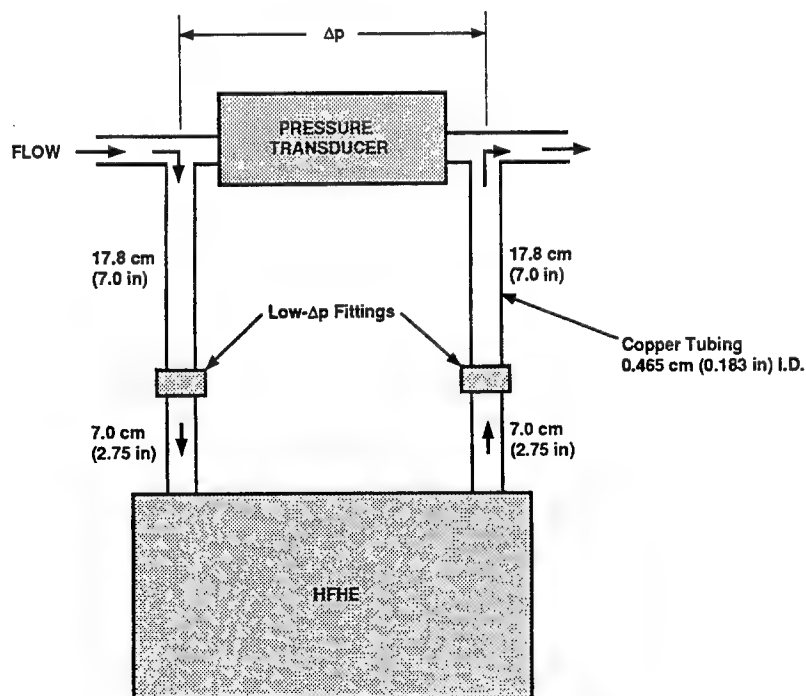
Figure G.1 Pressure Port Locations for HFHE Tests

Table G.1

Raw Pressure Drop Data, 10 °C Nominal Coolant Temperature

Test No. *	Test I.D. **	Flow Rate (gpm)***	Coolant Supply Temp. (°C)	Δp**** (psi)
26	54	0.31	10.87	5.92
26	55	0.31	10.87	6.09
Average		**0.31**		**6.00**
27	56	0.59	10.15	14.22
27	57	0.59	9.90	14.46
Average		**0.59**		**14.34**
29	58	1.14	9.00	36.89
29	59	1.13	9.70	36.26
Average		**1.135**		**36.58**

* Refer to Section 5.4.1, Table 17.

** A unique Test I.D. number was assigned to each test conducted, see App. F.

*** Gallons per minute

**** HFHE plus supply/return line pressure drop

Table G.2

Raw Pressure Drop Data, 20 °C Nominal Coolant Temperature

Test No. *	Test I.D. **	Flow Rate (gpm)***	Coolant Supply Temp. (°C)	Δp**** (psi)
1	2	0.35	20.00	5.55
5	12	0.35	20.40	5.49
5	13	0.35	20.54	5.81
13	37	0.35	20.26	5.89
13	38	0.35	20.24	5.48
25	74	0.35	20.36	6.18
25	75	0.35	20.29	5.71
29	92	0.35	19.22	5.87
Average		**0.35**		**5.75**
2	3	0.60	20.43	11.94
2	4	0.60	20.05	11.91
2	5	0.60	20.08	12.40
7	16	0.59	20.15	11.83
13	35	0.60	19.75	11.82
13	36	0.60	20.12	11.62
Average		**0.60**		**11.92**
3	6	0.90	20.24	21.65
3	7	0.89	19.46	21.54
3	8	0.90	20.34	21.43
8	20	0.89	19.61	21.37
8	21	0.89	19.96	21.47
12	78	0.90	20.25	21.47
12	79	0.89	19.56	21.45
12	80	0.90	20.53	21.24
Average		**0.895**		**21.45**
4	9	1.19	19.64	34.00
4	10	1.20	20.83	33.86
4	11	1.19	19.62	33.73
8	22	1.19	20.08	33.43
9	24	1.19	20.06	33.67
9	25	1.19	19.40	33.87
9	27	1.20	19.53	33.95
12	34	1.20	20.27	33.55
9	50	1.19	19.63	33.56
9	81	1.19	20.25	32.83
24	88	1.20	20.07	33.48
Average		**1.19**		**33.63**

* Refer to Section 5.4.1, Table 17.
** A unique Test I.D. number was assigned to each test conducted, see App. F.
*** Gallons per minute
**** HFHE plus supply/return line pressure drop

94

Table G.3

Raw Pressure Drop Data, 30 °C Nominal Coolant Temperature

Test No. *	Test I.D. **	Flow Rate (gpm)***	Coolant Supply Temp. (°C)	Δp**** (psi)
30	62	0.39	30.55	5.35
30	63	0.39	30.80	5.17
Average		**0.39**		**5.26**
32	64	0.88	31.80	18.58
32	65	0.88	30.80	18.24
Average		**0.88**		**18.41**
14	39	1.23	30.28	31.68
14	66	1.19	30.95	29.77
14	67	1.19	31.37	30.03
Average		**1.20**		**36.58**

* Refer to Section 5.4.1, Table 17.
** A unique Test I.D. number was assigned to each test conducted, see App. F.
*** Gallons per minute
**** HFHE plus supply/return line pressure drop

Table G.4

Raw Pressure Drop Data, 40 °C Nominal Coolant Temperature

Test No. *	Test I.D. **	Flow Rate (gpm)***	Coolant Supply Temp. (°C)	Δp**** (psi)
33	68	0.42	40.59	5.96
33	69	0.41	40.59	5.27
Average		**0.415**		**6.00**
35	70	0.89	41.36	17.52
35	71	0.89	41.41	17.16
Average		**0.89**		**17.34**
15	40	1.22	39.30	29.50
15	41	1.21	40.51	28.40
15	42	1.21	39.40	28.64
15	72	1.20	41.46	28.38
15	73	1.20	39.62	28.38
Average		**1.21**		**36.58**

* Refer to Section 5.4.1, Table 17.
** A unique Test I.D. number was assigned to each test conducted, see App. F.
*** Gallons per minute
**** HFHE plus supply/return line pressure drop

Step 2 - Tubing Pressure Drop

Figure G.2 shows the test configuration and pressure measurement port locations use to measure pressure drop in the copper supply/return lines. For these tests, the HFHE was removed and an additional 21.6 cm (8.5 in) of copper tubing was inserted in its place. The total length of tubing was 71.6 cm, as compared to 50 cm for the HFHE tests. Thus, Δp's obtained in these tests were multiplied by $50/71.6 = 0.7$, in step 3 below, to estimate tubing Δp in the HFHE tests. This method introduces some error because pipe entrance lengths, velocity profiles, and pipe turns between the two conditions (with versus without HFHE in flow loop) differ. However, using actual tubing pressure drop measurements, albeit with some error introduced, was deemed more reliable than using analytically derived Δp's of a complex flow configuration. Table G.5 shows tubing Δp measurement as a function of coolant supply temperature and flow rate.
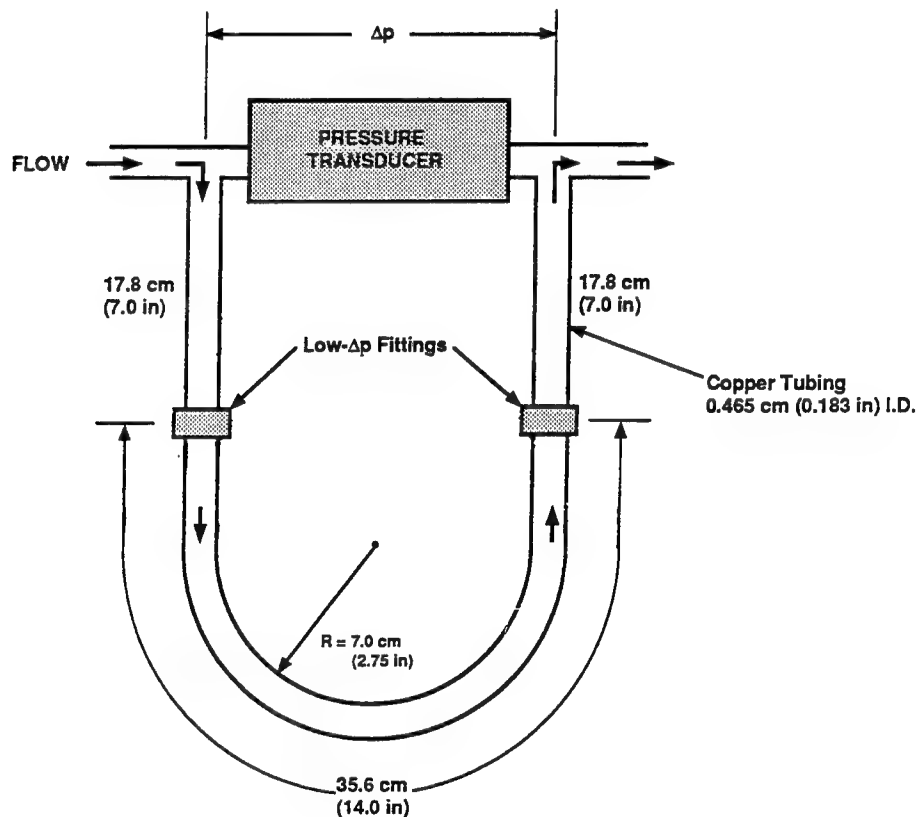

Figure G.2 Pressure Port Locations for Tube Pressure Drop Tests

Table G.5

Pressure Drop Measurement Through Copper Tubing

Note: All values are an average of two tests.
        Tubing length = 71.6 cm
        Tubing inner diameter =4.65 cm

Coolant Supply Temperature (°C)	Flow Rate (gpm)	Pressure Drop (psi)
10 °C Nominal Coolant Temperature		
9.68	0.45	4.41
10.01	0.60	6.19
9.78	0.90	11.08
9.88	1.20	17.49
20 °C Nominal Coolant Temperature		
20.53	0.505	3.81
20.37	0.60	5.09
20.30	0.90	9.47
20.45	1.20	15.00
30 °C Nominal Coolant Temperature		
29.99	0.54	4.01
29.99	0.60	4.57
29.73	0.90	8.40
30.30	1.20	14.23
40 °C Nominal Coolant Temperature		
40.06	0.60	4.33
40.06	0.90	8.43
40.04	1.20	13.41

Step 3 - Estimate HFHE Pressure Drop

Method employed: HFHE Δp = Δp from Step 1 - 0.7 * Δp from Step 2. Tables G.6 through G.9 show derived HFHE pressure drop as a function of coolant flow rate and temperature.

Table G.6
Derivation of HFHE Pressure Drop (10 °C Coolant Temperature)

Flow Rate (gpm)	Δp HFHE + 50 cm of lines (Step 1) (psi)	Δp (71.6 cm lines) (Step 2)* (psi)	Δp (HFHE) = Step 1 - 0.7* Step 2 (psi)
0.31	6.00	(3.04)	3.87
0.45		4.41	
0.59	14.34	(6.07)	10.09
0.60		6.19	
0.90		11.08	
1.135	36.58	(16.10)	25.31
1.20		17.49	

* Numbers in parentheses are interpolated or extrapolated.

Table G.7
Derivation of HFHE Pressure Drop (20 °C Coolant Temperature)

Flow Rate (gpm)	Δp HFHE + 50 cm of lines (Step 1) (psi)	Δp (71.6 cm lines) (Step 2)* (psi)	Δp (HFHE) = Step 1 - 0.7* Step 2 (psi)
0.35	5.75	(2.64)	3.90
0.505		3.81	
0.60	11.92	5.09	8.36
0.90	21.45	9.47	14.82
1.19	33.63	(14.82)	23.26
1.20		15.00	

* Numbers in parentheses are interpolated or extrapolated.

Table G.8
Derivation of HFHE Pressure Drop (30 °C Coolant Temperature)

Flow Rate (gpm)	Δp HFHE + 50 cm of lines (Step 1) (psi)	Δp (71.6 cm lines) (Step 2)* (psi)	Δp (HFHE) = Step 1 - 0.7* Step 2 (psi)
0.39	5.26	(2.90)	3.23
0.54		4.01	
0.60		4.57	
0.88	18.41	(8.14)	12.71
0.90		8.40	
1.20	30.49	14.23	20.53

* Numbers in parentheses are interpolated or extrapolated.

Table G.9

Derivation of HFHE Pressure Drop (40 °C Coolant Temperature)

Flow Rate (gpm)	Δp HFHE + 50 cm of lines (Step 1) (psi)	Δp (71.6 cm lines) (Step 2)* (psi)	Δp (HFHE) = Step 1 - 0.7* Step 2 (psi)
0.415	5.62	(2.99)	3.52
0.60		4.33	
0.89	17.34	(8.29)	11.53
0.90		8.43	
1.20		13.41	
1.21	28.66	(13.58)	19.16

* Numbers in parentheses are interpolated or extrapolated.

APPENDIX H

THERMAL PERFORMANCE DATA REDUCTION

H.1 Steady-State Tests

The objectives of this data reduction are to:

1) Determine wall-to-fluid thermal resistance as a function of coolant flow rate and temperature.
2) Assess uniformity of thermal performance among the four CHIC sites tested.
3) Determine the maximum heat flux tested.
4) Predict the maximum heat flux obtainable for operating conditions pushed to defined limits.

The first step required is the calculation of heat loss.

H.1.1 Conduction Heat Loss

The HFHE was designed for the simultaneous application of 100 W heat flux to twenty CHIC locations. During actual testing, however, only a single CHIC site was heated at any one time. Therefore, a portion of the heat applied was conducted away to the other nineteen CHICs. This heat loss was calculated and subtracted from the applied heat flux to obtain a net heat flux into the CHIC.

Method

Figure E.2 shows the top plate of the HFHE. Two of these plates, each 0.0381 cm (0.015 in) thick, permit heat conduction away from the CHIC. Figure E.3 shows the next plate in the stack, a target spacer also of 0.0381 cm thickness. This plate also provides a heat conduction path away from the CHIC. Beneath these top three plates lie orifice and spacer plates (Figures E.4 - E.6) which contain rectangular fluid passages which are assumed to block conduction. Based on this geometry, a conduction heat transfer thickness equal to the combined thickness of the top three plates, 0.1143 cm (0.045 in), was assumed. Heat which is conducted below these three uppermost plates was assumed to find its way to fluid passages or back into the CHIC. This would occur whether all twenty CHICs were heated simultaneously or if only one was heated, and therefore was not considered to be heat loss resulting from heating of only one CHIC.

Conduction heat loss was computed by measuring the surface temperature gradient away from the CHIC being heated, using a surface T/C arrangement as illustrated in Figure 17. These measurements were used to compute the surface temperature gradient at geometric symmetry boundaries and, using the thicknesses given above, to compute conduction heat loss using Fourier's law of heat conduction. This method is illustrated in Figure H.1.
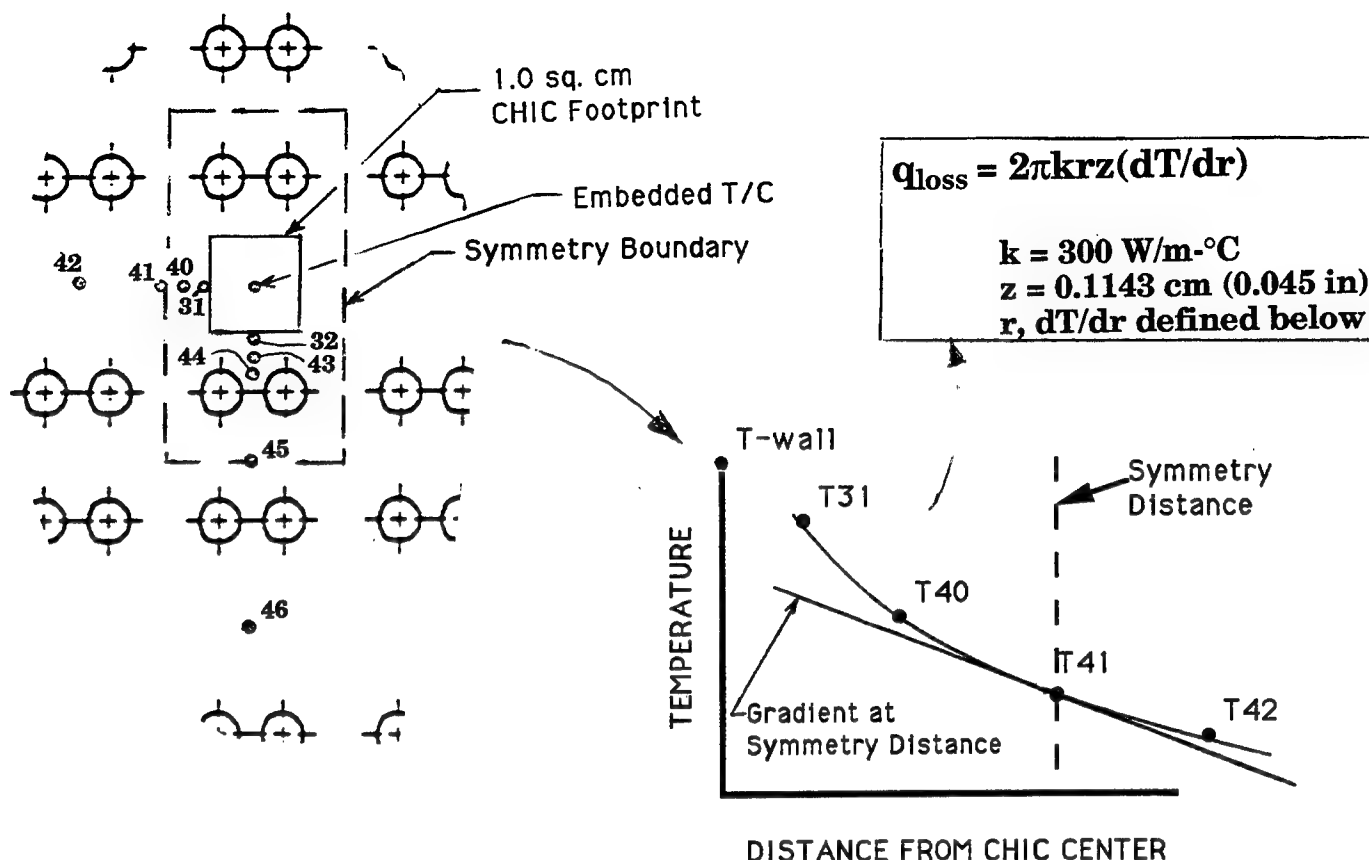
Figure H.1   Determination of Conduction Heat Loss

Using the methodology illustrated in Figure H.1, heat conduction losses were calculated, summarized in Table H.1. All calculations were performed at site "D" (shown in Figure 9) because this was the only CHIC site which had a thermocouple imbedded in the CHIC surface to provide a measure of wall temperature. In addition to calculated heat loss, Table H.1 also shows the net heat flux into the CHIC, and the ratio of conduction heat loss to applied heat flux. It was expected that heat loss should diminish as flow rate increases, since CHIC performance improves with increasing flow rate. A plot of heat loss, normalized to applied heat flux, versus flow rate is shown a Figure H.2. The trend is as expected, and a correlation was developed between heat loss and flow rate which was then used to expedite data reduction for tests at Sites A, B, and C. As a first-order approximation, it was assumed that heat loss was proportional to the number of adjacent CHIC sites. The correlation shown in Figure H.2 was derived from data obtained at site "D" (shown in Figure 9), which had four adjacent CHIC sites. Sites "A", "B", and "C" had four, two, and three adjacent CHIC sites respectively, so a factors of 1.0, 0.5, and 0.75, respectively, were applied to the Figure H.2 correlation.

Table H.1

Conduction Heat Loss Summary and Determination of Net Heat Flux

Test I.D.	Q-amplifier (W)	Temp. Grad. at Lines of Symmetry		Heat Conducted Across Line of Symmetry		Qloss.** (W)	Qnet*** (W)	Qloss/ Qamp
		dT/dx (°C)	dT/dy (°C)	$Q_{+/-x}$ * (W)	$Q_{+/-y}$ * (W)			
86	118.94	6.96	3.74	7.6	7.3	15.0	103.9	0.126
83	101.0	6.3	4.4	6.9	8.6	15.5	85.5	0.153
81	82.13	5.4	3.6	5.9	7.1	13.0	69.1	0.158
78	79.41	5.8	3.2	6.3	6.3	12.6	66.8	0.159
80	79.92	5.6	3.2	6.2	6.3	12.5	67.5	0.156
76	76.83	5.8	3.5	6.3	6.9	13.2	63.7	0.172
60	45.47	3.7	2.0	4.2	3.9	8.2	37.3	0.179
74	78.73	6.0	8.7	6.6	9.4	16.0	62.7	0.203

* $Q_{+/-x} = \pi k r_x t (dT/dx)$

* $Q_{+/-y} = \pi k r_y t (dT/dx)$ where:

    k = thermal conductivity = 300 W/m-°C,

    r_x = distance from CHIC center to symmetry boundary in x-direction = 1.01 cm

    r_y = distance from CHIC center to symmetry boundary in y-direction = 1.82 cm

    t = conduction thickness = 0.045 in

** $Q_{loss} = (Q_{+/-x} + Q_{+/-y})$

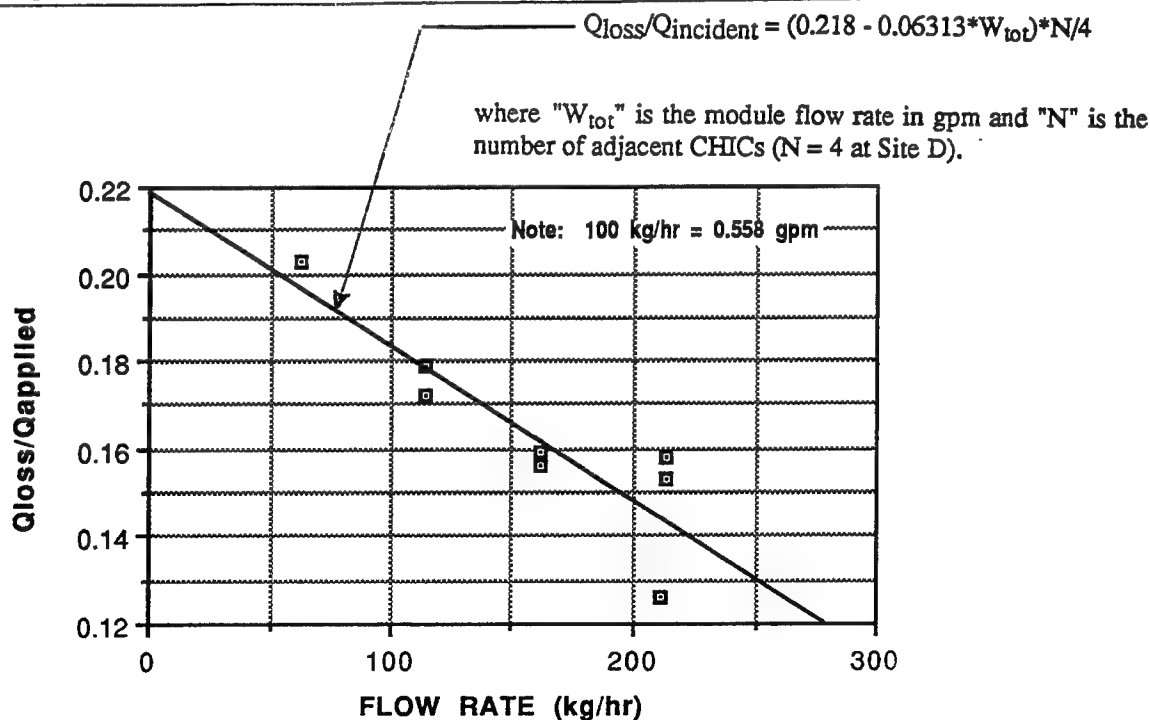*** $Q_{net} = Q_{amplifier} - Q_{loss}$

Qloss/Qincident = $(0.218 - 0.06313*W_{tot})*N/4$

where "W_{tot}" is the module flow rate in gpm and "N" is the number of adjacent CHICs (N = 4 at Site D).

Note: 100 kg/hr = 0.558 gpm

Figure H.2 Correlation Between Conduction Heat Loss and Flow Rate

102

H.1.2 Thermal Resistance Computation at Site D

Site D was the focus of data reduction because it was the only one of the four sites tested which had a thermocouple embedded in the heat exchanger skin at the CHIC location. This provided a direct measurement of wall temperature, necessary to determine wall-to-fluid thermal resistance. Thermal resistance is defined by the equation:

$$R_{wf} = (T_w - T_f) / Q_{net} \qquad (5)$$

where:
T_w = measured wall temperature at CHIC surface
T_f = coolant (fluid) supply temperature
Q_{net} = Applied heat flux (as measured through amplifier neck) minus conducted heat loss (obtained from Table H.1)

Using the net heat flux calculations from Table H.1, the following values of thermal resistance at site D were determined:

Table H.2

Thermal Resistance Computation - Site D (20 °C Coolant Temperature)

Test I.D.	Q_{net} (W)	T_w (°C)	T_f (°C)	Flow Rate (gpm)*	R_{wf} (°C/(W/cm^2))
86	103.9	45.95	18.80	1.18	0.261
83	85.5	43.00	20.24	1.19	0.266
81	69.1	38.83	20.25	1.19	0.269
78	66.8	39.58	20.25	0.90	0.289
80	67.5	39.73	20.53	0.90	0.284
76	63.7	39.72	19.87	0.64	0.312
60	40.6	32.12	20.01	0.64	0.298
74	62.7	43.22	20.36	0.35	0.365

* Gallons per minute

By applying the heat loss/flow rate correlation (Figure H.2), net heat flux and thermal resistance for other tests at site D could be estimated without the need to determine surface temperature gradients. Table H.3 shows heat loss, net heat flux, and thermal resistance for these tests.

Table H.3

Thermal Resistance Computation - Site D (10 °C, 30 °C, and 40 °C Coolant Temperatures)

Test I.D.	Flow Rate (gpm)	Qamplifier (W)	* Qloss/ Qamplif	Qloss (W)	Qnet (W)	Tw (°C)	Tf (°C)	Rwf (°C/(W/cm2))
75	0.35	78.60	0.197	15.48	63.12	43.26	20.29	0.364
54	0.31	51.75	0.199	10.30	41.45	26.44	10.87	0.376
56	0.59	53.15	0.181	9.62	43.53	24.12	10.15	0.321
58	1.14	56.44	0.147	8.30	48.14	22.15	9.00	0.273
62	0.39	49.38	0.194	9.58	39.80	45.33	30.55	0.371
64	0.88	49.19	0.163	8.02	41.17	43.86	31.80	0.293
66	1.19	49.65	0.143	7.10	42.55	42.57	30.95	0.273
68	0.42	44.63	0.192	8.57	36.06	53.68	40.59	0.363
70	0.89	46.39	0.162	7.52	38.87	52.66	41.36	0.291
72	1.20	45.55	0.143	6.51	39.04	51.70	41.46	0.262

* Based on Figure H.2 Correlation with Flow Rate

H.1.3 Thermal Performance at Sites A, B, and C

The objective of this task is to verify consistent thermal performance at several (four) CHIC sites. At Sites "A", "B", and "C", thermocouples were attached to the HFHE surface *adjacent to* the heat flux amplifier (and CHIC), but not *under* the amplifier; thus, these thermocouples measured a lower wall temperature. The following method for relating these temperatures to the wall temperature *under* the amplifier therefore was employed:

1) Use the heat loss correlation versus flowrate (Figure H.2) to estimate conduction heat loss and net heat flux into CHIC at Sites "A", "B", and "C".

2) Using wall temperature measurements at site "D", as illustrated in Figure H.1, determine relationship between wall temperature at CHIC center versus surface temperature profile.

3) Using surface temperature profiles measured at Sites "A", "B", and "C", use relationship from Step 2 to predict CHIC wall temperature.

4) Compute thermal resistance using eqn. 5 using wall temperature from Step 3 and net heat flux from Step 1.

Applying this methodology, wall-to-fluid thermal resistances derived at Sites "A", "B", and "C" are shown in Table H.4.

Table H.4

Wall-to-Fluid Thermal Resistances at Sites "A", "B", and "C"
(20 °C Coolant Temperature)

Site	Test I.D.	Flow Rate (gpm)	Q_{ampl} (W)	No. Adjacent CHICs (N)	Q_{loss} (W) (= N/4 * eqn. in Fig. H.2)	Q_{net} (W)	T_w-T_f (°C)	R_{wf} (°C/(W/cm2))
A	29	1.20	100.24	4	14.33	85.91	21.41	0.249
B	51	1.18	63.23	2	4.55	58.68	18.02	0.307
C	53	1.17	57.4	3	6.24	51.16	13.29	0.260

H.1.4 Maximum Heat Flux Measured

The maximum steady-state heat flux measured was limited by power availability, and is shown in Table H.5 as 106.8 W/cm². This exceeds the requirement of 100 W/cm². Also shown are limits on operating conditions, as defined by the design requirements.

Table H.5

Maximum Measured Steady-State Heat Flux

Test I.D.	T_f (°C)	Δp (HFHE) (psi)	Flow Rate (gpm)	T_w (°C)	Q_{amp} (W/cm2)	Q_{loss}/ Q_{amp}	Q_{loss} (W/cm2)	Q_{net} (W/cm2)
86	18.80	19.0	1.18	45.95	118.94	0.102	12.13	106.8
Limits	0 (min.)	45 (max.)		50 (max.)				

H.1.5 Projected Maximum Heat Flux

The maximum heat flux capability of the HFHE may be estimated by extrapolating the results shown in Table H.5 to limit operating conditions. For this extrapolation, coolant temperature is reduced to 0 °C and HFHE pressure drop is increased to 45 psi. At such conditions, flow rate is predicted to be 329 kg/hr (1.84 gpm) based on Figure 12. From Figure 10, for a flow rate of 329 kg/hr and coolant temperature of 0 °C, wall-to-fluid thermal resistance is 0.270 °C/(W/cm2). Thus, applying junction-to-case and case-to-wall thermal resistances from Section 2.1, maximum possible heat flux is calculated as:

$$Q_{max} = \frac{T_j - T_f}{R_{jc} + R_{cw} + R_{wf}} = \frac{90\,^\circ C - 0\,^\circ C}{0.20 + 0.20 + 0.27\,^\circ C/(W/cm^2)} = 134\,W/cm^2$$

H.2 Transient Tests

The objective of these tests was to characterize HFHE performance under transient heating conditions. The magnitude of the heat flux and its time dependence were to reflect heat dissipation characteristics of power switching devices. These characteristics vary considerably with device. A heat load profile increasing from zero to approximately 100 W/cm^2 in several seconds was selected for these tests because it was easily accomodated for by the test equipment, but does not reflect heat dissipation characteristics of any specific device.

The heat flux amplifier could not be used for transient heating because of the large thermal lag between the heat input end (top) and the delivered heat flux (bottom). Therefore, a thick-film ceramic heater, provided free of charge from Mini-Systems, Inc. (MSR-26), 1.0 cm on a side, was used for transient heating tests. Heat flux was controlled manually with a dial. All tests were conducted at nominal conditions of 20 °C coolant temperature and 215 kg/hr (1.2 gpm) module flow rate. These conditions were brought to steady-state prior to heat application, and held constant during heating.

Figure H.3 shows test results for steady-state heat flux ($Q_{applied}$ = 57.6 W), which provides a measure of wall-to-fluid thermal resistance. Using Figure H.2 to account for heat loss at the test condition flow rate of 215 kg/hr (1.2 gpm), a value of R_{wf} of 0.344 °C/(W/cm^2) is obtained. This compares high to the thermal resistance obtained using the amplifier (see Table H.2, R_{wf} for Test I.D.s 86, 83, and 81).

The time resolution of the data recording system was one second. Because of the short duration of the tests, there was some scatter in the data. Therefore, curves were plotted through the data to generate a smoother profile.
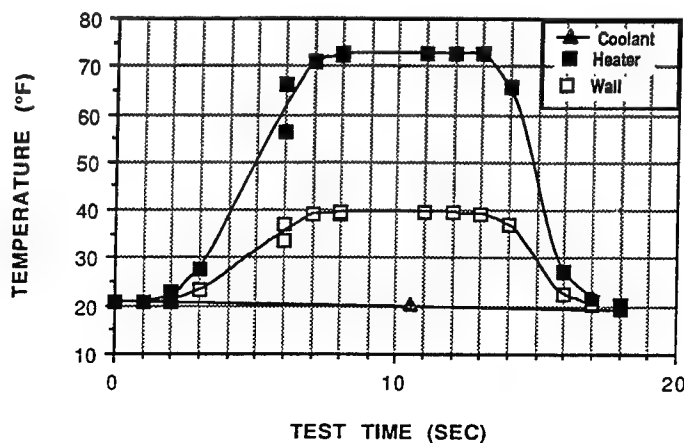

Figure H.3 Test Results - Ramp to Steady-State. Test I.D. 91

Figures H.4 and H.5 show test results for two different heat flux ramp-up rates. These results show that the HFHE responds to transient heating with very little time lag; i.e., wall temperature rises and falls with heat flux.
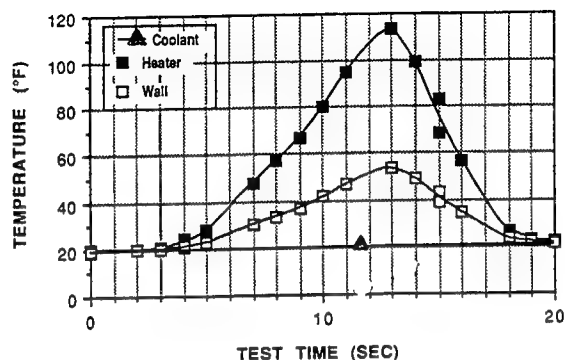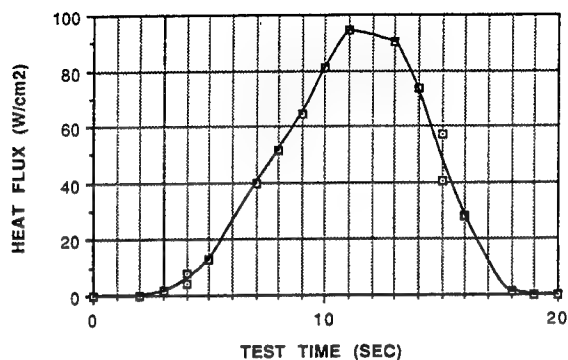

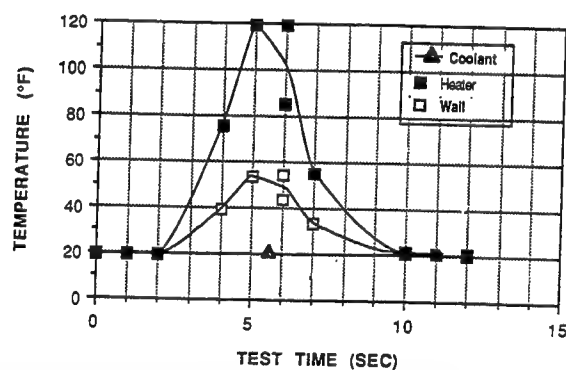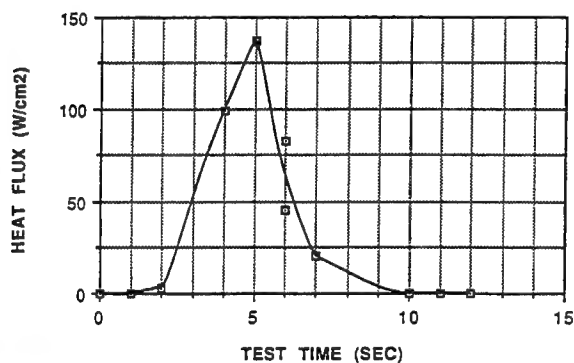**Figure H.4 Transient Heating Test Results, Slow Ramp. Test I.D. 97.**

Figure H.5 Transient Heating Test Results, Fast Ramp. Test I.D. 96.

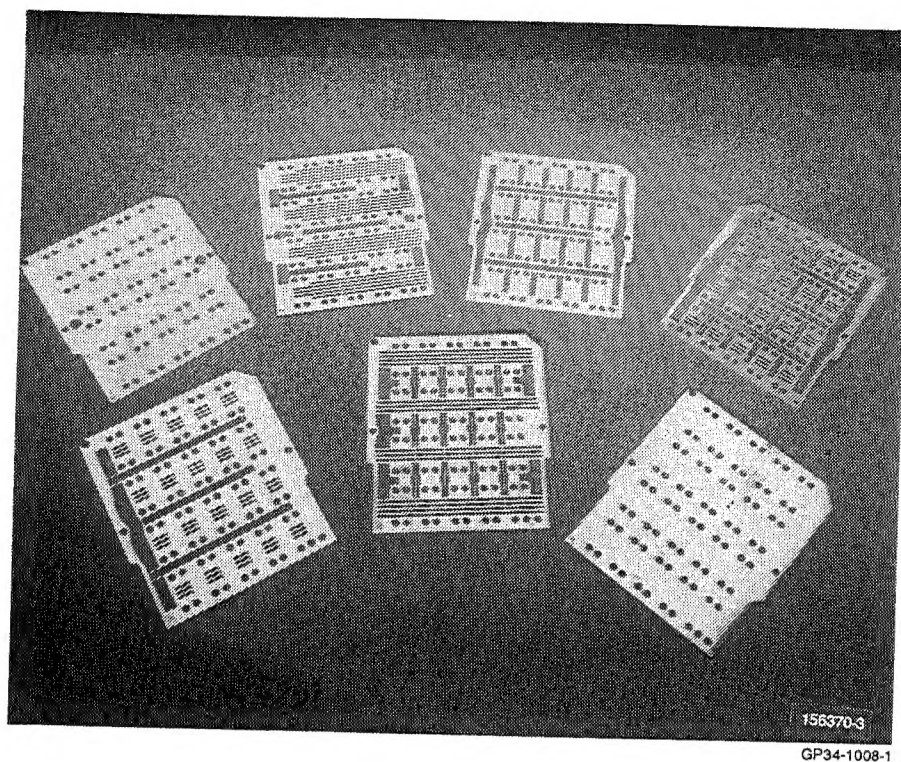107

APPENDIX I

PHOTOGRAPHS OF HFHE AND TEST SET-UP

156370-3

GP34-1008-1

Figure I.1. CHIC Laminates

ALUMINUM FRAME

GASKET
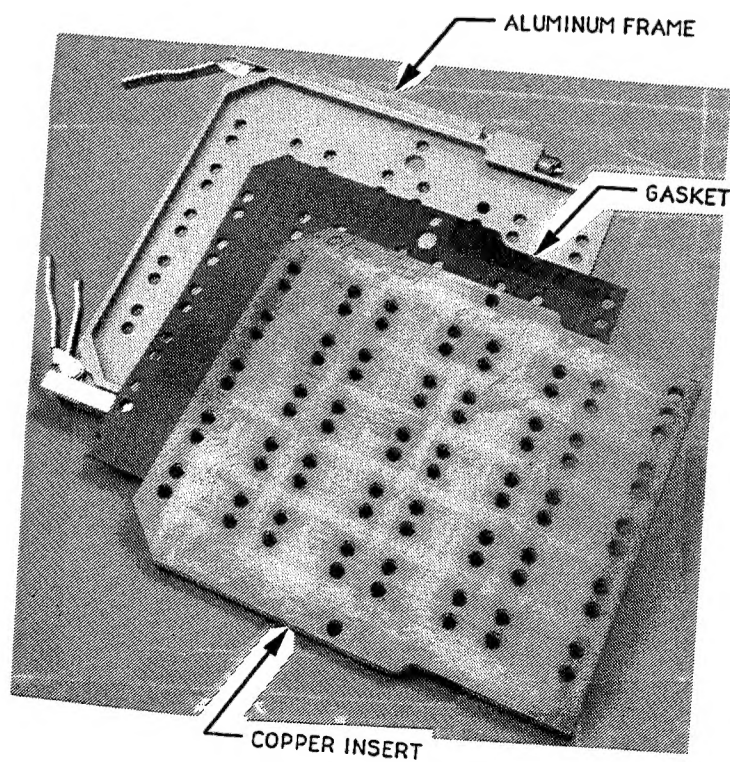
COPPER INSERT

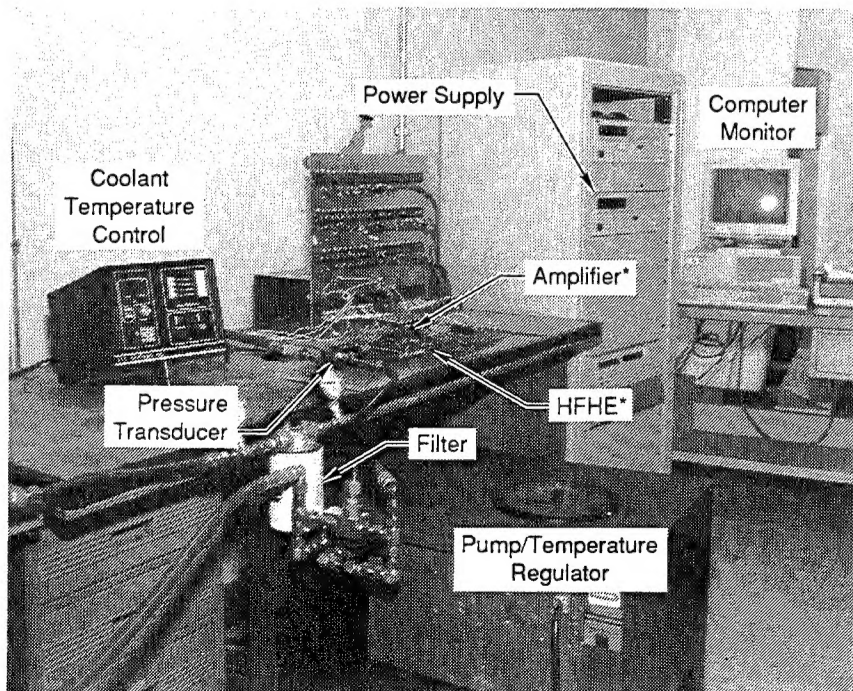Figure I.2. From Top to Bottom; Copper Inserts With Twenty CHICS, VITON Gasket, Aluminum Header Frame
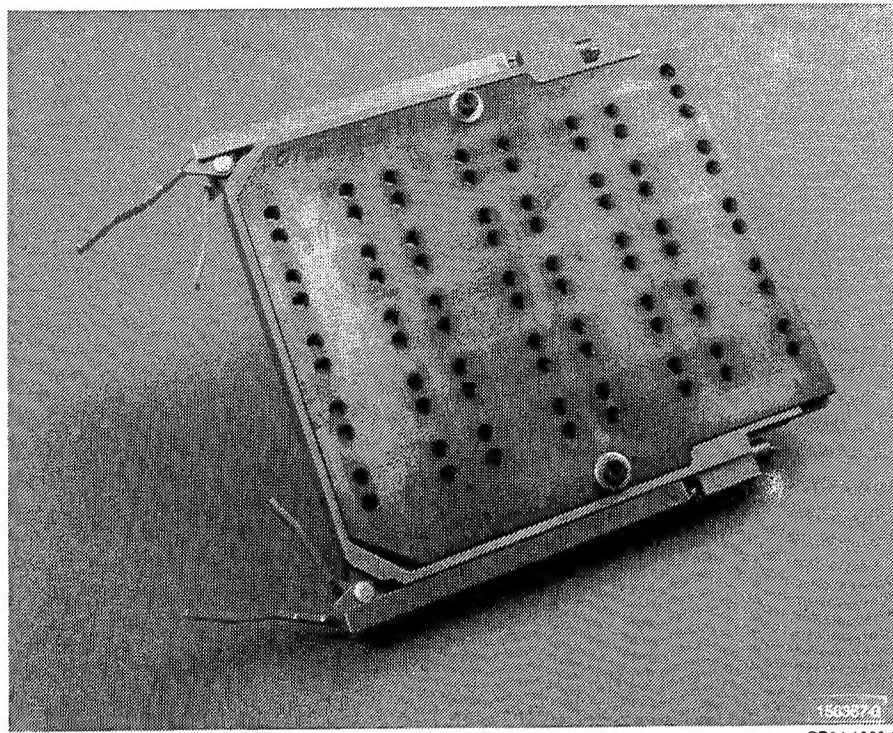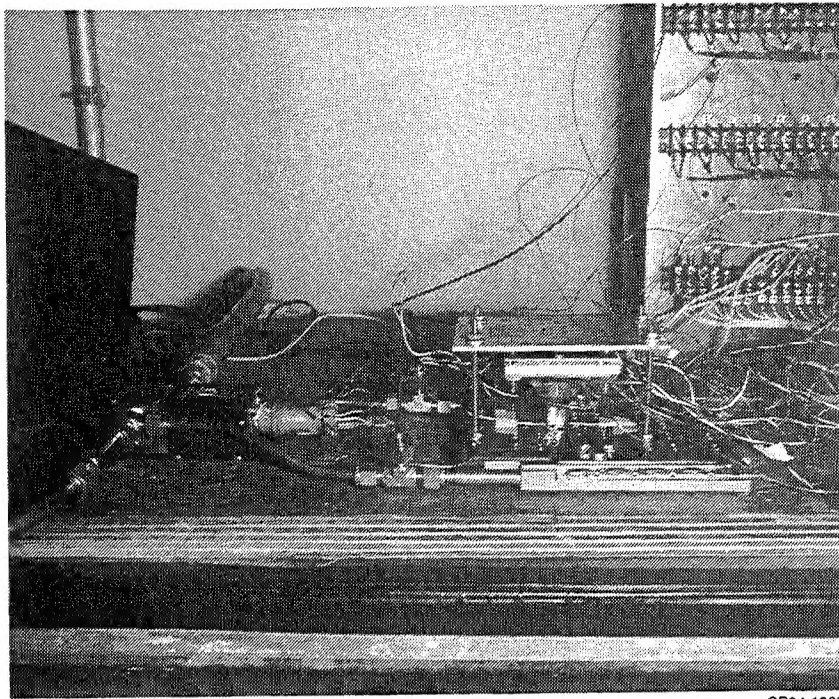
GP34-1008-3

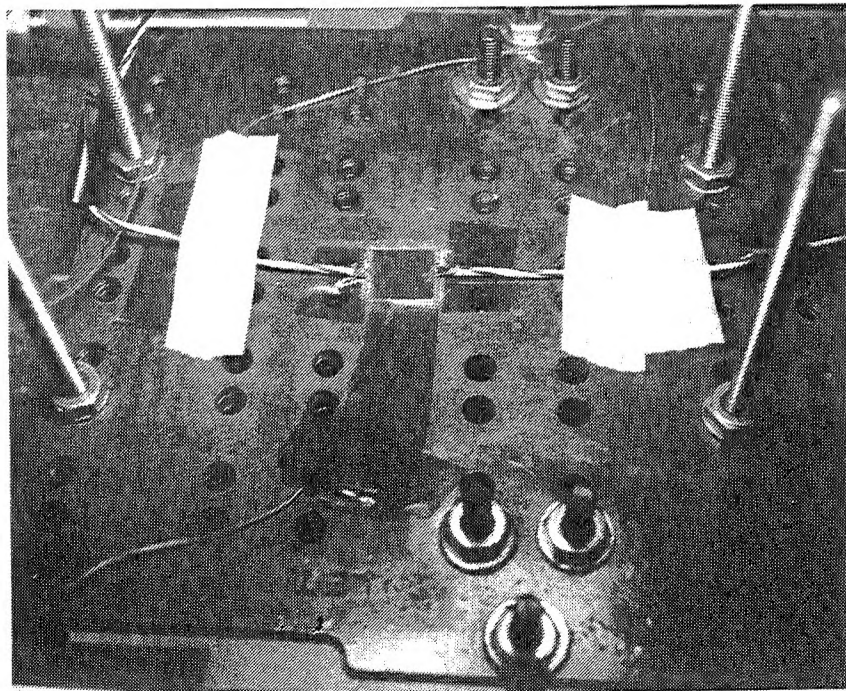**Figure I.3. Assembled HFHE**

*See Figure I.5 for detail

GP34-1008-4

Figure I.4. Laboratory Test Set-Up

110

GP34-1008-5

Figure I.5. Close-Up of Amplifier and HFHE

GP34-1008-6

Figure I.6. Thick Film Resistance Heater Used for Transient Heating Tests

111